Theoretical investigation of the adsorption of oxygen on TiO_2

Maria Dall Rasmussen
Interdisciplinary Nanoscience Center iNANO
Department of Physics and Astronomy
Faculty of Science
University of Aarhus

PhD Thesis
February 2005

This thesis is submitted to the Faculty of Science at the University of Aarhus, Denmark, in order to fulfill the requirements for obtaining the PhD degree in theoretical physics. The study has been carried out under the supervision of Dr. Bjørk Hammer at the Department of Physics and Astronomy from February 2001 to January 2005.

On the front page: The Wulff reconstruction of rutile TiO_2, reproduced from [1]. Picture of a rutile mineral crystal, commercially available from http://www.trinityminerals.com/munich/rutile.htm. Ball and stick model of the rutile $TiO_2(110)$ surface.

Contents

List of publications

[I] *Adsorption, diffusion, and dissociation of molecular oxygen at defected TiO_2(110): A density functional theory study,*
M. D. Rasmussen, L. M. Molina and B. Hammer, J. Chem. Phys. **120**, 2, 988-997 (2004)

[II] *Adsorption of O_2 and oxidation of CO at Au nanoparticles supported by TiO_2(110),*
L. M. Molina, M. D. Rasmussen and B. Hammer, J. Chem. Phys. **120**, 16, 7673-7679 (2004)

[III] *The charge state of oxygen on the TiO_2(110) surface,*
M. D. Rasmussen, L. M. Molina and B. Hammer, *In preparation*

[IV] *Charge transfer from sub-surface vacancies to adsorbates on TiO_2(110),*
M. D. Rasmussen and B. Hammer, *In preparation*

CHAPTER 1

Motivation

TiO_2 is an important material in many fields. In particular, it is important in catalysis, both as a support and as a catalyst. For instance, small gold clusters on titanium show great promise as a catalyst for the oxidation of CO. Many experimental studies concerning the oxygen chemistry of single crystal TiO_2 have left open questions. Some of these can only be expected answered by theoretical means. Theory has shown success in modeling the surface structure and reactivity so far, and we thus feel encouraged to study oxygen adsorption on the rutile (110) surface using density functional theory.

1.1 The material TiO_2

In the last couple of decades, the effort in environmental protection has been increasing. Part of these efforts has been to increase the control over the waste products let into the air and water from human production and transportation. This can be done in two ways: removing hazardous compounds for safer storage or converting them into harmless substances. Using the former technique demands that storage space be found for the harmful chemicals, and is consequently not a viable long term strategy for non-degradable compounds. Thus, many attempts are made at somehow changing unwanted compounds into forms that nature can deal with without problems. In these endeavours, catalysis often turns out to be an advantageous solution.

Catalysis describes the phenomenon of a compound accelerating a reaction without itself being consumed in the reaction. Usually this happens by the presence of the catalyst modifying the energetic barriers for conversion from reactants to products. Heterogeneous catalysis by nature happens on surfaces, as the bulk material is inaccessible to the reacting compounds. As many catalysts are also expensive materials, it is sensible to make the most of the material by adsorbing it in small clusters on a suitable support, so that most of the catalyst atoms are accessible to the reactants. This has two complications, which scientists must use to their advantage. Firstly, the properties of the catalyst material often changes drastically if cluster size becomes small enough. This is the case for e.g. noble metals as catalysts. Secondly, the right choice of substrate can enhance the activity of the catalyst.

TiO_2 is doubly important in catalysis; both as a catalyst substrate and as a catalyst in its own right. It enjoys widespread use as a photocatalyst for the removal of various pollutants from both water and air [2]. Many of these reactions are oxidation reactions, as the compounds are oxidated into small, relatively harmless molecules. The TiO_2 surface has also recently been found to be a very suitable support for heterogeneous catalysis, in particular for the low temperature oxidation of CO by Au catalysts [3, 4]. A reaction on a catalyst surface can be divided in three steps:

- Adsorption of reactants on the surface.
- Reaction on the surface.
- Desorption from the surface.

If either of the processes is not feasible, the catalyst does not work on the long term. If the reactants cannot adsorb or react at the surface, naturally catalysis is not taking place. If the desorption step does not happen, the surface is eventually covered by reaction products, and no more reactants can adsorb. This is known as poisoning. Consequently, investigating the adsorption, charge state and diffusion of oxygen on the TiO_2 is very interesting for e.g. oxidative catalysis.

Apart from catalysis, thin TiO_2 coatings have very interesting potential applications as gas sensors [5, 6], and the surface properties of titanium oxides are very important for the use of titanium as a biocompatible material [7] and for water disinfection [8]. Additionally, TiO_2 is used as pigment for a variety of different purposes. Therefore, a

good fundamental understanding of the intrinsic properties of TiO_2 surfaces and of their interaction with various adsorbates in general is called for, as this is of great importance for understanding the way these materials work and eventually improving them.

There exist two different technologically important phases of TiO_2, anatase[1] and rutile, with the anatase irreversibly transforming to rutile at high temperatures. For rutile, the most stable surface is the (110) facet [1]. We have limited out study to the rutile (110) surface, as it is the most stable surface of the most stable phase and ample experimental work already exists.

TiO_2 is a semi-conductor and has interesting properties when irradiated with UV light. It photo-catalyses a range of reactions [9], work in solar cells [10] and even simply irradiating the surface has an interesting effect: the wetability of the surface changes from hydrophobic to hydrophillic [11]. Why this happens has not yet been adequately explained. The principle driving the processes is the excitation of electrons from the valence band to the conduction band. The resulting hole and electron can take different pathways; in photo-catalysis of a chemical reaction, either a hole or an electron is transfered to one or more reactants. The excited state thus created induces the reaction. Sometimes, the hole and electron will recombine again, vanishing before inducing a reaction. As the original photon is then wasted, recombination is not wanted, and the system is usually tailored to optimize the quantum yield (the number of reactions per absorbed photon). In this context, the transfer of charge carriers to the reactants is an important issue. We will later find that on TiO_2 charge transfer from point defects to adsorbates can happen easily over long distances.

1.2 Why do theoretical modeling?

Theoretical modeling of the TiO_2 surface using density functional theory (DFT) has previously met with some success. The bulk lattice constants are well reproduced, as is the surface relaxation, [1], except for the bond lengths of the outermost oxygen atoms. Calculating these bond lengths is complicated by the presence of a soft, anharmonic mode. Simulated scanning tunneling microscopy (STM) pictures of the stoichiometric and defected surface [12], as well as the reconstructed surface [13], have shown satisfying similarity to real STM pictures, reproducing the electronic structure determined contrast. DFT has also successfully explained surface-adsorbate interaction for a number of adsorbates [14–16]. Based on this previous work, we expect that DFT should be able to contribute to the understanding of TiO_2 surfaces in predicting the electronic structure of the surface, with and without adsorbed molecules, and adsorption and reaction energies of adsorbates. This information can be used to judge the feasibility of the three steps in the catalytic reaction. Evaluating the adsorption energy determines whether adsorption of reactants is possible, and whether products will leave easily or the surface poisons. An estimate of the barriers for diffusion on the surface can provide insight into the reaction pathway; must reactants adsorb directly next to each other to

[1] The anatase phase is the one used most frequently as a pigment, since colloidal anatase is bright white, whereas rutile is slightly yellowish. Since anastase TiO_2 is used to colour products such as chewing gum, tooth paste and washing powder, the pure white colour is preferred.

react or can they diffuse and thereby meet and react? This is an important aspect in understanding a catalyst support, because it determines how easily reactants will reach the catalytic material adsorbed in clusters on the surface. The reaction barriers determines the rate of reaction, and therefore knowledge of the reaction barriers makes it possible to judge which reaction pathway will be chosen, and whether reaction happens fast enough to be practically useful. All this information helps in determining the performance of a catalyst and gives important clues in how to optimize it through the right choice of materials.

DFT, then, is a good tool to gain some theoretical insight. In particular, it is very well suited to complement STM observations in the identification of species present on the surface. There are drawbacks, though. Due to limited computational power, the size of the systems we can treat is finite. We can make it pseudo-infinite by using periodic boundary conditions, repeating a unit cell infinitely in all directions. However, this still imposes restrictions on the distance between defects and adsorbates and on the adsorbate-to-defect ratio. As it turns out, co-adsorption of different or even identical adsorbates is essential to the understanding of surface reactivity. This imposes a difference between the model system and the system of a chemical plant. In a production unit, the state of the catalyst is very far from the perfectly periodic single crystal described in calculations. Additionally, temperatures and pressures are usually high, whereas in calculations we address the ground state of the system, equivalent in principle to 0 K. Thus, the challenge is to draw from the simple model system conclusions which are helpful in the understanding of the complex system through a continuous interplay between theory and experiment.

1.3 Outline

The present thesis contains a theoretical study of the oxygen chemistry of the rutile TiO_2 (110) surface. The calculations have been done using density functional theory (DFT), the foundations of which are described in Chapter 2, as well as the implementation of DFT we are using, including the choice of basis functions, pseudopotentials and exchange correlation. A quick overview of the intricacies in finding transition states and diffusion paths is also found here.

In Chapter 3, the rutile TiO_2 (110) surface and its relaxations are described in detail. As TiO_2 is easily reducible, a description of the oxygen vacancies of the surface is given, together with the changes of the electronic surface characteristics introduced by vacancy creation. Additionally, the considerable change in the vacancy creation energy introduced by the electrophillic oxygen adsorbate is presented and related to vacancy segregation.

The interaction of oxygen with the TiO_2 (110) surface is of great importance due to the popularity of TiO_2 as a substrate for catalytic reactions involving the oxidation of small molecules, in particular CO. The oxygen chemistry of (110) surface is described in Chapter 4. First, experimental evidence is briefly described. Then the adsorption configurations and charge states of molecular oxygen found on the basis of DFT calculations are presented, and the interaction between oxygen adsorbates and defects in the surface

is discussed. Based on these insights, the co-adsorption of several oxygen molecules and of oxygen and CO is studied. As TiO_2 is used in the oxygenation of ozone, the interaction between the surface and ozone is investigated, based on the charge state of the surface.

Much experimental work has been done on TiO_2 already. Experimental evidence from temperature programmed desorption (TPD) measurements is reinterpreted in the light of calculations in Chapter 5, and an attempt is made to make a consistent designation of the species found in recent STM measurements.

On the first page of each Chapters 1-5, the reader will find a small abstract, summarizing the contents of the chapter.

Chapter 6 summarizes conclusions and presents an outlook on work yet to be done.

Chapter 7 contains an abstract of the thesis in Danish.

CHAPTER 2

Density Functional Theory

According to the Theorem of Hohenberg and Kohn, the ground state density of a bound system of interacting electrons in an external potential uniquely determines the potential. Therefore, all ground state information on the system is in principle inherent in the electronic density. This insight can be used to construct a method for self-consistently determining the ground state electron density and energy with much less computational cost than that involved in solving the corresponding Schrödinger equation. Knowing the exact form of the exchange-correlation of the system, the procedure would be exact; different attempts at establishing a functional form of the exchange-correlation have been done. Other approximations are necessary to use the computational scheme in practice. In describing periodical systems, it is advantageous to use Blochs theorem and expand the wave function in plane waves, including only those of lower energy in the calculation. Additionally, as the valence electrons strongly dominate electrical bonding, pseudopotentials are introduced to lessen the computational task.

2.1 The Hohenberg-Kohn Theorem

The foundation on which DFT rests is the theorem of Hohenberg and Kohn which was first published in 1964 [17]. It states that

The ground state density of a bound system of interacting electrons in some external potential $v(r)$ determines the potential uniquely [1].

I shall present the proof for a non-degenerate ground state. The generalization is straightforward [18], but more space consuming.

Proof: Let $n(r)$ be the non-degenerate ground-state density of N electrons in an external potential, $v_1(r)$. Let the corresponding wave-function of the many-body system be Ψ_1 and its energy E_1. Then the energy is given by

$$\begin{aligned} E_1 &= \langle \Psi_1, \widehat{H_1} \Psi_1 \rangle \\ &= \int v_1(r) n(r) d^3 r + \langle \Psi_1, (\widehat{T} + \widehat{U}) \Psi_1 \rangle, \end{aligned} \tag{2.1}$$

where $\widehat{H_1}$ is the total Hamiltonian corresponding to v_1, and $\widehat{T}$ and $\widehat{U}$ are the kinetic and interaction energy operators. Now, assume that another potential exists which is not identical to v_1 plus an additive constant. The ground state corresponding to this potential, Ψ_2, is not equal to Ψ_1, since it satisfies a different Schrödinger equation. Assume the ground state Ψ_2 produces the same density, $n(r)$. Then the energy is given by

$$E_2 = \int v_2(r) n(r) d^3 r + \langle \Psi_2, (\widehat{T} + \widehat{U}) \Psi_2 \rangle. \tag{2.2}$$

Since the ground-state Ψ_1 was assumed to be non-degenerate, and all non-ground-states have higher energy, the following inequality holds:

$$\begin{aligned} E_1 &< \langle \Psi_2, H_1 \Psi_2 \rangle \\ &= \int v_1(r) n(r) d^3 r + \langle \Psi_2, (\widehat{T} + \widehat{U}) \Psi_2 \rangle \\ &= E_2 + \int [v_1(r) - v_2(r)] n(r) d^3 r. \end{aligned} \tag{2.3}$$

The similar equation for E_2 is

$$E_2 \leqslant E_1 + \int [v_2(r) - v_1(r)] n(r) d^3 r, \tag{2.4}$$

since we did not make any assumption on the non-degeneracy of Ψ_2. Adding equations (2.3) and (2.4) reveals the contradiction:

$$E_1 + E_2 < E_1 + E_2. \tag{2.5}$$

[1] In this context, uniquely means up to an uninteresting additive constant.

This proves the theorem for a non-degenerate ground state. It is important to note the direction in the theorem: given the electron density, the external potential is determined, not the other way around. It should be noted that a random, well-behaved function is not necessarily a possible ground-state density corresponding to some $v(r)$. This means that a given function does not have to correspond to a physical system where it is the density [18, 19].[2] In the case where the function has a corresponding potential, however, the theorem states that the external potential, and as a consequence the full Hamiltonian, together with the number of electrons, N, is uniquely determined. This completely determines the system.

2.2 The Kohn-Sham equations

Using the theorem of Hohenberg and Kohn, we can derive the Hohenberg-Kohn variational principle. The following derivation is called the constrained search method and is due to Levy and Lieb [19–21]. The ground state energy is always given by

$$E = \min_{\tilde{\Psi}} \langle \tilde{\Psi}, \widehat{H} \tilde{\Psi} \rangle, \tag{2.6}$$

where the minimization runs over all possible $\tilde{\Psi}$. Every $\tilde{\Psi}$ corresponds to a density $\tilde{n}(r)$, and the minimization can then be done in a series of two steps, choosing first trial densities and minimizing with respect to all possible wave functions corresponding to the density, then minimizing with respect to densities. Here it is useful to define the constrained energy minimum, corresponding to the first step:

$$\begin{aligned} E_V[\tilde{n}(r)] &= \min_\alpha [\langle \tilde{\Psi}^\alpha_{\tilde{n}(r)}, \widehat{H} \tilde{\Psi}^\alpha_{\tilde{n}(r)} \rangle] \\ &= \int v(r)\tilde{n}(r) d^3r + F[\tilde{n}(r)] \end{aligned} \tag{2.7}$$

where

$$F[\tilde{n}(r)] = \min_\alpha [\langle \tilde{\Psi}^\alpha_{\tilde{n}(r)}, (\widehat{T} + \widehat{U}) \tilde{\Psi}^\alpha_{\tilde{n}(r)} \rangle] \tag{2.8}$$

and α numbers the wave functions corresponding to the density $\tilde{n}(r)$.[3] The second step is then the minimization of the constrained energy:

$$\begin{aligned} E &= \min_{\tilde{n}(r)} E_V[\tilde{n}(r)] \\ &= \min_{\tilde{n}(r)} \Big[\int v(r)\tilde{n}(r) d^3r + F[\tilde{n}(r)] \Big] \end{aligned} \tag{2.9}$$

Now, the problem has been formulated formally in the density only, but the wave function is still hiding in the expression for $F[\tilde{n}(r)]$. The next step is to obtain an expression

[2] The function is said not to be v-representable.

[3] The definition of $F[\tilde{n}(r)] = \min_\alpha [\langle \tilde{\Psi}^\alpha_{\tilde{n}(r)}, (T + U) \tilde{\Psi}^\alpha_{\tilde{n}(r)}]\rangle$ is equal to the definition $F[\tilde{n}(r)] = \langle \tilde{\Psi}, (T + U) \tilde{\Psi} \rangle$, where $\tilde{\Psi}$ is the ground state, in the case where $\tilde{n}(r)$ is v-representable. However, this approach works even if it is not.

for $F[\tilde{n}(r)]$ that takes advantage of the fact that it is only dependent of the density, as proven above. One expression is

$$F[\tilde{n}(r)] = T[\tilde{n}(r)] + \frac{1}{2}\int \frac{\tilde{n}(r)\tilde{n}(r')}{|r-r'|} d^3r d^3r' + E_{\mathrm{xc}}[\tilde{n}(r)] \tag{2.10}$$

The first term is the kinetic energy of a *non-interacting* electron gas.[4] The next term is the electrostatic energy, and the last term, called the exchange-correlation energy, encompasses the remainder of the functional. It is defined by (2.10), and much work has been put into the making of parametrizations of this term.

Now that we have an expression for $E_V[\tilde{n}(r)]$, we can return to the minimization problem (2.9), [22]. First consider a non-interacting system of electrons. According to the Hohenberg-Kohn Theorem there exists a unique energy functional

$$E[n(r)] = T[n(r)] + \int V_s(r) n(r) d^3r. \tag{2.11}$$

Since the system is non-interacting, the ground-state density can be found by finding the single-particle states

$$0 = \Big(-\frac{1}{2}\nabla^2 + V_s(r) - \epsilon_j \Big) \phi_j(r) \tag{2.12}$$

which make up the density

$$n(r) = \sum_{\mathrm{j}=1}^{\mathrm{N}} |\phi_{\mathrm{j}}(r)|^2. \tag{2.13}$$

Returning to the interacting case, $E_V[\tilde{n}(r)]$ is minimal when the variation with respect to the density is zero:

$$0 = \frac{\delta E_V[\tilde{n}(r)]}{\delta \tilde{n}(r)} = \frac{\delta T[\tilde{n}(r)]}{\delta \tilde{n}(r)} + v(r) + \int \frac{\tilde{n}(r')}{|r-r'|} d^3r' + v_{\mathrm{xc}} \tag{2.14}$$

where the exchange-correlation potential is defined by

$$v_{\mathrm{xc}}(r) = \frac{\delta}{\delta \tilde{n}(r)} E_{\mathrm{xc}}[\tilde{n}(r)] \Big|_{\tilde{n}(r)=n(r)}. \tag{2.15}$$

The corresponding equality for the non-interacting system is

$$0 = \frac{\delta T[\tilde{n}(r)]}{\delta \tilde{n}(r)} + V_s(r). \tag{2.16}$$

We then see that by inserting

$$V_s(r) = v(r) + \int \frac{\tilde{n}(r')}{|r-r'|} d^3r' + v_{\mathrm{xc}}(r) \tag{2.17}$$

[4] The assumption is made that the density is v-representable in the non-interacting case.

in (2.12) we get a system of equations producing the correct ground state density. These equations, together with the expression for the density (2.13), are called the Kohn-Sham equations. The ground state energy is then given by

$$E = \sum_j \epsilon_j - \frac{1}{2}\int \frac{\tilde{n}(r)\tilde{n}(r')}{|r-r'|} d^3r d^3r' - \int v_{xc}(r) n(r) d^3r' + E_{\mathrm{xc}}[n] \tag{2.18}$$

Since the Kohn-Sham equations simply derive from the mathematical similarity of (2.10) to the non-interacting electron equation, neither the Kohn-Sham wave functions $\phi_j(r)$ nor the corresponding energies ϵ_j have any real physical meaning, except from the highest occupied ϵ_j, which equals the ionization energy (relative to vacuum). In some cases, it has proven reasonable to use them as if they were indeed physical quantities, however. For instance the calculation of theoretical densities of states combined with the d-band model [23,24] reproduces binding trends well. DFT-based calculations of band structure is also based on this approximation.

2.3 Choosing exchange correlation potentials

All of the above equations are exact. Iteratively solving the Kohn-Sham equations produces the precise ground state density. However, this cannot be done since an expression for the exchange-correlation potential is still lacking. The major approximation inherent in DFT is the form of the exchange-correlation. All other approximations can be brought arbitrarily close to the actual value given enough computational effort. Even pseudopotentials could in principle be discarded by including all electrons as valence electrons (see below). Not so the exchange correlation; consequently large amounts of effort goes into finding better descriptions. The first approximation is the local density approximation (LDA) where the exchange-correlation energy density is dependent only on the local electron density. However, in truth the exchange correlation energy density depends on the values of the electronic density at all points, i.e. global information. As a consequence, the LDA is exact only for the uniform electron gas, since the local density in this case provides the global information. It has the form:

$$E_{\mathrm{xc}}[n] = \int n(r)\epsilon_{\mathrm{xc}}(r) d^3r. \tag{2.19}$$

It has been remarkably successful [25]. Near surfaces of molecules and solids, though, where the electron density decreases exponentially, the rapid change in density causes LDA to produce an over-binding. A lot of work has been put into advancing beyond the LDA. One of the successful attempts is the generalized gradient approximations (GGA) in which the energy density depends also on the gradient of the density. They are generally of the form:

$$E_{\mathrm{xc}}[n(r)] = \int f(n(r), \nabla n(r)) d^3r, \tag{2.20}$$

where spin dependence can also be taken into account (as for the LDA, which is then called LSD). This has resulted in a class of different functionals. In this thesis, I have

LDA	PW91	PBE	revPBE	RPBE	Exp.
7.10 eV	5.84 eV	5.81 eV	5.53 eV	5.51 eV	5.23 eV

Table 2.1: Binding energy of an oxygen molecule using different exchange correlation potentials. Taken from [27].

made use of two, the Perdew-Wang91 [26] and the RPBE [27]. Perdew-Wang91 (PW91) GGA is used frequently in the literature, and all the energies given in the present work are calculated self-consistently with this exchange correlation potential. If not specifically mentioned, energies are calculated using PW-91. RPBE results given for comparison contain several approximations: 1) The charge density is calculated self-consistently for the PW-91 functional. 2) Pseudopotentials are made based on the PW-91 exchange correlation. 3) Structures are optimized with respect to PW-91. The latter is the most important, according to [27]. As long as the two exchange correlation functionals both are GGA's, these approximations are reasonable. When using the LDA, though, using GGA parameters leads to errors of the order of 0.25 eV, again according to [27]. GGAs produce binding energies closer to experimental values, the reason most likely being the favouring of areas with large density gradients together with small local density which exists on surfaces. When an atom chemisorbs, the total surface of the system is diminished, and the chemisorbed state is less favourable than in the LDA. The RPBE is a further development of the PW-91 via the PBE [28] functional. It is identical to the PW-91 functional, apart from an interpolation. Nevertheless, the binding energies of O_2 in the two functionals differ by almost half an eV, see Table 2.3. RPBE is the better, even though the calculated value remains 0.3 eV larger than the experimental one. Thus, an error around 0.75 eV in absolute bond energies is inherent in the exchange correlation potentials.

2.4 k-point sampling

Because we investigate the properties of a surface, we have the opportunity to define our model as a periodic system. This is done by modeling the surface as a slab in a unit cell, which has the same dimensions as the slab in the directions parallel to the surface, but is larger in the direction orthogonal to the surface. When periodic boundary conditions are applied, the system becomes an infinite number of infinitely long and wide slabs. In an infinitely periodic system, we can take advantage of Bloch's theorem, which allows us to write the wave function as a plane wave part times a part with the periodicity of the lattice. The periodic part can then be expanded in a basis of a discreet set of plane waves with the wave vectors being the reciprocal lattice vectors of the crystal, allowing the whole electronic wave function to be expressed as a sum of plane waves:

$$\phi_j^{\mathbf{k}}(\mathbf{r}) = \sum_{\mathbf{G}} c_{j,\mathbf{k}+\mathbf{G}} \exp[i(\mathbf{k}+\mathbf{G})\cdot\mathbf{r}], \tag{2.21}$$

where $\mathbf{k}$ is the wave number for the wave-like part, the $\mathbf{G}$'s are the reciprocal lattice vectors and $c_{i,\mathbf{k}+\mathbf{G}}$ are expansion coefficients [29, 30].

The total energy expression in the infinite system turns into an integration over the first Brillouin zone [31]:

$$\sum_j \epsilon_j \rightarrow \sum_{\text{bands h}} \frac{V}{(2\pi)^3} \int_{BZ} \epsilon_h(\mathbf{k}) d^3\mathbf{k} \tag{2.22}$$

where V is the volume of the unit cell and all occupied bands must be summed. In an infinite system, the density of of k-points is infinite and therefore the number of k-points in the Brillouin zone is infinite. In practice it is reasonable to group points close in k-space and make the calculation on this grid. Picking these k-points in the right way leads to a very accurate approximation. Advantageous k-point sets have been calculated by Chadi and Cohen [32] and Monkhorst and Pack [33]. We use a Monkhorst and Pack type grid in our calculations. For a $c(4\times2)$ surface unit cell we find a grid of [2,2,1] to be sufficient. In calculations in different unit cells, the density of k-points are the same, or slightly larger.

Having limited the number of k-points, something must be done about the infinite number of terms in the sum (2.21). One solution is a crude cutoff, motivated by the coefficients $c_{i,\mathbf{k}+\mathbf{G}}$ being largest for smaller kinetic energy. The truncation of the basis set in this way naturally leads to an error. Ideally, more plane waves should be added to the set until the total energy converges, as should additional k-points. In practice, it is sufficient to add plane waves until the relevant energy difference (say, a surface energy) is converged, though. We have found a cutoff of 25 Ry to yield sufficiently converged values. Changing to higher cutoff, the adsorption energy of key states (V1 and V5, see Chapter 4) changes by no more than 0.01 eV. Unfortunately, if the core electrons shall be described, the cutoff must be very high. The solution to this is pseudopotentials.

2.5 Pseudopotentials

In practical calculations the time a given calculation takes to finish is of utmost importance. One of the ways of minimizing the time used in calculation is through the use of pseudopotentials.

Chemistry is almost only determined by the valence electrons. Therefore, core electrons do not have to be explicitly included in calculations. Pseudopotentials take advantage of the demand on valence and core electron wave functions to be orthogonal. The orthogonality means that valence electrons are less present near the core. This resembles a repulsion and has similar effects as a potential. To some degree, it cancels out the attractive potential of the atom core, leaving the valence electrons moving in a weak effective potential. A pseudopotential is then made mimicking the weaker potential and giving wave functions equal to the valence electron wave functions outside some cut off radius and approaching zero at the core. Often it will depend on the angular momentum quantum number (be non-local). This saves computer time both by cutting the core states out of the calculation all together and by the new pseudo wave functions having no radial nodes, necessitating fewer plane waves in mapping the wave functions. It introduces a few new considerations, though.

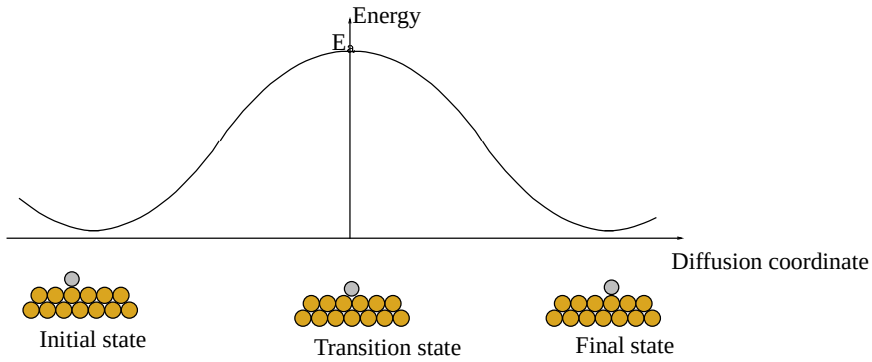

Figure 2.1: Schematic representation of one-dimensional diffusion.

To give accurate results a pseudopotential needs to function in different chemical environments. To save computer time it must not demand too many plane waves. Unfortunately, transferability (the quality of the pseudopotential mapping in different chemical environments) requires the cutoff radius to be small while softness (the lowering of the amount of plane waves needed to map the wave functions) requires a large cutoff. The same is the case for the number of electrons included as valence electrons: the fewer the faster and the larger the risk of cutting away too many electrons. A pseudopotential is therefore always a compromise between different demands, and a new task might demand a new pseudopotential. Different types exist; we have used Vanderbilt ultra-soft pseudopotentials [34], which sacrifice norm-conservation (a property indicating a certain transferability [35]) for large softness and are useful for atoms having partially filled d-orbitals (transition metals).

2.6 Hopping rates and determination of transition states

Diffusion on surfaces is experimentally seen to be dependent on temperature as

$$k = k_0 \exp\Big(-\frac{E_a}{k_\mathrm{b}T}\Big) \tag{2.23}$$

where k is the diffusion rate, i.e. the number of jumps per unit time. This observation can be explained through transition state theory. Assume that diffusion is happening in one dimension and that the potential energy surface looks like Fig. 2.1. The diffusion rate is then (under the assumption that the diffusing adsorbate remains in thermal equilibrium with the surface and that once it has passed the transition state, it will continue to the next minimum), given by [31, 36].

$$k_\mathrm{TST} = \frac{k_\mathrm{b}T}{h}\frac{1}{Z_0}\exp\Big(-\frac{E_a}{k_\mathrm{b}T}\Big) \tag{2.24}$$

where E_a is the energy in the transition state and Z_0 is the partition sum in the initial well. Assuming the harmonic approximation holds, $Z_0 = k_\mathrm{b}T/\hbar\omega_0$ and the final

expression becomes

$$k_{\mathrm{TST}} = \frac{\omega_0}{2\pi} \exp\Big(- \frac{E_a}{k_{\mathrm{b}}T}\Big) \tag{2.25}$$

where ω_0 is the vibration frequency in the first well. In general, the coordinate is not linear and the adsorbate may couple to several degrees of freedom, in which the partition sum in the transition state enters the expression explicitly:

$$k_{\mathrm{TST}} = \frac{k_{\mathrm{b}}T}{h} \frac{Z_{\mathrm{TS}}}{Z_0} \exp\Big(- \frac{E_a}{k_{\mathrm{b}}T}\Big). \tag{2.26}$$

Here, the harmonic approximation could of course be reintroduced, or the expression could be reformulated using the Helmholtz free energy, yielding

$$k_{\mathrm{TST}} = \frac{\omega_0}{2\pi} \exp\Big(\frac{\Delta S}{k_{\mathrm{b}}}\Big) \exp\Big(- \frac{E_a}{k_{\mathrm{b}}T}\Big) \tag{2.27}$$

where ΔS is the difference in entropy between the initial and final states. Normally, this difference is neglected, which is equivalent to assuming that the vibration frequencies orthogonal to the path are roughly the same in the transition and initial states.

Determining the transition state requires determining the diffusion path. This is a non-trivial problem. The diffusion path can be considered to be the lowest energy path through the coordinate space from the initial to the final configuration. However, to find it one needs to know the energy for all ionic configurations possible on the surface. To calculate the energy of merely one configuration can easily take days, and it is thus not feasible to map out the energy surface in coordinate space. The nudged elastic band method (NEB) [37] presents a good systematic method of solving this problem. First, the initial and final points are found. Then, a starting guess on a diffusion path is made. Along this path a sufficient number points in configuration space (hereafter termed 'images') are chosen and the energies of the configurations and the forces on the atoms are calculated. The individual images are then relaxed under the constraint that they follow the energy gradient orthogonal to the path in configuration space. The process is iteratively repeated. This allows the path as a whole to shift towards lower energies, and is effectively a path search. An extra constraint is introduced, which can be thought of as 'springs' connecting neighbouring images. During relaxation, images are not allowed to relax to far away from each other; this extra constraint serves to keep the path continuous and images evenly distributed along it. If it is removed, the images tend to relax away from the transition state. If a sufficient number of images are used, the initial guess is not too bad and the images along the path start out evenly distributed, this is a quite reliable way of finding diffusion paths, especially on surfaces which are structurally not overly complex. However, it is extremely demanding on computational time. When considering large structures, manually monitoring the process can be very computer time conserving. If the relaxation process is carefully monitored, images can be removed in the part of the paths where the barrier is not changing considerably and added around the transition state where they are more needed. The drawback on this method is that it demands constant attention.

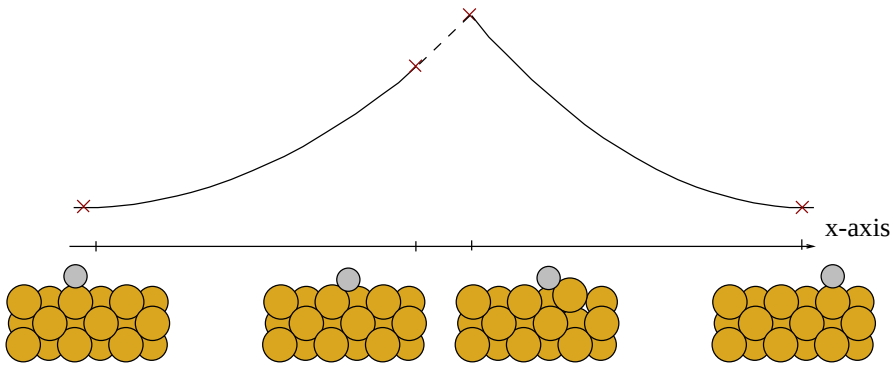

Figure 2.2: Illustration of a path, which appears coherent if judging by the x-coordinate by the diffusing atom, but by further inspection is not. Above, the barrier these calculations would produce. Dotted line represents the erroneous part of the barrier. Notice the cusp.

If the scientist believes that the diffusion path is simple and can be easily described, he can choose to assume a diffusion path and calculate the energy along it. This will then give an upper estimate of the energy barrier. The diffusion path is never known very well a priori. Therefore, for this procedure to be at all successful it must be possible to describe the diffusion path by a simple constraint on a few atoms. Then, the individual images are relaxed, keeping this key parameter fixed. A typical key parameter is a cartesian coordinate or a center of mass coordinate. However, this is problematic because the path may become discontinuous; if the diffusion distance is measured as the distance in the x-direction an atom has moved, two images, which are close in the sense that the selected atom has not moved very much from image A to image B, can actually be quite far apart if looking at the distance in coordinate space. The problem is illustrated in Fig. 2.2. In image A, the atom has moved somewhat from its equilibrium position, but all the substrate atoms remain close to the positions they had in the initial configuration. In image B, the diffusing atom has moved slightly to the new site *and* a surface atom has moved over to meet it, thus gaining the energy of the bond with the diffusing atom at the same time as loosing energy by the weakened bonding with the surface. Therefore, the actual transition state, where the surface atom is loosing coordination with the surface without having yet gained the benefit of bonding with the diffusing atom, is not found because no constraint was imposed on the substrate atoms, and the path turned out discontinuous in coordinate space. Often these errors result in a barrier with a cusp at the transition state. Adding images around the maximum point would eventually reveal the discontinuity of the barrier.

To avoid discontinuous paths, one must always envision the diffusion path as a path through the entire configuration space and calculate the distance between images in the entire space.

CHAPTER 3

The TiO_2 surface

Rutile is the most stable phase of TiO_2, and the (110) surface the most stable surface. The surface is built from stacked layers of whole TiO_2 units, tri-layers. The main features are titanium rows in the surface plane and bridging oxygen rows protruding from the surface plane. The surface relaxation appears to extend far into the sub-surface region and calculations have to take into account correspondingly many layers. The surface is easily reduced, bridging oxygen vacancies having the lowest vacancy formation energy of 3.0 eV. Vacancies interact strongly along bridging oxygen rows, less strongly orthogonal to the rows. The breaking of bonds involved in creating a vacancy frees two electrons to take part in bonding elsewhere. These electrons partially remain around the vacancies, partially spread to the titanium rows, from where they can move to electrophillic adsorbates. This charge transfer along titanium rows can take place over long distances, easily exceeding 10 Å. Evidence exists for the existence of sub-surfaces vacancies. These have higher formation energies than the bridging oxygen vacancy. The presence of oxygen on the surface lowers the vacancy creation energy by at least 2 eV. The charge transfer from the vacancy to the adsorbate is crucial to the stabilization of the configuration. Additionally, adsorbed oxygen facilitates the diffusion of sub-surface vacancies to the surface.

3.1 Introduction

Ample experimental and theoretical investigation of the TiO_2 surface exists. Early studies by Ramamoorthy *et al.* [1] and Bates *et al.* [38] focus on the (1×1) surface structure of the stoichiometric crystal, illustrated in Fig. 3.2. They generally find good agreement with experimental results [39], see Fig. 3.3 though bridging oxygen bond lengths are quite far from experimental ones. Harrison *et al.* [40] point to the existence of a soft, anharmonic vibration of mainly the bridging oxygen atoms (see below) as the reason for this deviation between calculations. Bredow *et al.* [41] have recently done a systematic investigation of the change in observables depending on the number of layers in the calculation and concludes that a large number of layers is needed to reach acceptable convergence. They find an oscillatory behaviour in odd-even numbers of layers attributable to the hybridization of surface Ti d-orbitals with O p-orbitals. The hybridization strengthens the interaction between the first and second layers and is only present in slabs which do not have a symmetry plane, which are precisely slabs with an even number of layers. These oscillations are reflected in the position of the top of the valence band and the bottom of the conduction band, as well as in the band gap itself. This leads to the expectation that a similar oscillation should be seen in the reactivity of the surface.

Much work has dealt with the structural determination of the ground state (1×2) surface reconstruction which is realized at moderate temperatures (above 500 K) [13, 42–49]. An agreement now seem to have been made on a ridged Ti_2O_3 structure. Other reconstruction-like structures can be grown by oxygen dosing in the same temperature range [46, 50].

A strong favouring of a spin polarized electronic structure has been reported on reduced rutile $TiO_2(110)$ [51, 52]. However, in the case of Ref. [51] it is assumed by the authors to be an error due to a low quality pseudopotential [53]. The structure described in Ref. [52] has the character more of a reconstruction than isolated vacancies since the coverage of vacancies is 100%. Bredow *et al.* [54] also find that the electronic structure of the vacancy is spin polarized. They do cluster calculations, and find that a spin triplet state is always favoured about a singlet state, independent of cluster size and embedding. For the largest cluster, the energy difference is 0.39 eV. Menetrey *et al.* [55] also report spin polarization which vanishes upon oxygen adsorption.

In a periodic Hartree-Fock study, focusing particularly on O_2 adsorption and spin-states, De Lara-Castells and Krause [56, 57] find that the vacancy electrons are spin-polarized, one locating on a Ti atom near the vacancy, the other on one of the second tri-layer Ti, where it remains strongly localized. However, with respect to the spin state, the electronic structure differs greatly depending on surface unit cell, going from strongly favoured ferromagnetic in a $p(2\times1)$ cell to slightly favoured anti-ferromagnetic in a $p(3\times2)$. Additionally, the authors point out that a large number of energy minima with almost equal energies exist in the calculation. Therefore, the calculations do not really allow to judge the electronic structure of an isolated vacancy.

Wu *et al.* [58] employ DFT using pseudopotentials and expansion in plane waves to investigate oxygen on TiO_2. They find essentially the same deformations of the electronic density around the vacancy as described later in this chapter and essentially the

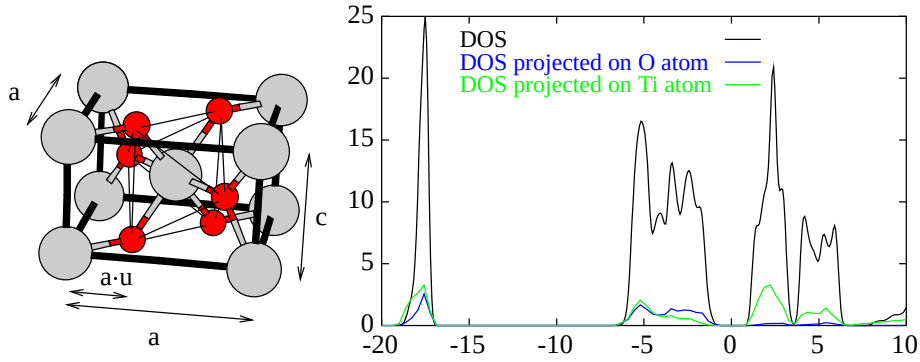

Figure 3.1: To the left, ball-and-stick diagram of the TiO_2 (110) rutile bulk unit cell showing the constituent octahedrons. The small, red balls represent oxygen atoms, the larger grey ones titanium. To the right, the total and atom projected density of states for bulk TiO_2. Units on the energy axis are eV and the Fermi level is set to 0.

same vacancy creation energy, except that they report '*a triplet state was found to be slightly more stable*' [than a singlet], much as in the large cell Hartree-Fock calculations. They do not report whether this magnetic moment changes significantly depending on cell size and shape.

Other authors [12, 59, 60] report no spin at all, and thus it appears that changing the spin polarization of the vacancy does not lead to significant energy changes, and spin will therefore probably differ between calculations. We find no spin on the vacancy.

3.2 Rutile bulk and the (110) surface

The rutile TiO_2 system has two lattice parameter, a and c, and an internal parameter, u, see Fig. 3.1. We find the theoretical values a=4.65 Å, c=2.98 Å and u=0.305, to be compared with experimental values of 4.59 Å, 2.96 Å and 0.305 [61]. Thus, the theoretical values are in agreement with the experimental ones within 1.5%. A ball-and-stick diagram of the bulk unit cell is found in Fig. 3.1. The structure consists of octahedrons with a titanium atom at the center and oxygen atoms at the apexes. Each oxygen atom is part of three octahedrons, two of which are parallel and one rotated 90° with respect to the others. In Fig. 3.1 the calculated density of states is shown. The bandgap is 2.3 eV, which is underestimated in comparison with experimental findings of 3.1 eV [62]. GGA is well known to underestimate semiconductor band gaps. As can be seen from the atom projected density of states, the conduction band edge mainly derives from titanium orbitals, while the occupied states are a mixture of oxygen and titanium states.

For most stable surfaces two conditions are met. As a gedankenexperiment, create a (110) surface by cleaving a crystal in a right and left half[1]. Firstly, the surface must be

[1] Experimentally, TiO_2 shatters rather than cleaves. However, the surface can be achieved by polishing and

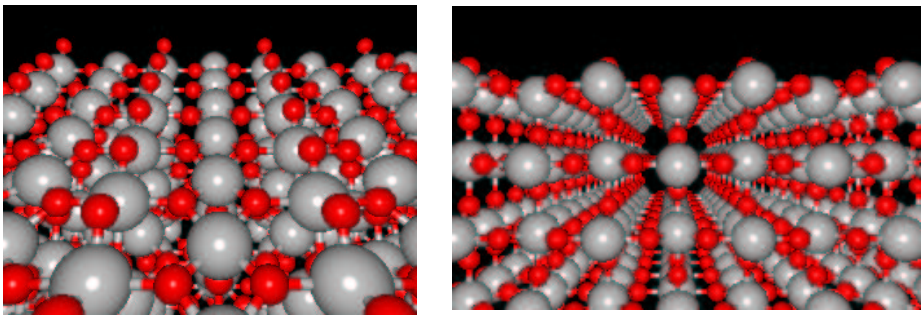

Figure 3.2: Ball-and-stick diagram of the TiO_2 (110) surface, seen from two different points. The small, red balls represent oxygen atoms, the larger grey ones titanium. The surface is a flat plane, divided into troughs by 'hedges' of bridging oxygen atoms.

auto-compensated [63]. This means that the excess charge from broken oxygen and titanium bonds must be the same. In the case of the (110) surface this means that the same amount of Ti-O and O-Ti bonds must be broken for the crystal to be stable. Secondly, the planes must not have both charge and a dipole moment [50,64]. This means that each layer is required to be a tri-layer of three atomic planes; one oxygen plane above and below and a mixed titanium and oxygen plane in the middle. This way, the whole unit has no dipole moment, nor is it charged, and the bond breaking restrictions are satisfied. The stoichiometric TiO_2 (110) surface, see Fig. 3.2, consequently becomes a flat plane with parallel 'hedges' separating it into troughs. The hedges consist of oxygen atoms twofold coordinated to titanium atoms below them in a bridge site configuration. These titanium atoms are sixfold coordinated, as are bulk titanium atoms. Between the rows of bridging oxygen atoms, in the same plane as the sixfold coordinated titanium atoms, are fivefold coordinated titanium atoms, coordinating each to four oxygen atoms in the surface plane, termed in-plane oxygen, and one oxygen atom directly below. The fivefold coordinated titanium atoms are also termed in-plane titanium atoms. Directly below the bridging oxygen atom is another oxygen atom which we will refer to as a sub-bridging oxygen atom. Together the bridging, in-plane and sub-bridging oxygen atoms and the in-plane and six-fold coordinated titanium atoms form the first of the above mentioned tri-layers. This is the first layer of full TiO_2 units, as illustrated in Fig. 3.3. Below the first tri-layer the structure is continued by additional tri-layers shifted by $a\sqrt{2}$ with respect to the immediate tri-layers above and below. The atoms in these layers are in the present work referred to as n'th tri-layer bridging, sub-bridging or in-plane, as consistent with the definitions in the first tri-layer. In Tables and Figures, this is denoted $\mathrm{Atom}^{\mathrm{tri-layer}}_{\mathrm{b,ip,sb}}$, see Fig. 3.3. Titanium atoms labelled by a star as $\mathrm{Ti}^{\mathrm{tri-layer}}_{\mathrm{ip*}}$ are the ones located directly beneath the bridging oxygen atoms in that tri-layer. If no tri-layer number is given, the atom is located in the first tri-layer; e.g. 'bridging oxygen atom' refers to one of the 'hedge' atoms in the first layer.

annealing. [50]

	relaxed layers		
slab layers	2	3	4
3	0.69	···	···
4	0.60	···	···
5	0.65	0.61	···
6	0.65	0.60	0.57

Table 3.1: The surface energy in J/m^2 as a function of layers in the slab, and the number of these layers that are allowed to relax.

3.3 The relaxations of the stoichiometric surface

We find, in accordance with previous work, that the relaxations of the (110) surface as compared to a truncated crystal are substantial. Achieving converged values requires slabs of considerable thickness. This is in all probability not an artifact. Thin layers of TiO_2 realized experimentally may very well behave in the same way [41]. As a consequence, the surface energy is similarly slow in convergence, see Table 3.1. The most pronounced relaxations occur on the top layer Ti atoms. The in-plane Ti atoms relax inwards by 0.21 Å, whereas the six-fold coordinated Ti atoms beneath the bridging oxygen atoms relax outwards by 0.16 Å. This is consistent with X-ray data by Charlton *et al.* [39] and partially with more recent data from Lindsay *et al.* [65], who find a larger relaxation inwards of the in-plane titanium atom. The only inconsistency with the Charlton X-ray data is the position of the bridging oxygen atom. This, we calculate, moves inward by a small amount of 0.04 Å whereas it is experimentally seen to move inwards by 0.27 Å. Here, we are consistent with Lindsay, however, who find relaxation of 0.12 Å. Our calculated surface energy is in agreement with Bredow *et al.* [41], though our value appears to converge in a less oscillatory manner. This supports the conclusion by Bredow that the oscillatory behaviour is caused by the presence and absence of slab symmetry. Our calculations always have a layer of atoms frozen in place at the bottom of the slab and are therefore never symmetric. Our most well converged surface energy is for a six layer slab with four layers relaxed, revealing a surface energy of 0.57 eV, to be compared with 0.63 eV by Bredow (ten layers, all relaxed). We find a somewhat larger band gab than Bredow, of 2.3 eV to be compared with 1.8 eV in the bulk.

3.4 Vacancy formation and mutual interactions

The most common defect on the TiO_2 (110) surface is the bridging oxygen vacancy, created by removing a bridging oxygen atom. This defect is easily created experimentally through annealing techniques. The coverage can be tailored with some precision. As a result, much work has been done on this system, and it is often termed a 'model system' for oxide surfaces. For a recent review, see [50].

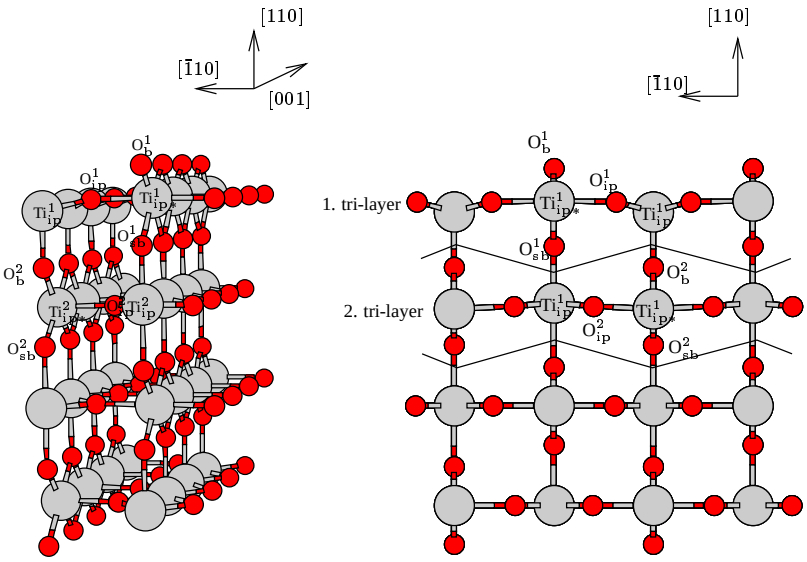

Atom	This work	Bates	Rama-moorthy	Charlton	Lindsay
O_b^1	-0.04±0.02	-0.02	-0.06	-0.27±0.08	-0.12±0.05
Ti_{ip*}^1	0.16±0.02	0.23	0.13	0.12±0.05	0.03±0.03
O_{ip}^1	0.01±0.02	0.18	0.12	0.05±0.05	0.05±0.08
Ti_{ip}^1	-0.21±0.01	-0.11	-0.17	-0.16±0.05	-0.40±0.03
O_{sb}^1	-0.04±0.03	0.03	-0.07	0.05±0.08	0.01±0.1
O_b^2	-0.02±0.01	0.03	0.02	0.00±0.08	-0.05±0.08
Ti_{ip}^2	0.01±0.00	0.12	0.06	0.07±0.04	0.07±0.05
O_{ip}^2	-0.03±0.02	0.00	-0.03	0.02±0.06	-0.02±0.12
Ti_{ip*}^2	-0.12±0.01	-0.06	-0.08	-0.09±0.04	-0.17±0.07
O_{sb}^2	-0.03±0.02	0.03	-0.01	-0.09±0.08	0.01±0.17

Figure 3.3: Above, the naming convention used in the present work for atoms in the TiO_2 surface and sub-surface region. The convention is $Atom_{b,ip,sb}^{tri-layer}$, where tri-layer denotes the tri-layer number, Atom the chemical identity of the atoms and b, ip and sb bridging, in-plane and sub-bridging posistion, repectively. Titanium atoms labelled by a star as $Ti_{ip*}^{tri-layer}$ are the ones located directly beneath the bridging oxygen atoms in that tri-layer. To the left, 3D ball-and-stick diagram. To the right, 2D picture of the [001] plane of the same structure. The small, red balls represent oxygen atoms, the larger grey ones titanium. In the table, the relaxations of the respective atoms in the [110] direction are presented including theoretical results by Bates [38] and Ramamoorthy [1] and experimental values by Charlton [39] and Lindsay [65]. The atomic displacements from this work are given as the average of the five and six layered slab displacements, ± the difference between the values.

	$p(2\times1)$				$p(3\times1)$				$p(4\times1)$			
	1	2	3	4	1	2	3	4	1	2	3	4
3	4.02	3.73	···	···	2.83	2.59	···	···	2.56	2.36	···	···
4	4.32	4.27	···	···	3.27	3.49	···	···	2.99	3.28	···	···
5	···	4.26	4.17	···	···	3.37	3.25	···	···	3.16	2.96	···
6	···	4.31	4.29	4.25	···	3.43	3.43	3.43	···	3.20	3.15	3.12

Table 3.2: The vacancy creation energy, in eV per vacancy, as a function of the number of tri-layers in the slab (rows), and the number of these tri-layers that are allowed to relax (columns). Calculations have been done in $p(2\times1)$, $p(3\times1)$ and $p(4\times1)$ unit cells.

The vacancy formation energy (VFE) is defined as

$$E_{\mathrm{vac}} = \left(E(\mathrm{Ti_N O_{2N-1}}) + \frac{1}{2}E(\mathrm{O_2})\right) - E(\mathrm{Ti_N O_{2N}}) \tag{3.1}$$

meaning the energy required to extract an oxygen atom from the surface to the gas phase and reuniting it with an identical oxygen atom. Exactly the same inherent difficulties is involved in calculating a converged value of the vacancy creation energy as in calculating the surface energy, with the added complication that the vacancies interact rather strongly along the bridging oxygen rows. At higher vacancy coverages the surface is known to reconstruct [42, 49]. Addressing first the issue of calculating a reasonably converged value, Table 3.2 shows the vacancy creation energy at several primitive unit cells ($p(2\times1)$, $p(3\times1)$ and $p(4\times1)$) as a function of both slab thickness and number of tri-layers allowed to relax. The dependence on both cell size and thickness is considerable. With respect to the latter, we observe again the kind of odd-even oscillation seen previously for the surface creation energy [38, 41]. Judging from the Table, for all unit cells the results obtained using four tri-layers (of which two are relaxed) are converged within 0.1-0.2 eV. Considering this a reasonable level of accuracy, slabs of this thickness have been used in the remaining chapters.

The strong dependence of the size of the unit cell reflects the vacancy-vacancy interactions which are markedly repulsive and decrease monotonously with distance. This calls for a more thorough investigation, varying both cell size and shape. A schematic view of the different cells employed in this investigation and of the vacancy configuration attained is presented in Figure 3.4. Different configurations represent different vacancy coverages. The use of primitive cells of increasing size gives an estimate of vacancy interactions along the bridging oxygen rows, while a comparison of the results obtained using either primitive or centered cells provides a measure of the strength of vacancy interactions across oxygen rows. The use of a primitive surface unit cell appears to cause a 0.1 eV increase in the vacancy formation energy as compared to what is calculated for a centered surface unit cell of the same vacancy concentration. Since the primitive and centered unit cells are identical with respect to the distribution of the vacancies in separate bridging oxygen rows for any given vacancy concentration, this energy difference is attributable to the inter-row interaction of vacancies. In-row vacancy-vacancy interactions are much stronger. The calculated vacancy creation en-

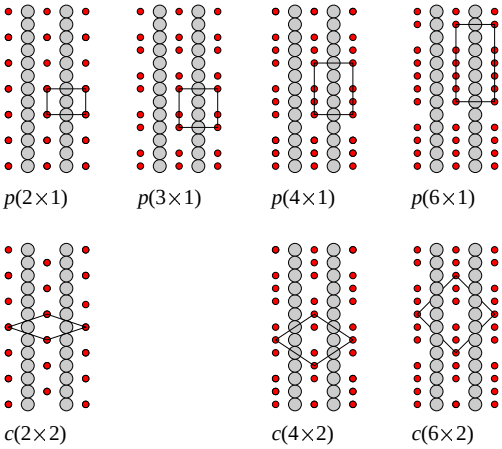

Structure	Θ_{vac}	VFE
$p(2\times1)$	0.50	4.27 eV
$p(3\times1)$	0.33	3.49 eV
$p(4\times1)$	0.25	3.28 eV
$p(6\times1)$	0.17	3.16 eV
$c(2\times2)$	0.50	4.17 eV
$c(4\times2)$	0.25	3.19 eV
$c(6\times2)$	0.17	3.03 eV

Figure 3.4: Schematic representations of some vacancy configurations. Large circles represent titanium atoms, small circles oxygen atoms. In the table, vacancy formation energy (VFE) in same configurations. Calculated with four tri-layers of which two are relaxed.

ergy ranges from more than 4 eV to about 3 eV from the smallest to the largest unit cell in the calculations.

One way of vizualising the vacancy-vacancy interactions is using a simplified model assuming that:

- The interaction can be described as pair interactions (no higher order interactions).
- Interactions can be split up as in-row interactions and inter-row interactions.

This model is very crude; for well separated vacancies, pair-wise, power law type electrostatic and (continuum) elastic interactions must be responsible for the interaction. For closely spaced vacancies, though, atomistic relaxation patterns, orbital overlaps and related effects can be expected to lead to a partial breakdown of the pair-interaction model.

Focusing first on in-row interactions, the formation energy for a single vacancy in a cell is:

$$E^j_{\mathrm{vac}} = E^0_{\mathrm{vac}} + \sum_{i=1}^{\infty} n^j_i V_i\,, \tag{3.2}$$

where V_i is the pair potential between vacancies i lattice sites apart and n^j_i is the number of such interactions in the j'th configuration (evaluated per calculational cell with interactions crossing the cell boundary being counted only half). The creation of vacancies

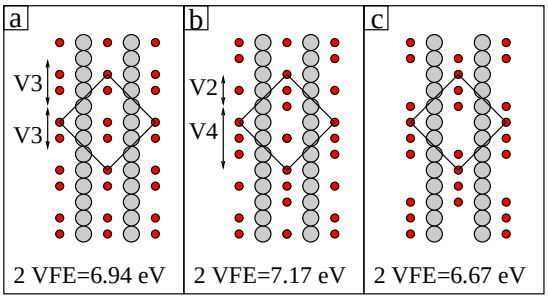

Figure 3.5: Schematic representation of some vacancy configurations and the creation energy of two vacancies in those configurations. Large circles represent titanium atoms, small oxygen atoms.

in the 50%, 33%, 25% and 17% coverage structures in this description are then given by

$$
\begin{aligned}
E_{\mathrm{vac}}^{p(2\times1)} &= E_{\mathrm{vac}}^{0} + V_2 + V_4 + \sum_{i=6}^{\infty} n_i^{p(2\times1)} V_i \\
E_{\mathrm{vac}}^{p(3\times1)} &= E_{\mathrm{vac}}^{0} + V_3 + \sum_{i=6}^{\infty} n_i^{p(3\times1)} V_i \\
E_{\mathrm{vac}}^{p(4\times1)} &= E_{\mathrm{vac}}^{0} + V_4 + \sum_{i=8}^{\infty} n_i^{p(4\times1)} V_i \\
E_{\mathrm{vac}}^{p(6\times1)} &= E_{\mathrm{vac}}^{0} + \sum_{i=6}^{\infty} n_i^{p(6\times1)} V_i .
\end{aligned}
\tag{3.3}
$$

Since vacancy-vacancy interactions appear to decrease monotonously along the rows, the parts of the sums involving $V_{i>4}$ are assumed to be negligible. Solving this linear system reveals the pair-wise interaction strengths $\mathrm{V}_2 = 0.99$ eV, $\mathrm{V}_3 = 0.33$ eV, and $\mathrm{V}_4 = 0.12$ eV, and a vacancy formation energy in a primitive cell, $E_{\mathrm{vac}}^{0} = 3.16$ eV.

The next step is then to address to which degree the model remains true for closely spaced vacancies. This is done by using the configurations in Fig. 3.5. Here, a $c(6 \times 2)$ super cell containing two vacancies separated by two, one, or no bridging oxygen atoms is realized. The structure with two bridging oxygen atoms between the vacancies (Fig. 3.5a) is identical to the $p(3\times1)$ structure in Fig. 3.4. According to our pair-wise interaction model (still neglecting inter-row interactions), the configuration with one bridging oxygen between the vacancies (Fig. 3.5b) is expected to be less stable by $V_2+V_4-2V_3 = 0.45$ eV per super cell than the structure of Fig. 3.5a. The full calculation, however, shows that it is only less stable by 0.23 eV. These calculations alone would therefore predict smaller pair-wise interaction strengths than determined above. Given the periodicity in the structures used to calculate the interaction strengths and the assumption of no second order interactions, the model is quite good. To complement the analysis

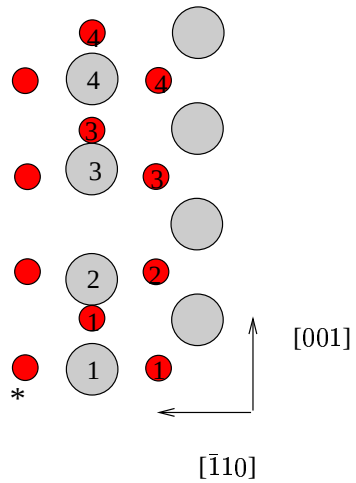

Atom	[$\bar{1}$10]	[001]	[110]
O^1_b 4	-0.018	0.000	0.147
Ti^1_{ip*} 2	0.001	-0.225	-0.335
Ti^1_{ip*} 3	0.002	0.225	-0.355
O^1_{ip} 1	-0.022	-0.011	-0.069
O^1_{ip} 4	-0.018	0.000	0.043
O^1_{ip} 1*	0.013	-0.005	0.132
O^1_{ip} 4*	0.013	0.003	0.130
O^1_{sb} 1	-0.001	-0.102	-0.002
O^1_{sb} 2	0.016	0.000	0.181
O^1_{sb} 3	-0.001	0.102	0.001
O^1_{sb} 4	0.000	-0.001	0.103
Ti^2_{ip} 1	0.001	0.019	-0.181
Ti^2_{ip} 3	0.001	0.019	-0.181

Figure 3.6: Main atomic displacements (in Å) upon the formation of an oxygen vacancy in a $c(4\times2)$ cell. To the left, a schematic view of the topmost atoms, illustrating the numbering. Atoms in lower layers are numbered accordingly. * denotes the leftmost row of in-plane oxygen atoms, as illustrated.

of the vacancy-vacancy interaction we further include in Fig. 3.5c a structure that has two vacancies in adjacent sites forming a double vacancy. Compared to the reference configuration of Fig. 3.5a 0.28 eV is gained, implying that vacancies may prefer to cluster together into double vacancies rather than being separated at very close distances. This behaviour, however, may be influenced by the distance between double vacancies, which in this calculation is quite small. The structure has only four bridging oxygen atoms between every double vacancy, and large possibility for inter-row interactions.

As mentioned above, the relaxations around vacancies are found to be substantial, in agreement with the findings of Ramamoorthy *et al.* [66]. This proves indeed to be the case around any kind of defect introduced into the structure. It will be illustrated below for oxygen adsorbates. The relaxations around the bridging oxygen vacancy are given in Fig. 3.6 relative to the relaxed stoichiometric surface. The calculational super cell was $p(4\times1)$. The Ti atoms just below the missing O are strongly pushed down and sideways while the O atom below these two Ti atoms is lifted upwards considerably. The neighbouring bridging oxygen atoms are pushed sideways, and the next bridging oxygen atom is pushed upwards. In light of these observations, it is understandable that the pair interaction model breaks down at short vacancy-vacancy distances.

The structural rearrangements are strongly coupled with important changes in the electronic structure upon vacancy creation. TiO_2 is an ionic crystal, implying that the charge transfer from Ti to O atoms is considerable. Upon creation of a vacancy by extraction of a bridging oxygen atom, this charge rearranges. This rearrangement is shown in Fig. 3.7, where the induced charge density upon removal of a bridging oxygen atom is plotted. In Fig. 3.7a, no relaxations are allowed from the stoichiometric positions

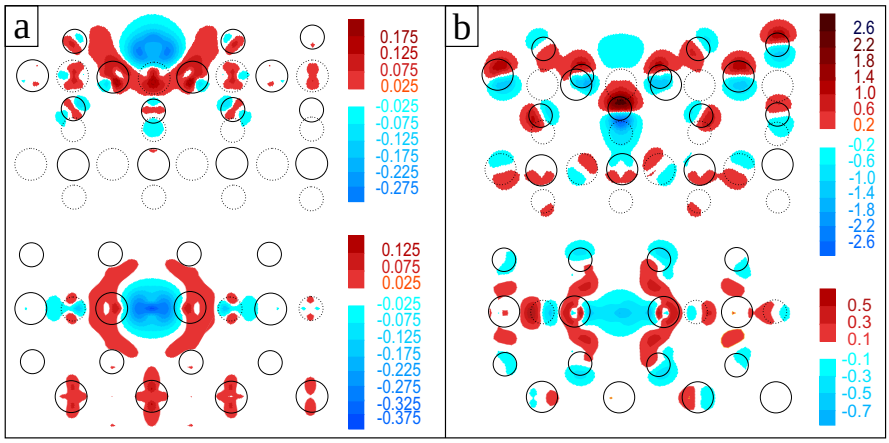

Figure 3.7: Changes in charge density upon the creation of a vacancy. Above, a cut through the slab along the bridging oxygen rows. Below, a top view. The induced charge densities have been integrated over the direction not plotted. Units are eV/Å^2. a) The surface has not been allowed to relax after the removal of the bridging oxygen atom. b) After relaxation.

while in Fig. 3.7b full relaxation of the top two slab layers is allowed (b). In the case of no relaxations, the charge remains around the vacancy to a large degree, primarily on the titanium atoms below the vacancy. A small amount relocates to the in-plane titanium atoms. When the surface is then allowed to relax, the charge spreads out somewhat more. The polarization-like signatures derive from the relaxation of the atoms. The electronic rearrangement is increased upon relaxation, as can be seen from the different scales in Figs. 3.7a and 3.7b. Although part of the electronic charge seems to spread, a sizable amount remains at the vacancy in both cases. We will see below that the presence of this charge is what makes the surface an attractive adsorption site for a number of electro-negative adsorbates.

Many semiconductors are well known to relax or reconstruct upon cleavage of the crystal to minimize the energy rise due to broken bonds. Looking at the density of states, this phenomenon is illustrated in the case of TiO_2. In Fig. 3.8a-b, the z-resolved electronic density of states (DOS) is plotted for the stoichiometric surface without and with relaxation of the upper two tri-layers of the slab. The z-resolved DOS is obtained by evaluation of the local density of states followed by integration over the x- and y-dimensions of the super cell. For the unrelaxed surface (Fig. 3.8a) a surface related state appears at the bottom of the band gab, decreasing the size of the band gap. It shifts down after relaxation (Fig. 3.8b) returning the band gap to its bulk value. Since all calculations have been done on slabs with at least two layers frozen in bulk positions, this state is visible in all DOS plots as an artifact of the calculation.

Since chemistry is almost only related to states around the Fermi level, the density of states in this energy range is of special interest. Fig. 3.9 zooms in on the energy axis around the Fermi level of the z-resolved DOS. Fig. 3.9a is the stoichiometric (relaxed) surface. The reduced surface with an oxygen molecule occupying the vacancy (see

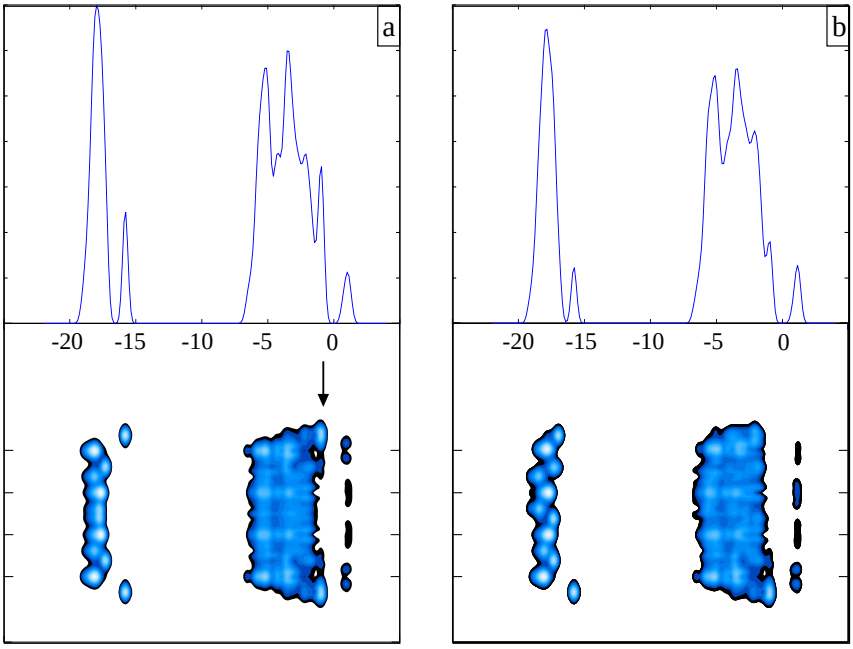

Figure 3.8: a) DOS for four layers bulk structure slab b) DOS for stoichiometric surface, four layers slab, two layers relaxed. The upper panels show the integrated (total) density of states. Marks at the vertical axis indicate the position of the center of each tri-layer. Units on the energy axis are eV and the Fermi level is set to 0.

configuration V1 in the next section), Fig. 3.9b, is very similar. In Fig. 3.9c, a vacancy concentration of 0.17 is realized while in Fig. 3.9d the concentration is 0.33. Since the TiO_2 bonding is of ionic character, the presence of vacancies does not introduce electronic states in the gap as would be otherwise expected for a covalently bonding semiconductor. Experimentally, such a state is reported [50]. However, DFT fails to reproduce it.

3.5 Other Oxygen Vacancy Types

The bridging oxygen vacancy is by far the most frequently mentioned in the literature, probably because it is the most abundant defect observed with STM. However, as STM is sensitive mostly to the first surface layer of atoms, other defects may be present immediately below the surface where they are observable only indirectly or by using techniques sensitive to the layers below the first. It is very difficult, however, to get experimental evidence for the vacancy concentration in the sub-surface region. Using two-photon photo-emission spectroscopy Onda *et al.* [67] have investigated the work function of differently prepared reduced surfaces. They find that while a defected surface created

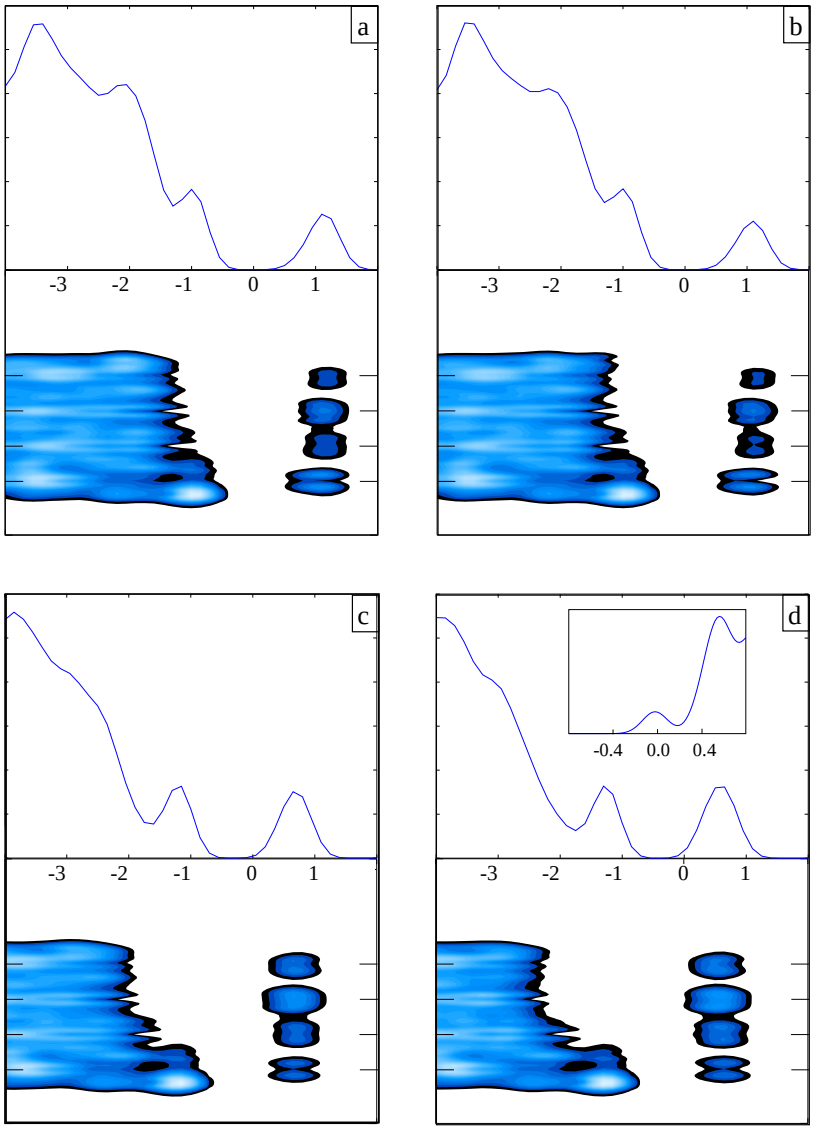

Figure 3.9: DOS around the Fermi level a) The stoichiometric surface b) The V1 configuration c) Vacancy coverage of 16.7 percent d) Vacancy coverage of 33.3 percent. The inset shows a closer zoom on the conduction band edge, showing the closet we get to resolve a split off, vacancy related state. To resolve it, the slab thickness had to be increased to five tri-layers and the electronic temperature had to be lowered to 0.08 eV. Units on the energy axis are eV and the Fermi level is set to 0.

by electron irradiation can be restored to stoichiometry[2], surfaces created by vacuum annealing cannot. The authors attribute this to the creation of sub-surface defects during the annealing procedure. Additionally they find that the capacity for O_2 adsorption is dependent on the annealing time. This is an indication of sub-surface vacancies somehow assisting in the bonding. These defects function as charge donors, just as the bridging oxygen vacancy, and may interact with adsorbates or even diffuse to the surface under some circumstances.

As for indirect evidence one might speculate that the tip-induced annealing of bridging oxygen vacancies observed by Diebold *et al.* [68] and attributed to tip-adsorbed oxygen relocating to the vacancies is partially due to sub-bridging oxygen atoms being drawn up into the bridging oxygen vacancies and leaving an STM-invisible sub-surface vacancy. Diebold also observes dark defects on the titanium rows which are tentatively attributed to sub-surface defects. Judging from their position they would be second tri-layer bridging oxygen vacancies (Fig. 3.13). Hebenstreit *et al.* [69] find that sulfur adsorption is heavily dependent on the bulk reduction state and propose an adsorption model where S induce bulk vacancy segregation, adsorbing in the newly-arrived vacancies. This they speculate to be a more general trend. Surface reconstruction upon oxygen exposure at elevated temperatures show a similar phenomenon [70]. Rodriguez *et al.* [16] support the S results using synchrotron-based high-resolution photo-emission, X-ray adsorption near-edge spectroscopy and DFT calculations. They calculate a vacancy formation energy of a second tri-layer in-plane vacancy to be comparable to the formation energy of a bridging oxygen vacancy. However, these calculations are done for small inter-vacancy distances (always a coverage of 50% vacancies).

Here, attention should be drawn to the fact that the oxygen content of the surface can change in two ways; either by diffusion of bulk oxygen vacancies as mentioned above or by diffusion of titanium interstitials as evidenced in the re-oxidation of sputter-damaged surfaces. Henderson has shown that at temperatures between 400 and 700 K both oxygen and titanium diffuse, whereas above 700 degrees the diffusion of titanium is strongly dominant [71, 72]. Below 400 K no diffusion is detected. This study was done in ultra-high vacuum, and it is quite possible that the presence of adsorbates may locally change the diffusion behaviour. Rodriguez [16] finds that sulfur facilitates the diffusion of sub-surface oxygen vacancies, but not titanium interstitials. In a study of the NO_2 chemistry on TiO_2 (110) Rodriguez [73] additionally finds that the migration of sub-surface vacancies is essential to the dissociation of adsorbed NO_2 and that the presence of NO_2 facilitates this migration.

We first move to investigating the nature of the relaxations around the different vacancies close to the surface.

3.5.1 The in-plane vacancy

Removing a first tri-layer in-plane oxygen is energetically unfavourable with the vacancy creation energy being 4.68 eV, to be compared to a bridging oxygen vacancy creation energy of 3.19 eV. The relaxations around the in-plane vacancy are large, as is expected

[2] As far as the work function goes, at least. The authors speculate that different ways of neutralizing the surface might give the same spectrum.

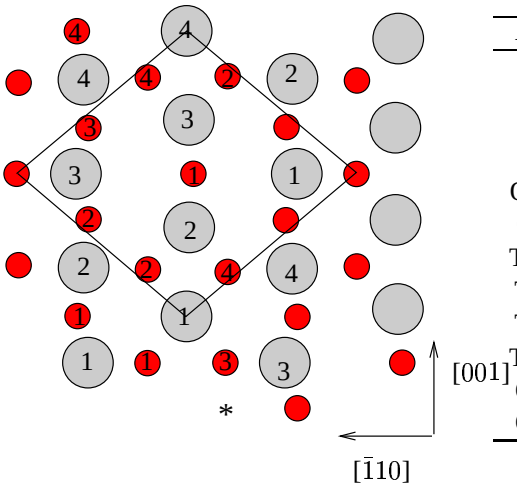

Atom	[$\bar{1}$10]	[001]	[110]
O_b^1 1	0.164	-0.021	-0.015
O_b^1 2	-0.178	0.049	-0.026
O_b^1 3	-0.176	-0.049	-0.023
O_b^1 4	0.184	0.022	-0.021
O_{ip}^1 1*	1.041	0.000	0.479
O_{ip}^1 1	0.020	-0.007	0.164
Ti_{ip*}^1 3	0.219	-0.001	-0.045
Ti_{ip}^1 2	-0.063	-0.206	0.074
Ti_{ip}^1 3	-0.050	0.205	0.075
Ti_{ip*}^1 1	-0.161	-0.000	-0.020
O_{sb}^1 2	-0.010	0.012	0.100
O_{sb}^1 3	-0.007	-0.013	0.102

Figure 3.10: Main atomic displacements (in Å) upon the formation of an in-plane oxygen vacancy in a $c(4\times2)$ unit cell. To the left, a schematic view of the first tri-layer atoms illustrating the numbering. Labelling of the atoms is consistent with the labelling of the atoms in the Fig. 3.6. However, a larger part of the surface is shown, and the unit cell indicated.

from the bridging oxygen case, see Fig. 3.10. The in-plane oxygen atom just across the titanium (labelled 1 in Fig. 3.10) relaxes towards the void left by the missing oxygen atom so strongly that it takes its final position bridging the in-plane titanium atoms, thereby making the defect symmetric around the titanium row. It also moves upwards by 0.48 Å. The bridging oxygen atoms surrounding the vacancy move towards it by 0.18 Å parallel to the surface. The titanium atoms beneath the bridging oxygens (Ti_{ip*}^1 1 and 3) move away from the vacancy by 0.22 Å and 0.16 Å. The row titanium atoms move away from the atom bridging them by 0.20 Å.

3.5.2 The sub-bridging vacancy

Proceeding down into the surface, the next vacancy is created by removing a sub-bridging oxygen atom. This can be thought of as a bridging oxygen vacancy which has diffused downwards. The creation energy is 3.75 eV. This is not low enough to expect to find these vacancies present on a surface in thermodynamic equilibrium. The number of second layer vacancies present in thermodynamic equilibrium at room temperature is to a very good approximation given by $\exp((E_{\rm sb} - E_{\rm b})/kT) = \exp(-0.55{\rm eV}/k * 300{\rm K}) = 5 \cdot 10^{-10}$ per bridging oxygen vacancy. Most experimental surfaces are specifically treated so as not to be in thermodynamical equilibrium but rather to have a much increased number of bridging oxygen vacancies (e.g. vacuum annealing at high temperatures). Therefore it is possible that vacancies of this kind remain, but as the barrier for a sub-bridging vacancy reverting into a bridging vacancy is only 0.2 eV, it is unlikely to find them in great numbers. The relaxations around the sub-bridging vacancy are

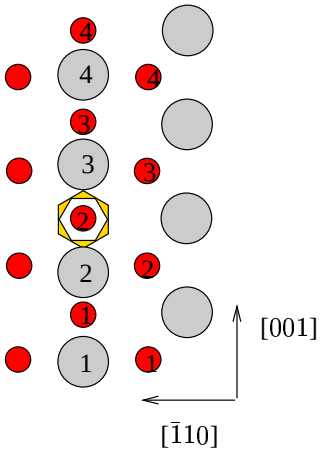

Atom	[$\bar{1}$10]	[001]	[110]
O^1_b 1	-0.004	-0.082	0.201
O^1_b 2	-0.006	0.000	-0.289
O^1_b 3	-0.004	0.081	0.201
O^1_b 4	-0.003	0.000	0.141
Ti^1_{ip*} 2	-0.005	-0.219	0.149
Ti^1_{ip*} 3	-0.005	0.218	0.148
O^1_{sb} 1	-0.005	-0.005	0.122
O^1_{sb} 3	-0.005	0.004	0.122
O^1_{sb} 4	-0.005	0.000	0.113
Ti^2_{ip} 2	0.002	0.000	-0.318
O^2_{ip} 2	0.031	0.051	0.127
O^2_{ip} 3	0.031	-0.052	0.127
O^2_{ip} 2*	-0.031	0.051	0.135
O^2_{ip} 3*	0.031	-0.053	0.134

Figure 3.11: Main atomic displacements (in Å) upon the formation of a first tri-layer sub-bridging oxygen vacancy in a $c(4\times2)$ unit cell. To the left, a schematic view of the first tri-layer atoms, illustrating the numbering. The yellow star illustrates the position of the vacancy.

substantial as well. The bridging oxygen atom above the vacancy (O^1_b 2 in Fig. 3.11) relaxes downward by 0.29 Å. The titanium atoms above the vacancy (Ti^1_{ip*} 2 and 3) follow downward by 0.15 Å while simultaneously moving outwards from the vacancy in the [001] direction by 0.22 Å. The titanium atom below the vacancy (Ti^2_{ip} 2) relaxes downwards by 0.32 Å whereas the oxygen atoms neighbouring it (O^2_{ip} 2 and 3) relax upwards by 0.13 Å. The bridging oxygen atoms next to the one directly above the vacancy (O^1_b 1 and 3) relax upwards by 0.20 Å. The oxygen atoms below them (O^1_{sb} 1 and 3) do likewise, although they relax to a lesser degree. As in the cases of the two previous vacancies, the pattern is thus that of titanium atoms relaxing away from the vacancy and oxygen atoms relaxing into it.

3.5.3 The second tri-layer bridging oxygen vacancy

The energy required to create a second tri-layer bridging oxygen vacancy is 5.66 eV, making it the energetically least favourable in the uppermost layers. Relaxations around the second tri-layer bridging oxygen vacancy are not above -0.09 Å for any atoms and are therefore not given.

3.5.4 The second tri-layer in-plane oxygen vacancy

A second tri-layer in-plane oxygen vacancy has a creation energy of 4.56 eV which is very similar to the first tri-layer creation energy. The relaxations are not as large, though, since the bulk-like environment does not allow space for an oxygen atom bridging the

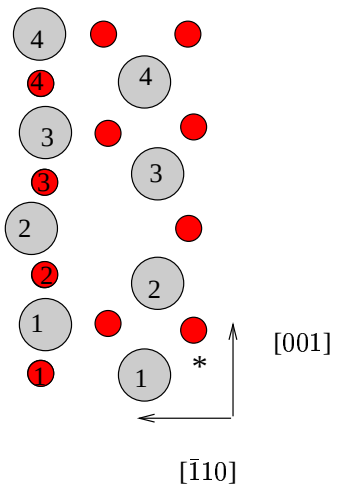

Atom	[$\bar{1}$10]	[001]	[110]
O_b^2 2	-0.108	0.077	0.005
O_b^2 3	-0.108	-0.077	0.005
Ti_{ip}^2 1	0.128	-0.026	0.005
Ti_{ip}^2 2	-0.277	-0.186	-0.045
Ti_{ip}^2 3	-0.277	0.186	-0.045
Ti_{ip}^2 4	0.128	0.026	0.004
Ti_{ip*}^2 1	-0.126	0.034	0.015
Ti_{ip*}^2 2	0.308	-0.000	0.041
Ti_{ip*}^2 3	-0.126	-0.034	0.015
Ti_{ip*}^2 4	0.057	-0.000	0.001
O_{ip*}^2 1	-0.069	-0.134	0.048
O_{ip*}^2 2	0.084	0.000	-0.044
O_{ip*}^2 3	-0.069	0.134	0.048
O_{ip*}^2 4	0.110	0.000	0.001
O_{sb}^2 2	-0.092	0.070	0.034
O_{sb}^2 3	-0.092	-0.070	0.034

Figure 3.12: Main atomic displacements (in Å) upon the formation of a second tri-layer in-plane oxygen vacancy in a $c(4\times2)$ cell. To the left, a schematic view of the second tri-layer atoms, illustrating the numbering. Atoms in lower layers are numbered accordingly. * denotes the rightmost row of in-plane oxygen atoms, as illustrated.

Ti^2_{ip} atoms. However, the oxygen atom opposite the vacancy, O^2_{ip*} 2 in Fig. 3.12, does relax towards the vacancy by 0.08 Å. The Ti^2_{ip*} 2 atom just opposite relaxes away from the vacancy by 0.31 Å whereas the neighbouring atoms relax 0.13 Å in the opposite direction and thereby drag the bridging oxygen atoms somewhat along with them. The Ti^2_{ip} atoms relax similarly. The ones closest to the vacancy relax away from the vacancy and the ones further in the opposite direction towards it. The large relaxations of all Ti atoms in the cell indicate that the unit cell is not of sufficient size to consider the vacancy properly isolated.

3.5.5 Comparison to other theory

Recently Oviedo *et al.* [74] have made a systematic study of different sub-surface vacancies focusing on the vacancy formation energy dependence on computational parameters. They conclude that the bridging oxygen vacancy is the most favourable but that differences in vacancy creation energy between species between different unit cells and slab thicknesses are significant. The most sensitive are the bridging and sub-bridging vacancy formation energies. The authors suggest solving the convergence problem by doing calculations for both even and odd number of layers and averaging.

They report relaxations only for the bridging and sub-bridging oxygen vacancies, since these are the most stable. The results are similar to this work. For the sub-bridging vacancies, they find that the bridging oxygen atom above the vacancy relaxes downward by 0.31 Å, to be compared with 0.29 Å in our calculations. The titanium atoms above the vacancy are computed to relax 0.40 Å/0.15 Å and the in-plane oxygen atoms relax only very little. The large difference in the relaxation of the titanium atoms is rather surprising. Possibly this is partially due to the choice of unit cell, but it seems rather a large difference nevertheless. In general the large relaxations around vacancies indicate a need for large unit cells in order to model truly isolated vacancies. Oviedo *et al.* have employed a $p(4\times1)$ unit cell in their calculations whereas we have employed a $c(4\times2)$ unit cell. For the bridging oxygen atoms, Oviedo finds a relaxation of the titanium atoms of 0.37 Å whereas we find 0.30 Å which is in better agreement. In this case our calculations have been done in a primitive cell as well. Unfortunately, Oviedo does not report which kind of structure is found for the in-plane oxygen vacancy. For the vacancy formation energies, we in general calculate lower energies than those found for four layer slabs and larger than those for five layer slabs. The agreement with the averaged values is reasonable, though. Oviedo finds vacancy formation energies of 3.07 eV for the bridging, 4.92 eV for the in-plane, 3.55 eV for the sub-bridging, 5.36 eV for the second tri-layer bridging and 4.58 eV for the second tri-layer in-plane vacancy. These are to be compared with the values in Figure 3.13. Possibly the reason for the closer resemblance of our calculations to the averaged values derives from our keeping the bottom layers fixed whereas Oviedo relaxes all layers. After the first four layers, our vacancy formation energies oscillates considerably less than Oviedo finds.

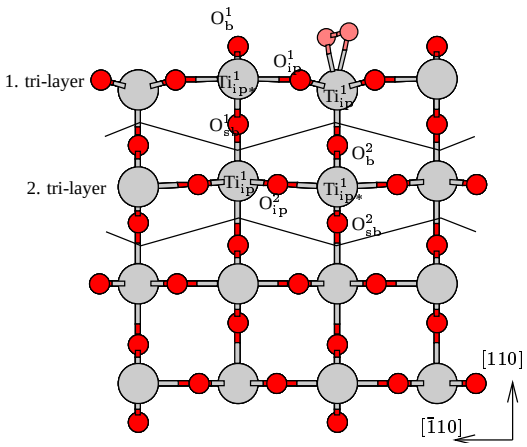

Vacancy	VFE	VFE w. O_2	d
O^1_b	3.19 eV	1.12 eV	1.42 Å
O^1_{ip}	4.68 eV	1.87 eV	1.43 Å
O^1_{sb}	3.75 eV	1.71 eV	1.40 Å
O^2_b	5.66 eV	2.30 eV	1.41 Å
O^2_{ip}	4.56 eV	2.58 eV	1.41 Å

Figure 3.13: Vacancy formation energy (VFE) of oxygen vacancies in the first four atomic planes, with and without co-adsorbed oxygen in a $c(4\times2)$ cell. The difference between VFE and VFE w. O_2 is the difference in binding energy of the oxygen molecule on the stoichiometric and defected surface. Above, schematic illustration of the naming of vacancies. The position of the oxygen molecule in the calculations where one was present is indicated in light red. Its bond length, d, is given.

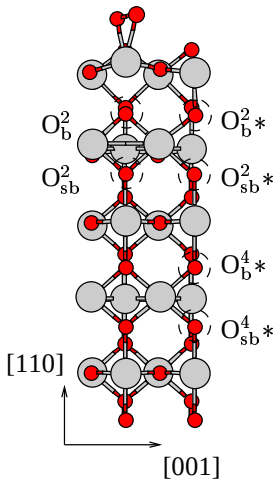

Vacancy	VFE	VFE w. O_2	d
O_b^2*	5.60 eV	3.29 eV	1.42 Å
O_b^2	5.60 eV	2.06 eV	1.42 Å
O_{sb}^2*	5.54 eV	2.65 eV	1.39 Å
O_{sb}^2	5.54 eV	2.95 eV	1.39 Å
O_b^4*	5.31 eV	3.30 eV	1.36 Å
O_{sb}^4*	5.58 eV	3.91 eV	1.35 Å

Figure 3.14: Vacancy formation energy of vacancies in increasing slab depth, with and without adsorbed oxygen. Bond distance, d, of the O_2 molecule adsorbed. The calculations employ a $c(2\times2)$ unit cell, eight tri-layers, top four layers relaxed. Atoms marked with * are not located directly below the adsorbed oxygen molecule but one lattice site removed.

3.6 Charge transfer from vacancies

Since all the vacancies are created by removing oxygen, they each contain two electrons which are now able to participate in a different kind of bonding or even leave the vacancy entirely to sit on an adsorbate. If an oxygen molecule is present on the surface, the vacancy charge will relocate to the adsorbate over surprisingly long distances. This charge gain can be monitored by the bond length and spin state of the molecule - this will be described in full detail in the next chapter. Here it suffices to remark that an oxygen molecule with a bond length of 1.40 Å or above has a net charge of two electrons and is named a peroxo species. An oxygen molecule of a bond length of about 1.35 Å has a net charge of approximately 1 electron and is termed a superoxo species. This charge transfer makes the creation of a vacancy more facile, which can be seen from the table in Fig. 3.13. The bridging oxygen vacancy creation energy in a $c(4\times2)$ surface unit cell is now lowered to 1.1 eV, and the second-plane vacancy creation energy is lowered correspondingly. Interestingly the creation energy of the in-plane vacancy is lowered even more and thus becomes only 0.75 eV less favourable than a bridging oxygen vacancy. The same is seen in the case of the third plane vacancy which is now only 1.2 eV less favourable than the bridging oxygen vacancy. In this case the energetic gain is not only from the charge transfer from vacancy to adsorbate. The molecule is adsorbed directly on top of the vacancy, changing the coordination of the Ti_{ip}^1 atom from four to six leading to an appreciable stabilization of the vacancy. The vacancies are not completely identical in their ability to donate charge, though very similar. The in-plane vacancy is the most effective with an adsorbate bond length of 1.43 Å.

Proceeding down into the slab, charge transfer from vacancies becomes less facile

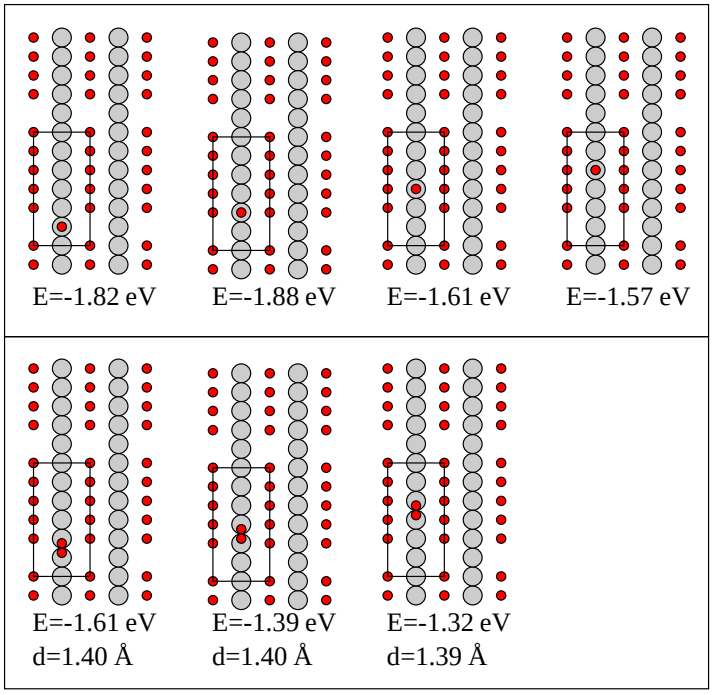

Figure 3.15: Bonding configurations of O and O_2 at increasing distances from an O vacancy, and associated adsorption reaction energies.

as distance increases, see Fig. 3.14. Nevertheless, charge can relocate over considerable distances. A distance of 11 Å still leads to a charge transfer of one electron. That charge transfer happens from sub-surface vacancies with such ease, is consistent with the suggestion by Onda *et al.* [67] that researchers should expect varying surface reactivity for differently treated substrates even if they look similar in STM.

Charge transfer to far away adsorbates is even more facile if it happens from bridging oxygen vacancies to adsorbates down the row. The surface has to be globally stoichiometric to substantially weaken the bonding. Simulating the bonding of O and O_2 to $TiO_2(110)$ by employing a very long $p(6\times1)$ unit cell with one oxygen vacancy and placing the adsorbates on the Ti row at increasing distance from the O vacancy reveals that charge transfer can take place over distances of several lattice spacings without considerable decline in adsorption energy, see Fig. 3.15. This remains true for both molecular and atomic oxygen. Adsorption potential energies remain numerically quite high at the largest distance from the vacancy that the $p(6\times1)$ unit cell allows to consider (approximately 10 Å).

This resolves an apparent discrepancy with STM measurement on this surface. Even though both theory and experiment shows evidence that no oxygen can adsorb on a stoichiometric surface, according to Schaub et al. [75] oxygen can diffuse along the titanium rows on a surface with vacancies. Since a surface containing vacancies is shown

above to be reactive to the adsorption of oxygen so far from vacancies that this is a global effect on surfaces with high vacancy coverages, this question is resolved. No contradiction exists with the results obtained by Schaub et al. [75] because the relatively large vacancy concentrations attained in the experiments ensure a rather short average vacancy-vacancy distance, and consequently a significant adsorbate-vacancy interaction. In addition it emphasizes the inadequacy of describing TiO_2 purely in covalent bonding-like terms. The semiconductor should also be thought of by its band structure.

3.7 Vacancy segregation to the surface

If the surface is free of O_2 molecules, the vacancy formation energies of sub-surface vacancies vary only little depending on depth, see Fig. 3.14. The O^2_b and O^2_{sb} vacancies and the O^4_{sb} have essentially the same vacancy creation energy. The O^4_b is slightly favoured over the others by 0.3 eV. However, if O_2 is present on the surface, the picture changes. The O^2_{sb} vacancy becomes favoured by 0.5 eV over the O^2_b and O^4_b vacancies, which are again favoured over the O^4_{sb} vacancy by 0.4 eV. This indicates that the presence of O_2 on the surface may have an influence on vacancy segregation to the surface. If the adsorbate is residing directly on top of the O^2_b vacancy, this position is much more favourable to the vacancy by 1.4 eV. Thus, a surface O_2 might draw a sub-surface vacancy up from the second layer position to the position just below the titanium atom. Here it would stay or segregate onwards to the surface depending on the local barrier size and the temperature. These values have been calculated using an 8 tri-layers, 4 tri-layers relaxed slab, and consequently they had to be done using only a $c(2\times2)$ surface unit cell. This leads us to expect vacancy creation energies to be systematically too large, leading also to a shift upwards in the difference in vacancy creation energy between systems with and without oxygen, as seen in Table 4.4 in the next chapter.

3.8 Stability of sub-surface vacancies

The presence of sub-surface vacancies is dependent, not only on their vacancy creation energy, but also on the barriers for their creation. In the case of the first tri-layer sub-bridging vacancy the transformation to a first tri-layer sub-bridging vacancy requires only small distortions of the surface. Therefore the barrier for the process is expected to be small. This turns out to be the case, see Fig. 3.16. As the vacancy creation energy generally differs depending on the abundance of O on the surface, the barrier has been calculated both with and without an adsorbed oxygen molecule. The barrier essentially remains the same. The barrier for the transformation of a bridging vacancy to a sub-bridging vacancy is 0.80 eV if oxygen is present and 0.68 eV if the surface is clean. The barrier for the reverse case is 0.22 eV if oxygen is present and 0.13 eV if the surface is clean. The barriers have been calculated using constrained minimization, constraining the coordinate of the diffusing oxygen atom in the [110] direction while allowing all other barriers to relax. The barrier for the transformation of a sub-bridging vacancy to a bridging vacancy is so small that sub-bridging vacancies should transform into bridging

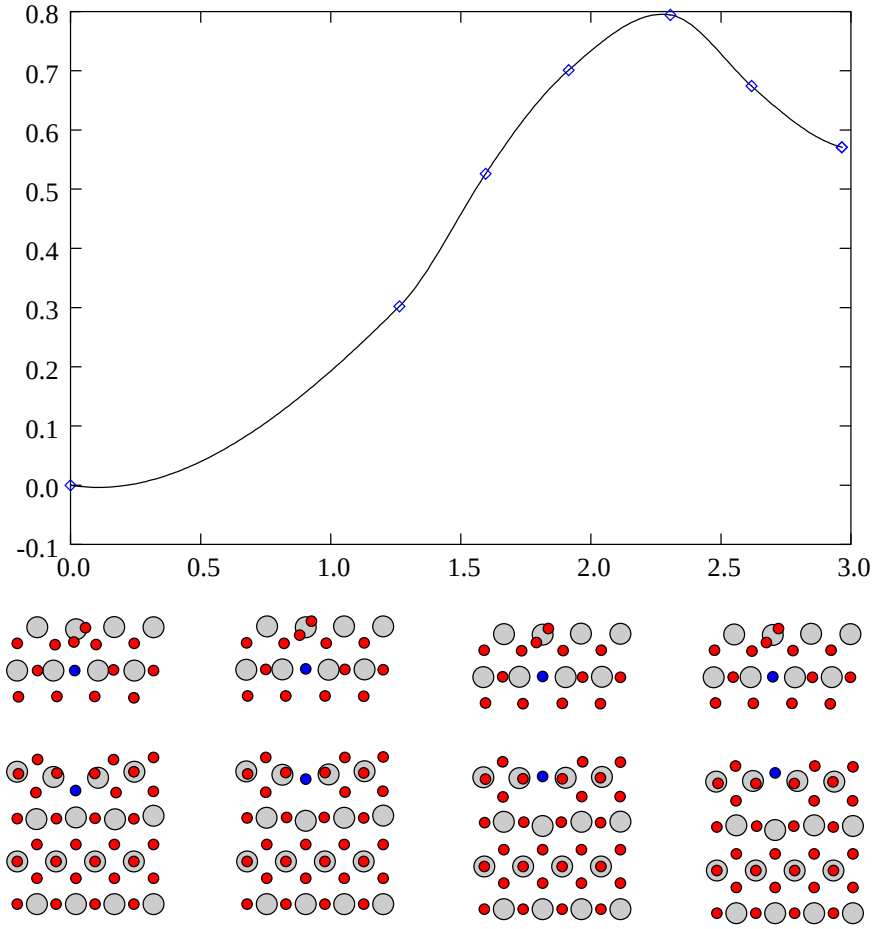

Figure 3.16: The diffusion barrier for the creation of a sub-oxygen vacancy in the presence of adsorbed O_2. The diffusing atoms has been marked in blue. Diamonds are calculated points, while connecting lines are splines, derived from the forces projected onto the transition path. The calculations have been made in a $c(4\times2)$ surface unit cell.

vacancies spontaneously. The reverse, however, is only feasible at high temperatures, and the sub-bridging vacancies would then revert to bridging ones instantly. Therefore, if these vacancies were somehow created, they are not likely to survive, and turning them into bulk vacancies is an endothermic process, as can be seen from the creation energy of e.g. the sub-titanium vacancy. There is a remote possibility of creating a double vacancy in the [110] direction during annealing. This is a bridging and a sub-bridging vacancy together. It proves to be a highly unstable configuration with a creation energy of 8.98 Å, to be compared with a creation energy of 6.67 Å for a double vacancy consisting of two bridging oxygen vacancies (no molecular oxygen present). If a horizontal double vacancy was ever created, it might possibly be meta-stable because of kinetic barriers, but eventually it would revert to two bridging oxygen vacancies. Thus, the sub-bridging vacancies appear to be of interest only as meta-stable stages in the vacancy diffusion.

The second tri-layer bridging oxygen vacancies have no such easy pathway for turning into first tri-layer bridging oxygen vacancies. Therefore, it is more likely that oxygen induced vacancy segregation can lead to the presence of this vacancy type at the surface. As they are much more stable beneath oxygen adsorbate covered titanium atoms than at a clean surface, they may be expected to gravitate to these adsorbates. Calculating the diffusion pathway for a second tri-layer bridging oxygen vacancy moving away from a surface titanium atom with an oxygen molecule on top to a neighbouring site using constrained minimization indeed turns out to be impossible. Keeping the coordinate in the [001] direction fixed and letting all other atoms, including the oxygen adsorbate, relax results in a diffusion path where the oxygen molecule moves to a bridge site configuration rather than staying adsorbed in the original atop site. As the diffusion pathway becomes complicated, constrained minimization is an insufficient technique to handle the calculation of the barrier. Thus, the barrier size of 1 eV for the reverse diffusion from a site beneath an undressed Ti to a Ti beneath an oxygen adsorbate should be taken as an order of magnitude only.

The barrier for the diffusion in the [001] direction if no oxygen is present can be estimated by calculating the energy of the configuration constraining the diffusing oxygen atom to the point exactly midway between two lattice sites. This produces a barrier of 1.3 eV. Thus, these vacancies appear stationary if oxygen is not adsorbed close by.

In general it would be interesting to investigate the barriers for vacancy diffusion in the bulk and sub-surface region. However, as constrained minimization appears to be insufficient, nudged elastic band calculations have to be employed. As this will be exceedingly costly in computer time, the study has been postponed.

CHAPTER 4

Oxygen on the TiO_2(110) surface

Oxygen does not adsorb on the stoichiometric surface. Upon the creation of vacancies, surface chemistry changes drastically and oxygen adsorption turns exothermic by as much as 2.2 eV in the vacancy and 1.7 eV on the titanium row. The stabilizing factor is the transfer of vacancy electrons to the adsorbate, resulting in oxygen becoming doubly charged (peroxo species). Peroxo species are characterized by bond lengths above 1.40 Å and vanishing magnetic moment. The surface valence can be tailored to allow for the existence of singly charged oxygen (superoxo species), either by changing the nature of surface defects or by changing the adsorbate to vacancy ratio above 1. Superoxo species are characterized by bond lengths around 1.35 Å and magnetic moments around 1 Bohr magnetons. O_2 and CO can co-adsorb on the surface, forming a pseudo-bond indicating a possibility for oxidation of CO. The surface is likely to poison to the reaction by annealing away the vacancies if they are not protected, for instance by adsorbing gold atoms therein. Adsorption of ozone is possible on the surface; if the surface is capable of effective charge donation, ozone will dissociate, leaving an oxygen ad-atom on the surface. If charge is scarce, ozone is stable on the surface.

4.1 Experimental findings

By now, both ample experimental and theoretical investigations into the oxygen chemistry on TiO_2 exist [44, 56–58, 60, 67, 68, 75–85] as well the chemistry of small oxygen containing molecules [73, 86–91]. Nevertheless, a consensus has yet to be reached on many important points. Naturally, surface chemistry is highly dependent on deposition temperature. At lower temperatures, oxygen adsorbs molecularly or dissociatively as adsorbates, whereas at higher temperatures it is incorporated into the lattice (see below).

Using photo-oxidation, Lu *et al.* [76] show the existence of two different oxygen species on the surface at low temperatures (105 K) which they term α and β oxygen. These two species are distinguished by the ability of the α species to photo-oxidize CO, as opposed to the β species, which instead undergoes fast photo-desorption. The α species can be converted into β species by heating to 200 K. Based on this, it is suggested that the β species binds stronger than the α species. Additionally, it is speculated that these species are most likely singly or doubly charged. Rusu and Yates [77] refines this study by finding that the α species divides into two species, α_1 and α_2, with different desorption cross sections.

Temperature programmed desorption (TPD) measurements by Henderson et al. [81] show a major first order desorption peak at 410 K. Adsorption crucially depends on the existence of vacancies; in the absence of vacancies no desorption of oxygen is seen. This study additionally supplies the information that at most 3 oxygen molecules are adsorbed on the surface which the authors envision as located in and around the vacancy. Only two thirds of these molecules are desorbed in the 410 K top, and these molecules are observed not to scramble with the surface. They are assumed to desorb from sites on the titanium rows. The remaining third is assumed to dissociate at vacancy sites, annealing the vacancies and leaving oxygen adatoms on the surface. This process is described in more detail in an earlier paper [78]. Sequential exposures of $^{16}O_2$ and $^{18}O_2$ evidence that the probability that a given molecule chooses a particular channel is not predestined by the time at which it was dosed. This is attributed to an exchange of oxygen molecules between the vacancy and in-plane titanium sites. Additionally, the experiments illustrate the adsorption configuration sensitivity to adsorption temperature, as molecules adsorb molecularly at 120 K, whereas molecules adsorb dissociatively at 150 K.

Schaub *et al.* [75] observe diffusing oxygen molecules on the surface using scanning tunneling microscopy (STM). These species are active in mediating the diffusion of surface oxygen vacancies. The authors suggest a mechanism where one oxygen atom dissociates at the vacancy, filling it and then recombining with another bridging oxygen, leading to vacancy diffusion. This process, however, scrambles surface and adsorbate oxygen, in conflict with Henderson *et al.*'s claims of no scrambling. In a later paper [83] the same group presents a suggestion for a charge transfer driven diffusion process on the surface, since diffusion seems not to be phonon-mediated.

At higher temperatures (above 500 K) bulk titanium interstitial atoms are believed to be mobile. Li *et al.* use STM combined with LEIS (low-energy He^+ ion scattering) to reveal that oxygen adsorbed on the surface in this temperature range recombines with titanium interstitials diffusing to the surface where they form rosette-like structures, strands and (1×1) islands [43–47]. These structures are all variations of incomplete TiO_2 layers,

ranging from rosettes over Ti_2O_3 strands to full layers as the temperature rises. At some temperatures these features co-exist. The restructuring depends on the bulk reduction state of the crystal, as larger reduction leads to a higher degree of incorporation of gas phase oxygen and more disordered structures. The structure of the rosettes is supported by DFT calculations. The authors have done LEED (low-energy electron diffraction) on the surfaces and point out that a (1×1) LEED pattern by no means has to indicate a well-ordered (1×1) surface.

The strands are the same as those of the (1×2) reconstruction reported by Onishi and Iwasawa [42], which is not surprising as sample preparations are similar. They assign the strands to a structure much similar to a stoichiometric continuation of the surface on every other titanium row and all bridging oxygen rows, strained inwards towards the covered titanium rows. This structure is supported by a thorough theoretical investigation by Elliott and Bates [13, 48, 49]. Investigations of reconstructions related to the growth of TiO_2 during annealing are numerous, and it is outside the scope of the present work to review them. The reader is referred to Diebolds review from 2003 [50].

4.2 Adsorption on stoichiometric and defected surfaces

From the results of Henderson [81] no oxygen is expected to adsorb on the stoichiometric surface. This is supported by theory, as illustrated in Figure 4.1a. Introducing one bridging oxygen vacancy per unit cell, Figure 4.1b presents five stable configurations on the Ti rows for O_2 in $c(4\times2)$ unit cells. This is equivalent to a 25% vacancy coverage which is not too far from experimental coverages of 8%-16%. The introduction of the vacancy changes the binding of O_2 dramatically, adsorption becoming strongly exothermic.

Figure 4.1b shows a clear correlation between binding energy and bond distance of the adsorbed O_2 molecule. The configurations parallel to the surface V5-V8 have bond lengths of around 1.40 Å and are stable by 1.0-1.7 eV. The less stable configuration V9 with O_2 in an upright orientation have a shorter bond length of 1.29 Å. This last configuration also retains some magnetic moments, as opposed to the other, more stable configurations. It is a well established fact that the charging of a diatomic molecule leads to an increase in bond length [92]. A bond length of more than 1.40 Å is indicative of a charged O_2 molecule carrying a charge around 2 electrons. In this case all electrons are paired, and no magnetic moment remains. Shorter bond lengths are indicative of less charge, and some magnetic moment is expected to be present. Comparison with the stoichiometric surface confirms this point. Calculated oxygen molecule bond lengths are around 1.30 Å which is only moderately more than the value for gas phase O_2, calculated to be 1.24 Å. This reflects that the molecule does not gain electrons by interacting with the surface. Consistently, O_2 retains part of the magnetic moment characteristic of the gas phase molecule (2 μ_B); the spin on the adsorbed O_2 molecule is 1.1 μ_B at the top site and 1.5 μ_B at the bridging one. It can therefore be concluded that whenever an oxygen vacancy is present there is an important charge transfer to the O_2 adsorbate. This finding is in good agreement with in the presence of excess electronic charge in the region of the vacancy, cf. Fig. 3.7 in the previous chapter. The most stable configuration

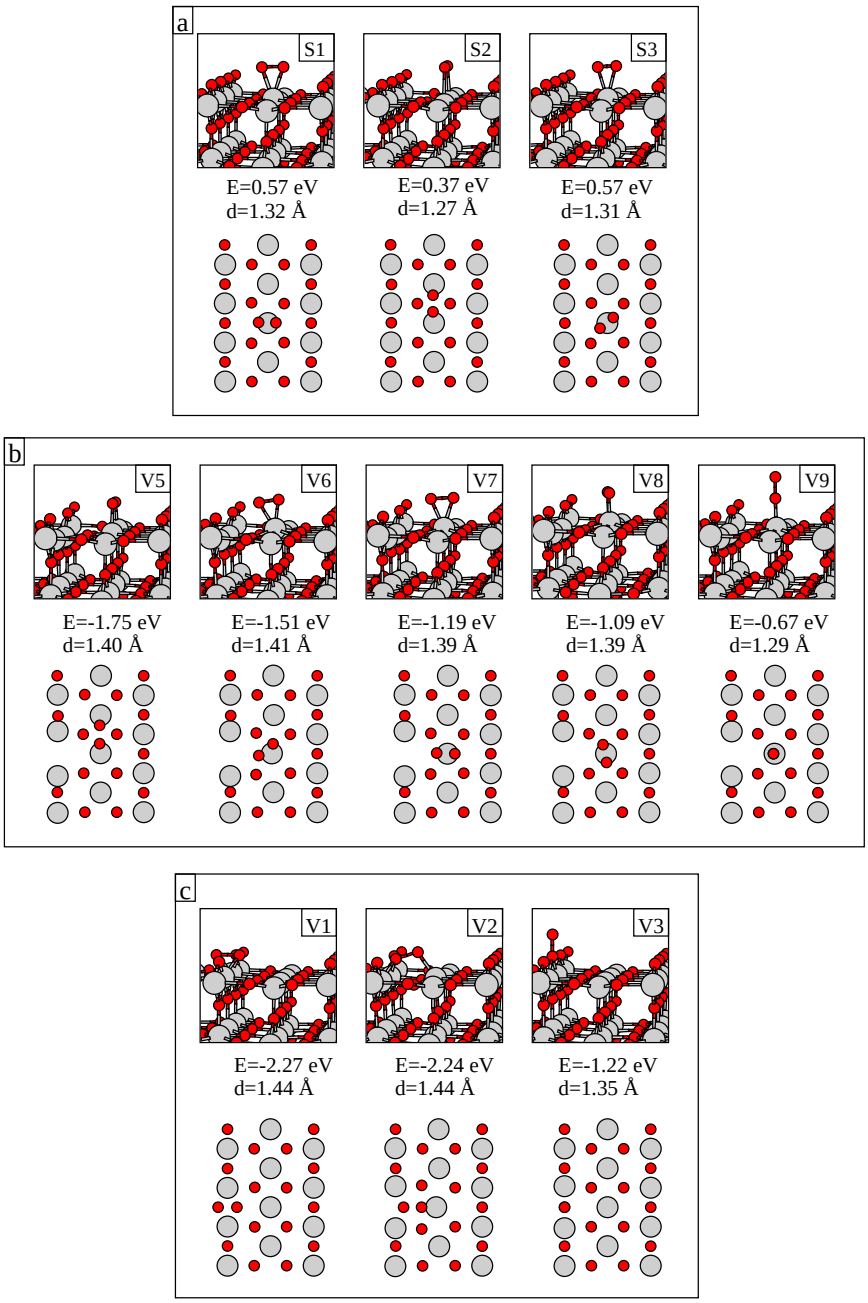

Figure 4.1: Some stable configurations after the adsorption of molecular oxygen on a $c(4\times2)$ surface with zero or one bridging oxygen vacancy prior the the adsorption. The adsorption energies, E, and bond lengths, d, are given. Below,, schematic presentation, above, ball and stick model of the same configurations. Large grey balls/circles represent titanium atoms, small red ones oxygen atoms.

in the atop site is turned 45° with respect to the bridging oxygen rows. This can be understood in terms of general coordination arguments. Upon O_2 adsorption the TiO_2 defected surface undergoes varying structural relaxations depending on the specific O_2 binding configuration. Whenever an oxygen atom or molecule is positioned on top of a Ti atom in the row, this atom relaxes strongly outwards (by up to 0.7-0.8 Å as in the V6 case). Therefore, O_2 binding results in the breaking of the Ti-O bond to the second tri-layer. The Ti thus becomes effectively 6-fold coordinated. The oblique orientation is then the one better resembling the ideal octahedral arrangement of oxygen atoms around a Ti found in bulk rutile TiO_2. Wang *et al.* [60] formalize this argument using frontier orbital theory. The large relaxation of the Ti atom reflects the general tendency of the surface to relax to a large degree if any defect is introduced, as commented upon in the previous chapter. Any other adsorbate can be expected to introduce similar large-scale relaxations. This provides a computational challenge to DFT, as quite large unit cells containing 100-150 atoms are necessary to obtain any useful information about isolated adsorbates.

Henderson proposes adsorption in the vacancy, and it turns out that the vacancy is indeed an attractive adsorption site. Figure 4.1c presents three adsorption configurations in the vacancy. The two configurations parallel to the surface (V1 and V2) have expanded O-O bond lengths of 1.44 Å whereas the V3 configuration, which is orthogonal to the surface, has a bond length of only 1.35 Å. Thus, the general picture from the row repeats. Parallel configurations are favoured and have long bond lengths indicative of doubly charged molecules (peroxo species), whereas orthogonal species bind less and have shorter bond lengths indicative of singly charged molecules (superoxo species). The relaxations around the adsorbed molecule serve to lift the surface deformation introduced by the vacancy, and the V1 configuration indeed restores the surrounding surface almost to stoichiometry. In the previous chapter, this was seen also to reflect in the electronic structure and in the DOS, which returns to that of the stoichiometric surface when O_2 is adsorbed in the V1 configuration.

4.3 Charge states of O_2 on the surface

As the S2 and V5 states illustrate, the adsorption energy of oxygen on TiO_2 is strongly dependent on the amount of charge the molecule can gain from the substrate. In literature, several charge states are mentioned (see Ref. [9] and references therein) but on single crystals with bridging vacancies the adsorbate appears to be singly charged [81, 93, 94]. Bond lengths of 1.40 Å and above and no magnetic moments indicate, however, that our calculations of oxygen adsorbates in the vicinity of vacancies describe doubly charged molecules. Calculations of Wu *et al.* and Wang *et al.* [58, 60] support this. We shall see later in this chapter that this is probably linked to the amount of oxygen adsorbed at the surface. As only a limited amount of vacancies exist, only a limited amount of adsorbates can be stabilized by charge from these adsorbates, and only one electron is left for every oxygen molecule. However, the interactions of the adsorbed oxygen molecules and single atoms are complicated, and therefore we first investigate an isolated, singly charged oxygen molecule and establish the bond length, stability and

	Defect type	Φ	E_{ads}	E_{top}	E_{brd}	μ_{top}	μ_{brd}	d_{top}	d_{brd}
I	V1	6.2	-2.27 eV	0.62 eV	0.34 eV	1.0	1.5	1.32 Å	1.26 Å
II	No defect	6.3		0.56 eV	0.36 eV	1.1	1.6	1.31 Å	1.27 Å
III	Cl in vacancy	5.7	-3.63 eV	-0.79 eV	-0.68 eV	0.9	0.8	1.33 Å	1.32 Å
IV	P substituent	7.1		-0.91 eV	-0.74 eV	0.9	0.8	1.35 Å	1.32 Å
V	Vacancy on Al subst.	5.2		-0.80 eV	-0.69 eV	0.8	0.9	1.35 Å	1.32 Å
VI	H in vacancy	5.5	-3.15 eV	-0.80 eV	-0.65 eV	0.8	0.8	1.36 Å	1.33 Å
VII	OH in vacancy	4.8	-4.79 eV	-0.84 eV	-0.76 eV	0.8	0.8	1.35 Å	1.33 Å
VIII	V3	6.0	-1.22 eV	-0.84 eV	-0.72 eV	0.7	0.7	1.36 Å	1.34 Å
IX	Br in vacancy	5.7	-2.76 eV	-0.84 eV	-0.78 eV	0.9	0.9	1.34 Å	1.32 Å
X	Au in vacancy	5.3	-1.95 eV	-0.86 eV	-0.80 eV	0.7	0.3	1.38 Å	1.36 Å
XI	Gold rod	5.2		-0.84 eV	-0.65 eV	0.3	0.0	1.41 Å	1.39 Å
XII	H_2 in vacancy	4.9	-0.10 eV	-1.59 eV	-1.75 eV	0.2	0.0	1.41 Å	1.39 Å
XIII	Vacancy	4.9		-1.59 eV	-1.74 eV	0.0	0.0	1.41 Å	1.40 Å
XIV	Gold rod on vacancy	5.3		-1.63 eV	-1.61 eV	0.0	0.0	1.44 Å	1.41 Å

Table 4.1: Work function of the system prior to oxygen adsorption in the titanium row, Φ. Adsorption energy of adsorbate in the vacancy, if applicable, E_{ads}. Adsorption energies, E, magnetic moments, μ, and bond lengths of the adsorbed oxygen molecule, d, of oxygen in the top and bridge configurations. The systems are presented in Fig. 4.2, see next page.

magnetic moment to ease the identification of such species later on.

4.4 O_2 binding charge dependence

Creating a singly charged adsorbed oxygen molecule could in principle be done by simply adding an electron to a calculation of an adsorbed molecule on a stoichiometric surface. Our attempts to do this failed. The electron locates on the unrelaxed back of the slab instead of on the adsorbates. Furthermore, calculations were unstable and often failed to converge entirely. We have thus discarded this model as unsuitable.

A more promising possibility is changing the character of the surface itself. This choice has the advantage of simultaneously estimating the sensitivity of adsorbate properties to the character of the charge donor. Thus, it leaves us the possibility of evaluating whether the properties of adsorbed oxygen, such as charge state, adsorption site and configuration, contain sufficient information to determine with which defects oxygen shares the surface. As it turns out oxygen properties are independent of the nature of defects on the surface in so far as these defects are equally efficient charge donors or acceptors.

Thus, we attempt to model a monovalent surface. This can for instance be done by substituting a chlorine atom for a bridging oxygen atom, which can also be viewed as adsorbing a chlorine atom in a bridging oxygen vacancy. As the chlorine needs only one electron to fill its outer shell, this leaves the last vacancy electron free to relocate to an oxygen adsorbate. Other atoms share this property, for instance H and Au. The charge on the oxygen molecule should then reflect the electronegativity on the adsorbate. The

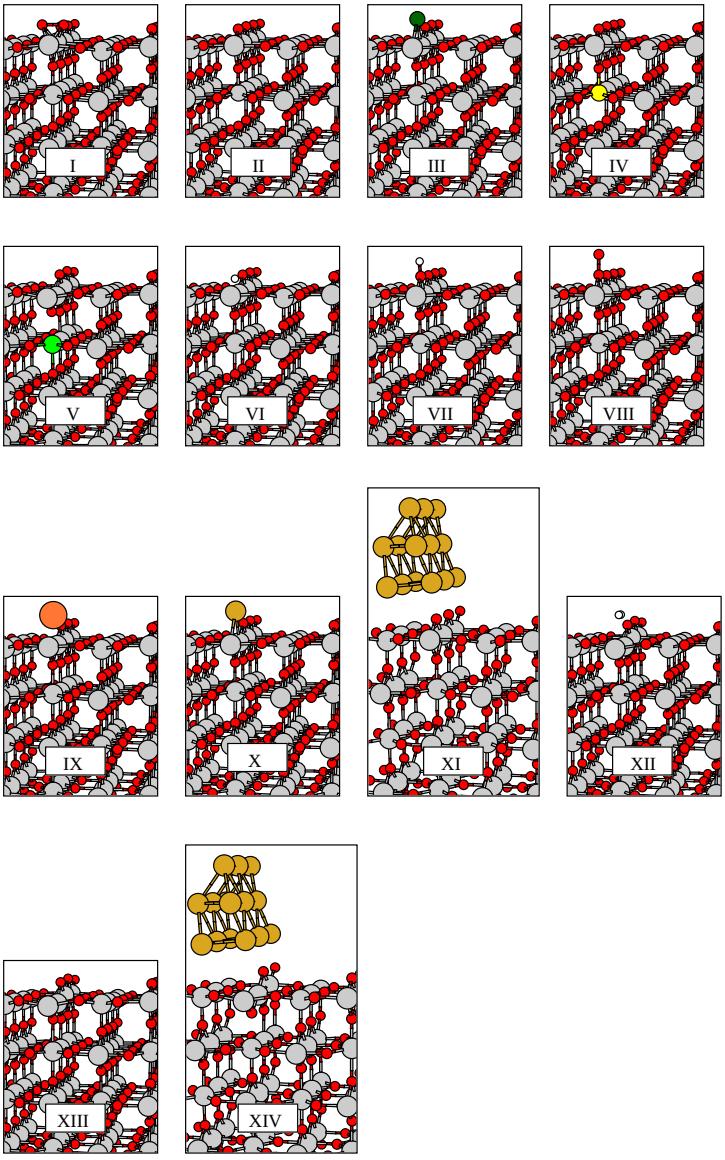

Figure 4.2: Ball-and-stick models of the different systems described in Table 4.1. XI and XIV were calculated in a $p(3\times2)$ cell, all other systems were calculated in a $c(4\times2)$ cell. I An O_2 lying in a vacancy. II The stoichiometric surface. III A Cl atom in a vacancy. IV A P atom in the stoichiometric surface. V A vacancy above an Al atom. VI An H in a vacancy. VII A OH in a vacancy. VIII O_2 upright in a vacancy. IX A Br atom in a vacancy. X An Au atom in a vacancy. XI A gold rod on the stoichiometric surface. XII H_2 in a vacancy. XIII Vacancy. XIV Gold rod on a vacancy.

Site	Bridging O_2	Atop O_2
0	-0.69 eV	-0.80 eV
1	-0.72 eV	-0.81 eV
2	-0.70 eV	-0.79 eV
3	-0.71 eV	-0.80 eV

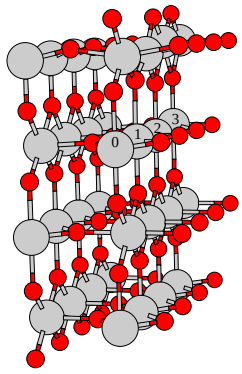

Table 4.2: Adsorption energies of an oxygen molecule in the atop and bridge site as a function of aluminum substituent position.

Mulliken-Jaffe electronegativity[1] of the three atoms is Cl 3.10, H 2.25 and Au 1.87 in Pauling units [95]. The adsorption energy of the atoms in the vacancy should also follow this trend, which is indeed the case. The binding energies of the substituents calculated with respect to the defected surface and a free atom in vacuum reflect the trend as well. They are -3.63 eV, -3.15 eV and -1.95 eV for Cl, H and Au, respectively (see Table 4.1). The bond lengths of the oxygen molecule in the bridge configuration on the row are in these three cases 1.32 Å, 1.33 Å and 1.36 Å, following the expected trend, as do the magnetic moments with 0.8. 0.8 and 0.3 Bohr magnetons. Oxygen binding energies likewise increase slightly as -0.79 eV, 0.80 eV and the -0.84 eV. The bond lengths and magnetic moments reflect the new adsorbate charge of around one electron, a little more in the case of Au.

Adsorbing an atom in the vacancy provides a good model system as long as adsorption configurations on the row are being investigated, but makes it impossible to investigate adsorption in the vacancy. This can be remedied by leaving the vacancy open and instead substitute an aluminum atom for the titanium atom underneath the vacancy. This also leaves only one electron to relocate to the adsorbate, as the other one fills the acceptor level induced by the Al substituent. Commercially available rutile TiO_2 is often doped with Al to suppress undesirable photoactivity. Experiment support that with low amounts of dopants Al atoms do indeed substitute Ti [96]. Adsorption potential energies, bond lengths and magnetic moments can be found in Table 4.1. They are consistent with a singly charged adsorbate, fitting neatly between the systems with Cl and H in the vacancy. The adsorption energy and bond lengths are not heavily dependent on the specific site of the substitution, see Table 4.2. However, moving the Al to the third tri-layer where the atoms are not allowed to relax but kept in bulk positions reduces its ability to accept charge efficiently. Adsorption in the vacancy turns out to be much less favourable when the Al atom has been substituted. The V1 state now has an adsorption potential energy of -0.47 eV. The V3 is more favourable, having an adsorption potential energy

[1]The Mulliken-Jaffe electronegativity is defined as the average of the electron affinity and the ionization potential with respect to a specific valence state.

of -0.85 eV. The V2 has an adsorption potential energy of -0.69 eV. Bond lengths are shortened compared to the vacancy with no substituents, being V1 1.39 Å, V2 1.36 Å, and V3 1.31 Å. These values should be compared with V1 1.44 Å, V2 1.44 Å, and V3 1.35 Å. Thus, the V1 and V2 configurations are similar to singly charged adsorbates whereas the V3 has a slightly smaller charge, supported by a magnetic moment of 1.2 Bohr magnetons.

Since the use of Al appears successful, it is natural to investigate what happens if no vacancy or vacancy-like defect is present on the row and instead substitute a P atom for a Ti atom. This is an attempt to model a surface without the relaxations introduced by the vacancy while still being monovalent and should model the surface far away from vacancies. Adsorbates become singly charged just as the Al case, but the binding energies are slightly increased corresponding to the cases above. This may simply reflect that it is more favourable to adsorb on a locally stoichiometric environment if the necessary charge is present. This effect would serve to smooth the potential energy surface on the Ti rows. As the adsorbate moves away from the vacancy, the charge transfer is slightly inhibited. However, the steric arrangement of the surface is slightly more favourable. Thus, no dependence on the distance to the vacancies is seen with STM, as long as vacancy coverage remains high. Moving the P atom to the third tri-layer makes it a less efficient donor just as the Al atom became a less efficient acceptor. This is apparently primarily due to the atoms around it not being allowed to relax. The phenomenon is also seen if a bulk vacancy is introduced in an unrelaxed layer; it relinquishes very little charge to a surface adsorbate. Relaxing the layer, however, increases the charge transfer by about one electron. This was also seen in the induced charge density plot of the bridging oxygen vacancy in the previous chapter, see Figure 3.7. Thus, the facile charge transfer on the surface is crucially dependent on the surface relaxations.

4.5 Evaluating the charge on adsorbates

We have chosen to evaluate molecule charge by bond length and magnetic moment. It is well known that bond length correlates to adsorbate charge [92] just as HO_2 and H_2O_2 have longer O-O bonds than the oxygen molecule. We calculate values of 1.24 Å for the oxygen molecule, 1.35 Å for HO_2 and 1.49 Å for H_2O_2. Nevertheless, using this parameter alone to determine adsorbate charge is error prone since the bond length is also sensitive to the local geometry on the surface. Thus, the added consideration of magnetic moment is imposed. Neutral oxygen in the gas phase has a magnetic moment of two Bohr magnetons, deriving from the partial filling of the two anti-bonding π^*_{2p}-orbitals [97]. Filling one orbital results in a singly charged molecule with a magnetic moment of 1 Bohr magneton, which vanishes completely as the last state is filled and the molecule becomes doubly charged. Looking at Table 4.1, it is clear that even the adsorbates on the essentially stoichiometric surface (I and II) are slightly charged. In particular the molecule adsorbed in the atop site has a magnetic moment indicative of this, about one Bohr magneton. This is consistent with the bond length of 1.32 Å. Progressing downwards through the Table, the adsorbates change their charge gradually, and thus it is somewhat of a simplification when we above addressed molecules as

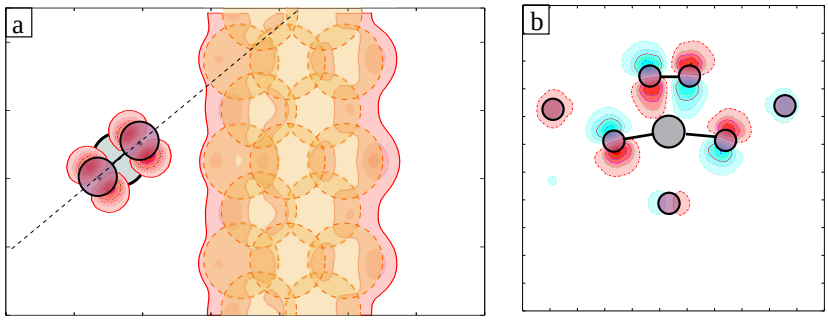

Figure 4.3: a) Contour plot of the square modulus of the two states closest to the Fermi energy in the XI system (TiO_2 with a gold rod) with an oxygen molecule in the V6 configuration. In this system, the filled oxygen π state can actually be resolved, b). The orbital is also located on the substrate oxygen atoms, and thus not only π in character.

discreetly singly or doubly charged (system IX being a case in point). The bridge configuration is more sensitive to the charge changes on the surface, possibly because it bonds to only two in-plane titanium whereas the atop site has an interesting orbital involving also two in-plane oxygen and a sub-surface oxygen, see Figure 4.3. Consequently, the charge on adsorbates in the bridge configuration ranges from about 0.5 to 2 electrons. All spin is located on the adsorbate in what appears to be an anti-bonding π^*_{2p}-orbital. Integrating spin up and spin down charge densities in the direction perpendicular to the slab and subtracting them reveals the shape of the spin polarized orbital, see Fig. 4.4. It is identical in all systems with magnetic moment. It is tempting to try to resolve this spin-polarized state by finding the corresponding Kohn-Sham eigenfunction. However, it turns out that no single eigenfunction is responsible for all spin because the filled spin-polarized state is shifted all the way down into the valence band. An unfilled state just above the Fermi level can be resolved, though. This state has π^*_{2p} character.

The charge transfer from the defect to the adsorbate is visualized for the atop configuration in Fig. 4.5 by plotting the induced charge density. It is calculated as the charge density of the slab with adsorbate (O_2) and substituent (Cl) minus the charge density of the adsorbate minus the charge density of the substituent minus the charge density of a stoichiometric slab plus the charge density of an oxygen atom in place of the Cl atom (n(TiO_2(vac)+Cl+O_2)-n(O_2)-n(Cl)-n(TiO_2)+n(O)). Only key atoms are relaxed since the polarization signatures are otherwise too large to distinguish the charge transfer. As mentioned above, this is likely to change the charge transfer, but as the bond length of the molecule remains almost the same as in the fully relaxed case, we judge the approximation to be reasonable.

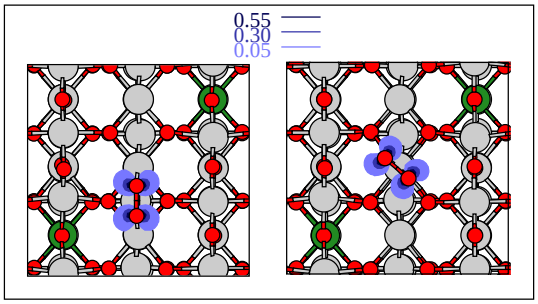

Figure 4.4: Difference of spin up and spin down charge densities in the top and bridge configuration, integrated over the [110] direction. Units are electrons/Å^2.

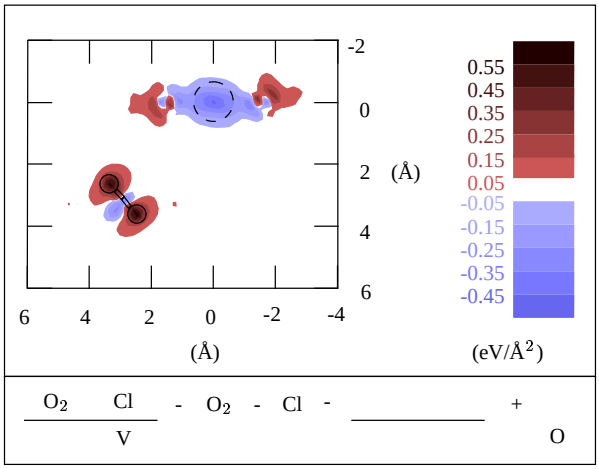

Figure 4.5: Induced charge density in the top configuration, (n(TiO_2+Cl+O_2)-n(O_2)-n(Cl)-n(TiO_2)+n(O)). The systems have been indicated below the plot. Only key atoms are relaxed. The dashed circle represents the vacancy, the ball-and-stick the adsorbed oxygen molecule.

4.6 Interaction with realistic defects

Having established the possibility to create a singly charged adsorbate and conformity of the properties of bond length, adsorption potential energy and magnetic moment, it is interesting to investigate some defects which realistically may be present on the surface, even if they are not created intentionally. Hydrogen adsorbed in the vacancy might be such a case, as hydrogen is known to be present in large amounts in the TiO_2 bulk. However, literature indicates that atomic hydrogen would adsorb more favourably on the bridging oxygen atoms [98]. This would produce a drastically different surface, as both a divalent vacancy and a monovalent hydroxyl group would be present. A hydrogen molecule is a different case. Having a binding potential energy of -0.1 eV, it does not

realistically stay molecularly adsorbed on the surface. This vanishing interaction with the surface means that it does not modify the vacancy charge donation characteristic, and the surface remains divalent. A much investigated defect [12, 50, 98–101] is the bridging hydroxyl, which is a hydrogen atom adsorbed on top a bridging oxygen atom. It turns out to donate a charge of about one electron as well. So does an oxygen molecule adsorbed in the vacancy in the V3 configuration. However, if the oxygen molecule is adsorbed in the vacancy in the V1 configuration, it effectively neutralizes the vacancy. Adsorption becomes endothermic to the same degree as on the stoichiometric surface, and bond lengths change accordingly. It is interesting to note that if the row adsorbate is in a top site it is more favorable to have an oxygen molecule in the V3 configuration and another on the row than leaving the vacancy adsorbed oxygen in the V1 configuration. The adsorption potential energy is -2.06 eV in the first case and -1.65 eV in the second case. If the adsorbate is in the bridge configuration, the energies are even at -1.93 eV and -1.94 eV. Thus, the interaction with row adsorbates could be what keeps all vacancies from being filled with oxygen molecules in the V1 state. This remains a strange apparent inconsistency between STM experiments [75] and theory; it seems likely that all vacancies should be filled with oxygen molecules in some configuration. This would also be in agreement with TPD experiments [81]. Additionally, the STM signature of a V1 state would most likely be very close to that of a vacancy. DFT even calculates a density of states having two states in the band gab at an energy of 0.80 eV and 1.09 eV, see Fig. 4.6, which are roughly where the vacancy derived state is found experimentally. The defects responsible for the defect state associated with the vacancy are known to vanish upon adsorption of molecular oxygen at room temperature. This does not disprove the possibility of 'vacancies' actually being V3 states, though, as STM data shows 'vacancies' vanishing simultaneous with the creation of an unknown complex. Indeed, the oxygen chemistry of the surface turns out to be very complex [102]. In so far, the question remains unresolved.

To properly address the question of O_2 adsorbate characteristics dependence on charge origin, we need to examine defects which are not in some way modified vacancies. Metal clusters are efficient charge donors and are therefore a logical choice. We have settled on gold, because gold clusters are interesting as catalysts and reported to donate charge to adsorbed oxygen molecules [94]. Since we use periodic boundary conditions, we have implemented the gold clusters as infinitely long rods along the [001] direction. In this way we achieve a metallic state. Adsorbing O_2 on the in-plane titanium atoms results in bond lengths of 1.40 Å, in consistency with doubly charged molecules, as is the almost vanished magnetic moments. The binding energies are those of a singly charged molecule, though. Thus, the gold cluster serves as a transition case to the very charge rich systems. Adding a vacancy beneath the gold rod increases binding to the same level as a lone vacancy. The presence of the gold cluster seems to increase the adsorption potential energy of the bridge site, favouring binding in the atop site. The local geometric environment is the same in both cases, excluding a geometric effect due to the gold cluster.

The last thing to be noted in the Table is that the site preference changes depending on the charge state. In a system containing enough charge to sustain O_2^{2-} molecules, the most favourable adsorption site is the bridge site, but if charge is limited, the top site

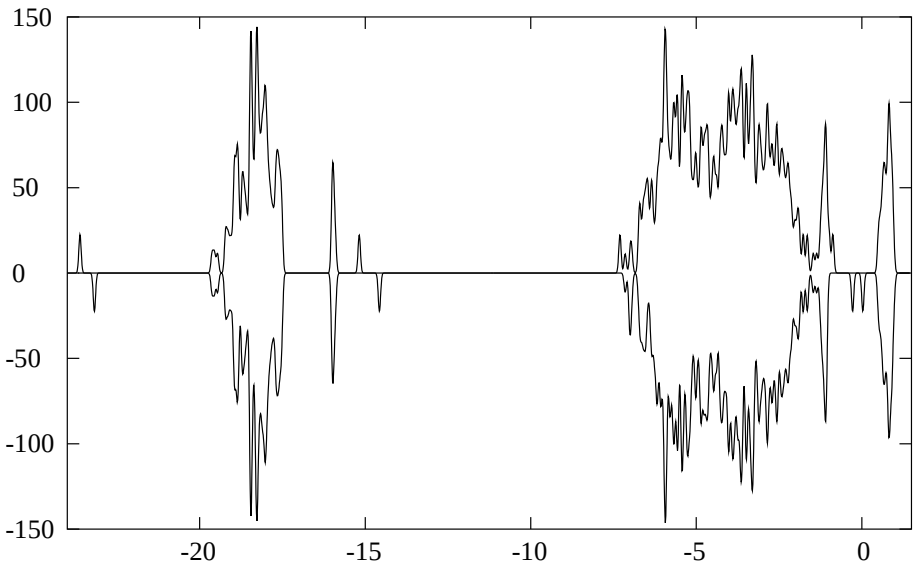

Figure 4.6: Spin-resolved density of states of a TiO_2 surface with an oxygen molecule adsorbed in the vacancy in the V3 configuration. The energy scale is eV with the Fermi level set to 0. The spin-polarized states in the band gab are clearly visible.

Author	V1	V2	V3	V5	V6	V7	V8	V9
This work	-2.27	-2.24	-1.22	-1.75	-1.51	-1.19	-1.09	-0.67
Wang *et* al.	-2.72	-2.52	-1.02	-2.04	-1.92	-1.44	-1.34	n.a.
Wu *et* al.	-2.87	n.a.	n.a.	n.a.	-0.98	n.a.	n.a.	n.a.

Table 4.3: Comparison of the calculated adsorption energies for the most stable configurations of molecular oxygen on TiO_2(110) by Wang *et al.* [60], Wu *et al.* [58] and this work.

becomes preferred. The top site preference is consistent with STM observations [83]. This subject will be treated in more detail in Chapter 5.

4.7 Other theory

The first theoretical study of O_2 binding on TiO_2(110) was done by Shu *et al.* [80]. However, their model is using clusters so small (Ti_2O_9) that the results have little, if any relevance to adsorption on a surface.

De Lara-Castells and Krause [56, 57, 82] investigate the V1, V3 and V9 states using periodic Hartree-Fock calculations. Contrary to our results they find the V3 state to be more stable than the V1 state with adsorption energies of 3.39 eV and 1.97 eV, respectively. The spin states are the same as we find for the adsorbates, V3 being most favourable as singlet and V1 as triplet. The V3 triplet state is almost dissociated, as is the V1 singlet state. The discrepancy between their and our results seem to derive from

the discrepancy in the description of the vacancy; de Lara-Castells and Krause find that one electron is strongly located on a Ti atom.[2] Consequently, the electron is likely not as readily moved to an adsorbate as the electrons in our calculation, and de Lara-Castells and Krauses results should rather be compared to our results containing Al dopants with which they are consistent, excepting the absolute size of the adsorption energy of the adsorbate in the vacancy. As the thickness of the slabs in the Hatree-Fock calculations is only three tri-layers with adsorbates symmetrically placed, the agreement is as good as can be expected. The authors support the possibility of adsorbing three oxygen molecules on the surface, as found by Henderson [81].

As mentioned in the previous chapter, Wu *et al.* [58] use DFT, pseudopotentials, and expansion in plane waves, as we have done. Contrary to us they use the Perdew-Burke-Ernzerhof gradient corrections. As the studies are so similar, similar results should be found. This is indeed the case. Using our terminology, they find a vacancy creation energy of 3.55 eV, and adsorption energies of 2.45 eV for the V1 state in a $p(4\times1)$ cell. This should then be compared with a vacancy creation energy of 3.28 eV in the same cell in our calculations and a 2.27 eV adsorption energy in the V1 in a $c(4\times2)$. For the V6 state, Wu *et al.* calculate the adsorption energy only in a $p(2\times2)$ cell, finding a value of 0.98 eV. We find a value of 1.51 eV in a $c(4\times2)$ cell. The study by Wu *et al.* also agrees with ours in the large stabilizations of adsorbates found when the ratio of adsorbates to vacancies is changed below 1.

Wang *et al.* [60] calculate adsorption energies for most of the same configuration as we do, see Table 4.3, obtaining almost identical results. They do DFT calculations using slabs of five tri-layers and surface unit cells of $p(3\times2)$. Their choice of exchange correlation is not reported. They find slightly higher binding energies than we do, which is to be expected as the calculational cell of Wang *et al.* have three lattice constants between oxygen vacancies compared to four in our calculations. The only exception is the V3 configuration where they calculate a slightly lower energy.

4.8 Co-adsorption of oxygen

Henderson *et al.* [81] report a saturation oxygen coverage of three molecules per vacancy. In the light of the insights above, this must be due to charge transfer from the vacancies. Assume for simplicity of discussion that the first adsorbates adsorb on the row and sit in an atop site in the V6 configuration, see Fig 4.7. The adsorption potential energy is then -1.59 eV (using the unmodified vacancy model). Some of the molecules, according to Henderson, end up in the vacancies. If they realize the V1 configuration, the surface has been completely neutralized, as can be seen from Table 4.1. No more oxygen can be adsorbed and the row must be empty. If instead they realize the V3 configuration, however, the adsorption potential energy of the two co-adsorbed molecules is still -2.06 eV with respect to two molecules in the gas phase. Therefore the second molecule must adsorb in the V3 configuration, if adsorbing in the vacancy. The adsorption potential energy of the whole configuration declines as the third molecule is added

[2] The reader is cautioned that de Lara-Castells and Krause number their layers by atomic layers, not by triple layers, as chosen here.

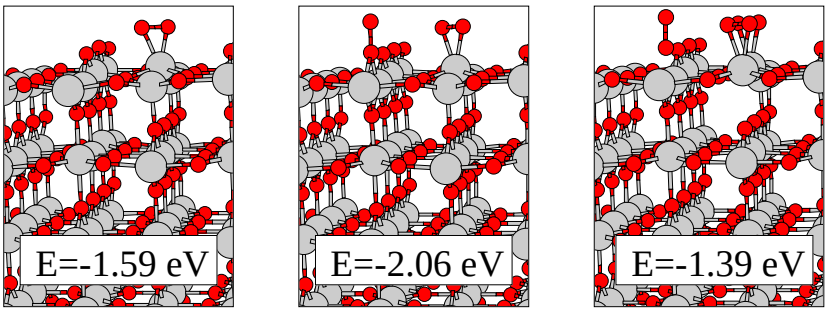

Figure 4.7: Energy of co-adsorption of O_2. The binding potential energies given beneath each system are of all the adsorbates relative to the surface with one vacancy, $E_{slab+nO_2}$-E_{slab}-nE_{O_2}

to a value of -1.39 eV. Thus, the third molecule is not stable. Judging from the bond lengths of the molecules, the one to leave the surface would be the one in the vacancy, as it has a bond length of only 1.27 Å as opposed to 1.33 Å for the ones on the row. Consequently, at higher coverages the presence of adsorbates on the row changes the vacancy to a less favourable adsorption site. This may be what keeps the vacancies free of adsorbates in STM experiments. Any other way of removing the charge from the vacancies is likely to have the same effect. The model of two molecules in the V6 configuration on the row and one in the V3 configuration in the vacancy is unsuccessful in reproducing three adsorbed oxygen molecules in Hendersons experiment. Possibly binding could be strengthened a little by optimizing the configuration of the molecules, e.g. moving the oxygen molecules further apart or changing adsorption site or configuration. However, this is unlikely to be the real explanation. In light of the study of surface vacancy distribution by Onda *et. al* [67] the crystal used by Henderson is expected to contain sub-surface vacancies. As these are also capable of charge donation to the adsorbates, the charge needed to stabilize the third adsorbate by 0.7 eV is probably found here. A lot of intricacies in the adsorption process exists depending on the order surface sites are occupied. If O_2 is first adsorbed in the vacancies, it might realize the V1 configuration and neutralize the surface. The configuration where one atom is adsorbed in the V1 configuration and one is in the gas phase is 0.21 eV more favourable than the two-atom co-adsorption configuration of Fig. 4.7. However, kinetic barriers may prevent the V1 configuration from ever being realized. Indeed, it has never been observed in STM. If an oxygen molecule gets close to the surface and the V1-adsorbed O_2, it is energetically favourable by 0.42 eV for the vacancy-bound oxygen to rotate and the oxygen nearing the surface to chemisorb at the atop site it is approaching. This is then a lower estimate of the barrier for the reverse process happening if the V1 configuration suddenly should become accessible (say, by the temperature rising in a TPD experiment).

In many studies atomic oxygen is reported on the surface. The possibility of atomic and molecular oxygen species co-existing on the surface is determined by the adsorbate-to-vacancy ratio. Atomic oxygen cannot coadsorb with molecular oxygen if the adsorbate-

to-vacancy ratio exceeds approximately 1.5. Adsorbing both an O_2 and an O on the titanium row next to a vacancy is endothermic by 0.98 eV. This is due to the O scavenging all the charge. It can be rationalized by looking at the DOS for the systems of O and O_2 on the surface. The state corresponding to O is lower in energy, and thus both electrons locate spatially on the O and O_2 is not stabilized. At least one additional electron must be free to relocate to adsorbates for the situation to stabilize. Therefore, if the adsorbate coverage is small in comparison to the vacancy coverage, both species should be able to coexist, since charge is ample. When determining the ratio, one should keep in mind that also sub-surface vacancies are capable of charge donation to adsorbates and therefore should be counted in. When molecules dissociate, charge is being used up fast and no more oxygen can adsorb. How much was adsorbed prior to dissociation is critical to the population on surface. If only little oxygen was adsorbed (or the temperature was so high that oxygen essentially dissociates instantly on the surface), all can dissociate and the surface is left covered with atomic oxygen and poisoned to further O/O_2 adsorption. If more was adsorbed, a large portion may dissociate, but as charge becomes scarcer, dissociation will stop because O_2 requires less charge to be stable than two O atoms. Indeed, a bridging oxygen molecule is more stable than two oxygen atoms by 1.8 eV in a cell containing one bridging oxygen vacancy. This issue will be revisited in Chapter 5, section 5.1.

In a recent combined experimental and theoretical study of the surface structure of the (011) surface, Beck *et al.* [103] point to doubly bonded oxygen atoms (titanyl groups) in the surface lattice as the source of enhanced photocatalytic activity of this surface. It is interesting to note that these atoms appear similar to the doubly charged adsorbed oxygen atoms on the (110) surface. The coordination of the oxygen atom is one in both cases, and the bond lengths are almost identical. The adsorbed oxygen atom on the (110) surface has a bond length of 1.64 Å whereas the oxygen atom in the titanyl group on the (011) surface has a bond length of 1.62 Å. The bonding in the titanyl groups appears to be the stronger, though.

4.9 Consequences for O_2 binding versus vacancy coverage

Because of the charge transfer, bonding properties of O_2 and O vary with vacancy coverage. Table 4.4 presents the binding energy of O_2 in the V1 and V5 configurations. Oxygen is postulated to dissociate in the vacancy, annealing it and leaving an oxygen atom on the row. The adsorption energy is also given for this state (D1). Configurations are presented for unit cells of increasing size ($p(3\times1)$, $c(4\times2)$ and $c(6\times2)$) and also for a $c(6\times2)$ cell with two O vacancies per adsorbed O_2 molecule (and thereby per unit cell). The vacancy distribution in the latter case is identical to the distribution achieved by using a $p(3\times1)$ unit cell. When only one vacancy is present for every adsorbed oxygen molecule the V1 configuration is clearly the most stable one, being around 0.5 eV more stable than the D1 one.

Interestingly, O_2 binding steadily decreases as the unit cell is enlarged. The trend follows the decrease in vacancy creation energy as can be seen from the Table. Since O_2

Structure	Θ_{vac}	Θ_{ads}	E_{V1}	E_{D1}	E_{V5}	VFE
$p(3 \times 1)$	0.33	0.33	-2.53	-1.69	-1.90	3.49
$c(4 \times 2)$	0.25	0.25	-2.27	-1.53	-1.75	3.19
$c(6 \times 2)$	0.17	0.17	-2.04	-1.57	-1.55	3.03
$c(6 \times 2)$	0.33	0.17	-2.81	-5.29	-2.24	3.49

Table 4.4: Comparison between O_2 binding energies (in eV) at the V1 (O_2 in vacancy), D1 (O_2 dissociated in the vacancy, leaving an oxygen atom on the Ti row) and V5 (O_2 on the Ti row) configurations, as a function of the adsorbate and vacancy coverages. Trends follow the vacancy creation energy, VFE. As the vacancy distribution is identical in the $p(3\times1)$ cell with one vacancy and the $c(6\times2)$ cell with two vacancies, the VFE is identical per definition.

takes up vacancy charge upon adsorption, the binding increase is most probably due to vacancy-vacancy interaction; if the electrons are on the adsorbate the vacancies interact less strongly, and the adsorbates do not interact to a similar degree, in spite of also being charged. The larger the cell, the smaller the vacancy-vacancy interactions and thereby the smaller the adsorption energy. The trend of O_2 binding thus reflects the distance between vacancies. In this light it is not surprising that the *difference* in adsorption potential energy between V1 and V5 states is remarkably independent of the size of the unit cell.

The binding in the V1 and V5 configurations is strengthened by adding another vacancy to the cell, changing the adsorbate to vacancy ratio to 1/2. This may reflect larger charge transfer, but also that it is favourable for vacancies not to release all their charge to adsorbates. The adsorbate bond length in the V5 case changes from 1.39 Å to 1.41 Å when adsorbate coverage per vacancy is halved, supporting the idea that added charge transfer is at least partially responsible.

The dependence of the adsorption energy on charge availability is much more evident in the case of the D1 state. The introduction of an additional vacancy in the unit cell dramatically changes the energetic order between V1 and D1 states, making the dissociative configuration D1 strongly favoured. This is inherent in the dissociated state, as the dissociation serves to anneal the vacancy. In the one adsorbate per vacancy case this results in a stoichiometric surface. When two vacancies are present per adsorbate, one vacancy remains for the dissociated state, serving as the charge donor to the adsorbed O atom on the Ti row. If only one vacancy is present per adsorbate, we evaluate an endothermic adsorption potential energy of +1.38 eV for O atop a Ti atom in the row (calculated using a $c(6 \times 2)$ unit cell with respect to $\frac{1}{2}O_2(g)$). In a similar configuration but now with an adjacent O vacancy so that there are two vacancies per adsorbate, this quantity is stabilized to -1.58 eV (exothermic reaction). This is not at all surprising, since the enhancement of binding experienced by molecular O_2 upon the creation of a vacancy on a stoichiometric surface is likewise dramatic.

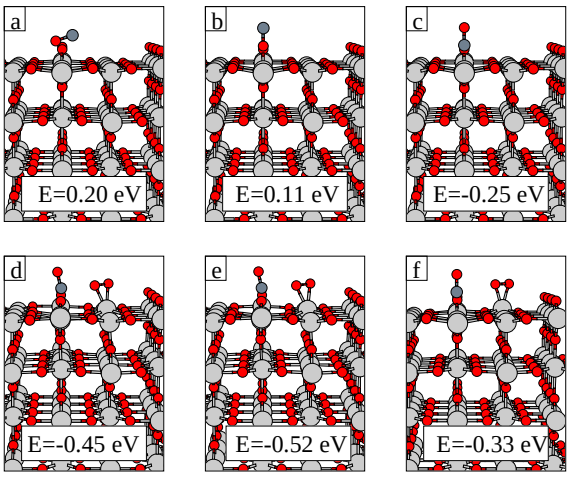

Figure 4.8: Energy of adsorption of CO. a), b) and c) CO in the vacancy in a $c(4\times2)$ unit cell. d) CO in the vacancy with O_2 on the row in a $c(4\times2)$ unit cell. e) and f) CO in the vacancy with O_2 on the row in a $p(4\times1)$ unit cell. Large, light gray spheres represent Ti atoms and small, red spheres represent oxygen atoms, as in previous figures. Small, grey spheres represent C atoms.

4.10 Co-adsorption of CO and O_2

The binding of CO has already been the subject of theoretical study [86–89, 98]. CO is less electrophillic than O_2. As such, it is not surprising that CO is not binding strongly in the vacancy. Adsorbing in the most favourable configuration in the vacancy with the carbon-end towards the surface, binding is barely exothermic, the adsorption potential energy being -0.25 $eV_{c(4\times2)}$[3], see Fig. 4.8a-c. On the row, the adsorbate binds weakly with an adsorption potential energy of -0.24 $eV_{c(4\times2)}$. This is consistent with the calculations of Wu *et al.* [86] who find a binding potential energy on the row Ti of -0.22 $eV_{p(2\times2)}$ and -0.37 $eV_{p(2\times2)}$ C-end down in the vacancy and with Menetrey *et al.* [98] who find energies of -0.28 $eV_{p(3\times1)}$ and -0.37 $eV_{p(3\times1)}$. Menetrey *et al.* use three tri-layer slabs and only partial relaxation of the first layer.

Binding is enhanced if O_2 is pre-adsorbed on the surface next to the vacancy, see Fig. 4.8d-f. As the vacancy charge relocates to the oxygen molecule and a pseudo-bond to the oxygen molecule is formed, CO adsorption potential energy decreases to -0.45 $eV_{c(4\times2)}$. Conversely, if CO has adsorbed in the vacancy prior to surface exposure to oxygen, the binding energy of oxygen is -1.48 $eV_{c(4\times2)}$. The adsorption potential energy of an oxygen molecule in the same configuration without CO is -1.51 $eV_{c(4\times2)}$. This reflects relative O_2 charge state independence of CO adsorption in the vacancy. The bond length of the O_2 is slightly increased; 1.40 Å compared to 1.39 Å at the

[3]To enhance clarity, the calculational surface cell has been indicated on the calculated energies in this section.

adsorbate-free vacancy. If O_2 is present on the surface, binding on the row becomes exothermic by 0.49 $eV_{c(4\times2)}$. Wu *et al.* [86] find that adsorbing an oxygen molecule has no effect, but this is most likely due to the adsorption site chosen. They choose to adsorb the oxygen molecule in the vacancy and parallel to the surface (V1). In this case, the oxygen molecule is already fully saturated by charge from the vacancy and therefore does not interact significantly with CO. Simultaneous binding of CO and O_2 still requires a donor; on the stoichiometric surface it is endothermic by 0.52 $eV_{c(4\times2)}$ whereas it is exothermic by 1.99 $eV_{c(4\times2)}$ if a bridging oxygen vacancy is present.

Calculating the CO binding energy in a $p(4\times1)$ cell gives similar results. Adsorption potential energy in the vacancy is -0.38 $eV_{p(4\times1)}$, enhancing to -0.52 $eV_{p(4\times1)}$ when O_2 is pre-adsorbed. As is evident from Fig. 4.8, the CO and O_2 molecules establish a pseudo-bond when O_2 is adsorbed next to a CO in the vacancy. Breaking this bond by moving the oxygen molecule two lattice sites costs 0.19 $eV_{p(4\times1)}$.

The pseudo-bond indicates a possibility for the two molecules to react. Reaction is favourable, forming CO_2 and a surface O. If the initial configuration has the CO in the vacancy and O_2 on the row, and the remaining oxygen atom is left on the row, the energy gain is 3.21 $eV_{c(4\times2)}$. If the remaining oxygen is instead left in the vacancy, the energy gain is higher, 4.56 $eV_{c(4\times2)}$, as the vacancy is annealed. If the vacancy-consuming process happens, the surface will rapidly be annealed, leaving it inert to the adsorption of O_2 and CO as the adsorption potential energy of a CO and an O_2 molecule together on the stoichiometric surface is positive.

The catalytic properties of gold on titania has attracted much attention in later years, in particular with respect to the oxidation of CO [4, 104–106]. Theoretical modeling has been employed as well [107–115]. It has been argued in the literature [116] that the active species in the catalysis of the water-gas-shift ($CO + H_2O \leftrightarrow CO_2 + H_2$) on gold on ceria are not large gold particles but rather single gold atoms, distributed on the substrate surface. This makes the behaviour of CO and O_2 on gold atoms adsorbed in the vacancies highly interesting. Additionally, if gold is already adsorbed in the vacancy, it blocks the vacancy healing process described above so that the surface is not as easily rendered inactive.

The adsorption of a gold atom in a vacancy is exothermic by 1.95 $eV_{c(4\times2)}$ per atom. The subsequent adsorption potential energy of oxygen on the row is typical for that of a surface allowing only the formation of singly charged oxygen, -0.86 $eV_{c(4\times2)}$. If the oxygen is placed directly in front of the gold atom rather than translated one lattice site, the binding potential energy is -1.11 $eV_{c(4\times2)}$. The oxygen can actually form a bond to the Au atom, see Fig. 4.9, but this is less favourable than simply adsorbing on the row by 0.51 $eV_{c(4\times2)}$. The configuration bears some similarity to the V2 configuration. A similar configuration is formed on larger clusters, see Fig. 4.9, which is also less stable than the corresponding configuration on the row. This weaker bonding originates at least in part from charge transfer considerations as can be seen from the bond lengths. The gold-coordinated molecules have shorter bond lengths which reflects less charge, leading to weaker binding. CO adsorbs on the gold atom weakly, as on the vacancy; the configuration is the same. If O_2 is pre-adsorbed on the surface, CO binding is strengthened by 0.2 eV. Thus, it is quite possible to form a complex where O_2 and CO is adsorbed on the gold atom. This may then form the precursor for the reaction. The reaction is

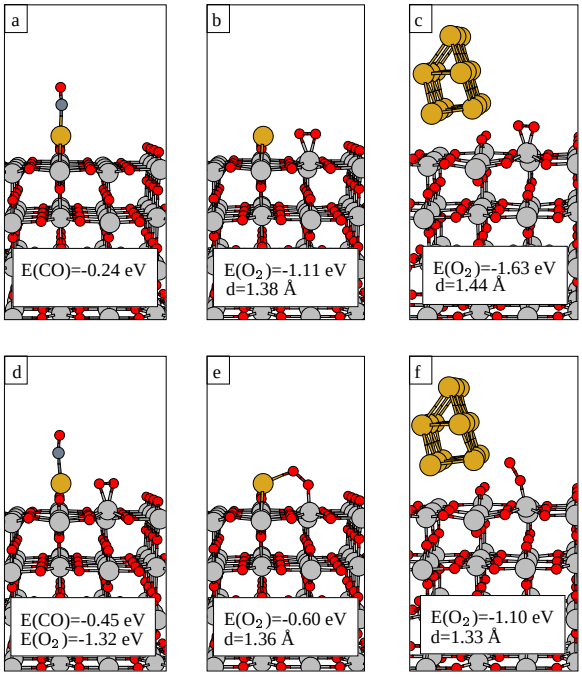

Figure 4.9: Adsorption potential energies and O_2 bond lengths in key configurations of CO and O_2 near an Au atom or an Au cluster. a), b) d) and e) are calculated in a $c(4\times2)$ cell, c) and f) in a $p(3\times2)$ cell. Large, light gray spheres represent Ti atoms and small, red spheres represent oxygen atoms, as in previous figures. Small, grey spheres represent C atoms and large, golden spheres Au atoms.

exothermic by 3.16 $eV_{c(4\times2)}$.

4.11 O_3 adsorption

Having investigated the adsorption of O_2 and O on the surface, we turn to investigating the interaction of O_3 with the surface. O_3 is used in conjunction with TiO_2 in a variety of oxygenation reactions [117–122] many of them in waste water treatment [123–128]. Additionally, TiO_2 both with and without platinum clusters has shown the ability to dissociate O_3 [124, 129–131]. In many of these studies photo-catalysis is involved, but some reactions happen in darkness as well, at least until the surface undergoes poisoning. Therefore, it is highly interesting to investigate the bonding, stability and charge state of O_3 on the surface.

The investigation of ozone adsorption is complicated by the enormous amount of configurations a tri-atomic molecule can realize on a surface as richly structured as TiO_2 coupled with the size of the molecule itself. We have chosen to investigate a large

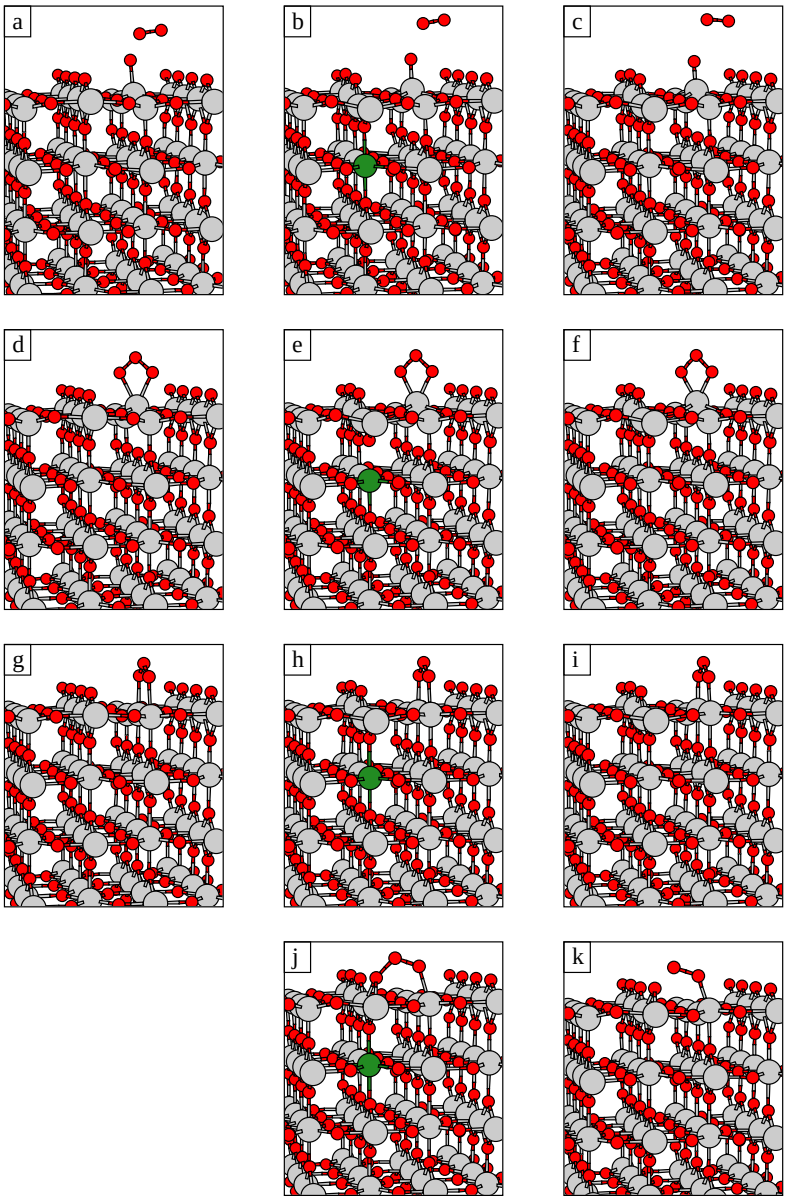

Figure 4.10: The most stable structures of O_3 on TiO_2 surfaces of different valence. a), b) and c) O_3 adsorbed singly binding in the atop site at the stoichiometric surface, by an aluminum substituted vacancy and by a vacancy. d), e) and f) O_3 adsorbed doubly binding in the atop site at the stoichiometric surface, by an aluminum substituted vacancy and by a vacancy. g), h) and i) O_3 adsorbed doubly binding in the bridge site at the stoichiometric surface, by an aluminum substituted vacancy and by a vacancy. j) and k) O_3 adsorbed doubly binding in the vacancy, with and without aluminum substitute.

Adsorbate	Vacancy		Aluminum vacancy		Stoichiometric surface	
	E	d	E	d	E	d
O	-1.84 eV	1.64 Å	-0.21 eV	1.67 Å	1.67 eV	1.69 Å
O_2(top)	-1.59 eV	1.41 Å	-0.80 eV	1.35 Å	0.56 eV	1.31 Å
O_2(brd)	-1.74 eV	1.40 Å	-0.69 eV	1.32 Å	0.36 eV	1.27 Å
$O_3(top_1)$	-1.11 eV	2.37 Å	0.09 eV	2.04 Å	1.26 eV	1.51 Å
$O_3(top_2)$	-1.03 eV	1.41 Å	-0.08 eV	1.38 Å	1.27 eV	1.35 Å
O_3(vac)	-2.31 eV	1.40 Å	-1.05 eV	1.36 Å	n.a.	n.a.
O_3(brd)	-1.58 eV	1.41 Å	-0.74 eV	1.38 Å	0.50 eV	1.35 Å

Table 4.5: Adsorption energies, E, and characteristic bond lengths, d, of pure oxygen molecules on the surface. The characteristic bond lengths are the O-Ti distance for atomic O, the O-O bond length for O_2, and the O-O bond length for the O-O bond closest to the Ti atom (see Fig. 4.11) for the O_3 complexes. The calculations have been made in a $c(4\times2)$ cell.

number of configurations in smaller unit cells, $c(4\times2)$ with three tri-layers in the slab, knowing that adsorption energies in this system are not converged due to the small slab thickness. However, these calculations allow us to discriminate sufficiently to make it possible to choose the more stable configurations and repeat the calculations with slabs of four layers. In Table 4.5, the energies and bond lengths of the four most stable configurations are presented along with the most stable configurations on the Ti row of O and O_2.

Binding of ozone on the surface essentially follows the charge dependency trends from mono- and di-atomic oxygen. On the divalent surface with one vacancy, ozone adsorbs strongly on the titanium rows. The most stable of the configurations on the titanium row with an adsorption potential energy of -1.58 eV is bridging two titanium row atoms. The molecule may also bond to the vacancy, bridging the vacancy and the closest row titanium. With an adsorption potential energy of -2.31 eV, this configuration is more stable. Binding in an atop site either coordinating with one or both ends is less favourable with energies of -1.11 eV and -1.03 eV, respectively. The binding energies have not been calculated with respect to a free ozone molecule but rather with respect to $\frac{3}{2}$ free oxygen molecules:

$$\mathrm{E_{ads}} = \mathrm{E_{surf+O_3}} - \mathrm{E_{surf}} - \frac{3}{2}\mathrm{E_{O_2(g)}}$$

This way, the adsorption energies can be directly compared to those of atomic oxygen. If the quantity

$$\Delta\mathrm{E} = \mathrm{E_{surf+O_3}} - \mathrm{E_{surf+O}} - 1\mathrm{E_{O_2(g)}}$$

is positive, it is more favourable for adsorbed ozone to eventually dissociate. For the chosen definition of $\mathrm{E_{ads}}(O_3)$, ΔE is identical to $\mathrm{E_{ads}}(O_3)$-$\mathrm{E_{ads}}$(O). On the titanium row of a surface containing vacancies, the adsorption energy of O is -1.84 eV, whereas the most stable configuration of ozone on the titanium row has an adsorption energy of only -1.58 eV. Consequently, ozone would eventually dissociate. If the ozone molecule adsorbs in a vacancy, it appears partly dissociated already, see Fig. 4.10 and 4.11. The bond

distance between the O atom closest to the vacancy and its neighbour in the molecule is 1.91 Å, whereas the bond distance between the middle atom and the one coordinating to the titanium row is only 1.40 Å. Dissociation would be favourable, since the adsorption energy of atomic oxygen in the vacancy is identical to the vacancy formation energy of 3.19 eV. Whether the split off O_2 would most likely leave to the gas phase or adsorb on the surface would depend on the number of vacancies nearby. If none were present, the molecule would leave to the gas phase, independent on whether the vacancy had been annealed or not. Co-adsorption with the adsorbed O atom next to the vacancy is endothermic and so is adsorption on a stoichiometric surface.

On a monovalent surface, dissociation is not favoured. The binding of O_3 on the row is stronger than the binding of O by 0.53 eV. As a consequence, the molecule should be able to adsorb on the surface and stay there undissociated. Possibly the outcome of the adsorption process depends on the exact path followed by the molecule, as some configurations are close to being dissociated; e.g. the atop configuration which has only one bond to the surface as well as the molecule adsorbed in the vacancy. If O atoms were present on the surface, they could even attract O_2 from the gas phase. The most stable configuration remains the vacancy configuration with a binding potential energy of -1.05 eV, closely followed by the titanium row bridging molecule. The least stable configurations are the two atop configurations.

This pattern repeats on the stoichiometric surface. The vacancy coordinating configuration does not exist as such, since there are no vacancies. None of the configurations are stable on the surface if compared to $\frac{3}{2}$ gas phase oxygen molecules. However, compared to a gas phase ozone molecule, the bridge configuration is stable by 0.82 eV while the atop configurations are in reality unbound, as they have binding potential energies of mere -0.05 eV and -0.06 eV. The ozone molecule is stable to dissociation by more than 1 eV, and it is therefore theoretically possible to saturate the surface with ozone. However, achieving a sufficiently perfect surface for this to be tested experimentally would require some effort.

The bond lengths in the different adsorbed ozone complexes reflect the surfaces valence, see Fig. 4.11. The bridge complex and the atop complex having two bonds to the surface (O_3(top$_2$)) are symmetric in nature and similar to the two most stable O_2 adsorption configurations only with an added atom. Bond lengths in the molecule are the same for both configurations and increase as charge becomes available as 1.35 Å for the stoichiometric surface, 1.38 Å for the surface with one vacancy and one subsurface aluminum atom and 1.41 Å for the surface with a proper vacancy. For the free ozone molecule we find bond lengths of 1.29 Å and a bond angle of 118°. The bridge adsorbed ozone has a very similar bond angle which decreases as 120°, 119°, 116°as charge becomes available, whereas the atop configuration has a much smaller bond angle of 106°, 103°, 100°. The difference in binding energy is probably partially due to this difference and partially to the lower coordination in the atop site. The distances to the surface titanium atoms follow the trend but reversed; the stronger the charging, the stronger the bonding and the shorter the adsorbate-substrate distance. The distances are 2.12 Å, 2.04 Å, 1.92 Å for the bridge configuration and 2.14 Å, 2.06 Å, 1.99 Å for the atop configuration. The bridge configuration is very slightly asymmetric, with the shorter bond furthest away from the vacancy.

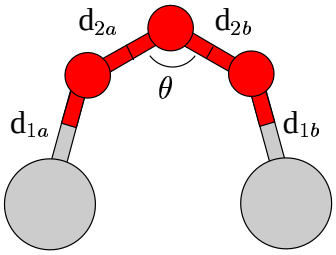

Parameter	Vacancy	Al vacancy	No defect
d_{1a}	1.92 Å	2.04 Å	2.12 Å
d_{1b}	1.90 Å	2.03 Å	2.12 Å
d_{2a}	1.41 Å	1.38 Å	1.35 Å
d_{2b}	1.41 Å	1.38 Å	1.35 Å
θ	116°	119°	120°

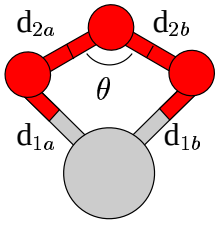

Parameter	Vacancy	Al vacancy	No defect
d_{1a}	1.99 Å	2.06 Å	2.14 Å
d_{1b}	1.99 Å	2.06 Å	2.14 Å
d_{2a}	1.41 Å	1.38 Å	1.35 Å
d_{2b}	1.41 Å	1.38 Å	1.35 Å
θ	100°	103°	106°

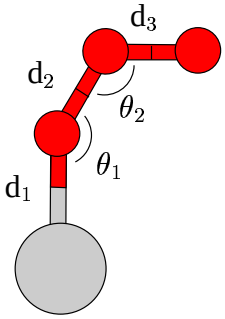

Parameter	Vacancy	Al vacancy	No defect
d_1	1.62 Å	1.69 Å	1.89 Å
d_2	2.37 Å	2.04 Å	1.51 Å
d_3	1.23 Å	1.21 Å	1.25 Å
$\theta 1$	158°	157°	155°
$\theta 2$	104°	118°	118°

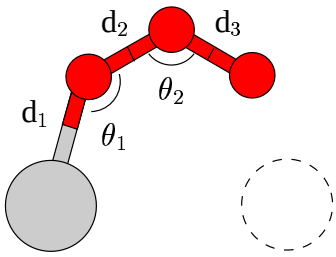

Parameter	Vacancy	Al vacancy	No defect
d_1	1.91 Å	2.07 Å	n.a.
d_2	1.40 Å	1.36 Å	n.a.
d_3	1.49 Å	1.44 Å	n.a.
$\theta 1$	127°	125°	n.a.
$\theta 2$	114°	116°	n.a.

Figure 4.11: Bond lengths of the four most stable O_3 complexes in environments of different charge. Above, the bridging configuration, followed by the doubly coordinating atop configuration, the singly coordinated atop configuration and the vacancy coordinating configuration.

The other atop adsorbed configuration and the configuration where the ozone molecule is adsorbed in the vacancy are very different in nature. They both primarily coordinate to one titanium atom on the row. The distance between this atom and the nearest oxygen atom reflects the charge state of the surface as 1.89 Å, 1.69 Å, 1.62 Å for the atop configuration and 2.07 Å, 1.91 Å for the vacancy coordinating one. In the molecule adsorbed on the row the bond between the oxygen atom binding to the substrate and its neighbour in the molecule is very extended, ranging through 1.51 Å, 2.40 Å and 2.37 Å as charge becomes available. When singly or doubly charged, the molecule is hardly coherent anymore, as the bond is so long that the complex should rather be described as an oxygen molecule loosely adsorbed on an adsorbed O atom. As can be seen from Table 4.5, the atop configuration is indeed less stable than if the bond extended further, leaving the O_2-like part to drift off into the vacuum. This could be a precursor states to desorption. One could visualize the ozone adsorbed in the bridge site capturing an electron released by photo-excitation, breaking one bond with the surface and letting this part of the molecule desorb.

The possibility of poisoning by annealing the vacancy sites arises here. Possibly this process is part of the reason that TiO_2 with platinum clusters is more active for ozone oxygenation; here, the defects cannot simply be annealed away. However, since that study has been done on a powder sample with an anatase structure rather than a rutile, comparisons should not be attributed too much weight. Rather, our investigation exemplify how the substrate charge state reflects on the adsorbate stability in a way that may lead to dissociation.

4.12 Exchange correlation

The choice of exchange correlation potential is the only true approximation involved in density functional theory. Even errors from pseudopotentials could in principle be eliminated by including all electrons as valence electrons. To give an estimate of the error introduced in the binding energies of oxygen on titanium, the adsorption potential energies have been calculated for different exchange-correlation functionals, see Table 4.6. The values calculated are not completely self-consistent. In principle, the lattice constants, relaxations and bond lengths should have been calculated separately for all three functionals as should electronic densities in the subsequent calculations to derive adsorption potential energies. However, we are only interested in an estimate of the error introduced by the description of the exchange correlation. Therefore, we have simply optimized the structures and calculated the electronic density using PW-91 and only in the last step in calculating the energy used different functionals. As described in Chapter 2, this gives a reasonable estimate of the binding energies with an error of the order of 0.25 eV for LDA, better for RPBE. As RPBE is created to be similar to PW-91, this is expected. If binding does not happen or is very weak, the three different functionals yield almost identical results. Otherwise, LDA gives the stronger binding energies which is a well established phenomenon. RPBE gives slightly smaller binding energies than PW-91. The difference between the two GGAs is at most 0.7 eV. The relative difference between binding energies is smaller. RPBE favours the top configurations slightly

more than PW-91, approximately 0.1 eV for both configurations. On the contrary, LDA favours the bridge configuration. In summary, we expect the GGAs to give adsorption energies closer to experimental ones. The error in adsorption energies, we expect to be at most 0.75 eV. When establishing the most favourable adsorption site, error is expected to be around 0.1 eV, since we then compare adsorption energies relative to each other. Changing the GGA to RPBE would change none of the conclusions in the this chapter.

Adsorbate	Vacancy		
	LDA	PW-91	RPBE
O	-2.10 eV	-1.84 eV	-1.75 eV
O_2(top)	-2.25 eV	-1.59 eV	-1.27 eV
O_2(brd)	-2.65 eV	-1.74 eV	-1.27 eV
O_3(top_1)	-1.70 eV	-1.11eV	-0.85 eV
O_3(top_2)	-1.96 eV	-1.03 eV	-0.54 eV
O_3(vac)	-3.57 eV	-2.31 eV	-1.59 eV
O_3(brd)	-2.84 eV	-1.58 eV	-0.90 eV

Adsorbate	Aluminum vacancy		
	LDA	PW-91	RPBE
O	-0.18 eV	-0.21 eV	-0.19 eV
O_2(top)	-1.19 eV	-0.80 eV	-0.52 eV
O_2(brd)	-1.35 eV	-0.69 eV	-0.25 eV
O_3(top_1)	-0.37 eV	0.09 eV	0.34 eV
O_3(top_2)	-1.04 eV	-0.08 eV	0.46 eV
O_3(vac)	-2.20 eV	-1.05 eV	-0.36 eV
O_3(brd)	-1.89 eV	-0.74 eV	-0.08 eV

Adsorbate	Stoichiometric surface		
LDA	PW-91	RPBE	
O	1.61 eV	1.67 eV	1.76 eV
O_2(top)	0.16 eV	0.56 eV	0.89 eV
O_2(brd)	-0.12 eV	0.36 eV	0.73 eV
O_3(top_1)	0.80 eV	1.26 eV	1.54 eV
O_3(top_2)	0.45 eV	1.27 eV	1.77 eV
O_3(brd)	-0.54 eV	0.50 eV	1.13 eV

Table 4.6: Adsorption energy dependence on exchange correlation potential. All electron densities are calculated self-consistingly using PW-91 and structures use PW-91 bond lengths.

CHAPTER 5

Species on the surface

The charge state and relative electrophillicity turns out to be a key feature in explaining TPD spectra. Oxygen adsorbs on the surface molecularly. Adsorption is precursor mediated. After adsorption, oxygen may dissociate if sufficient charge is present that the resulting atomic oxygen species can have a charge of two electrons. As dissociation happens at different rates at different temperatures, different atomic-to-molecular oxygen ratios are observed. Diffusion of molecular oxygen adsorbates is reported from STM measurements. The diffusion of vacancies is only partially described by DFT; barriers exceed 1 eV and thus are inconsistent with observed rates. Diffusion barriers are seen to depend on the adsorbate-to-vacancy ratio. A charge transfer driven diffusion process is suggested to explain STM data. This model is to some degree supported by theory. The assignment of observed STM signatures to ozone, coexisting on the surface with molecular oxygen, is not supported by calculations. Attributing the same signatures to atomic oxygen and a Schottky defect is more consistent with calculations. The question remains open.

5.1 TPD experiments

From the work of Henderson [72], the surface chemistry of TiO_2 appears relatively simple. At lower temperatures (120 K) the molecular adsorption of O_2 is precursor-mediated. Some molecules adsorb irreversibly, others reversibly with a desorption temperature of 410 K. The irreversible adsorption is attributed to dissociative adsorption, oxidizing the vacancies. This is based on the EELS feature from the vacancies vanishing. The EELS feature is attributed to charge transfer to the Ti atoms immediately beneath the vacancy. However, we know from calculations that electrons also transfer from the vacancies to the titanium rows. When this charge is transfered to adsorbates, it may be seen in the spectra as the oxidation of Ti^{3+} to Ti^{4+}. Therefore, it is possible that some vacancies remain, but their charge is located entirely on oxygen adsorbates. For dissociation of O_2 to happen, the resulting atomic species must have a charge of two; otherwise, dissociation is endothermic. This evaluation is based on the stability of O and O_2 relative to surface valence, see Fig. 5.1 and Chapter 4, section 4.9 and 4.11. If four electrons are present per oxygen molecule, the binding energy will be roughly twice the adsorption potential energy of a doubly charged oxygen atom, or -3.8 eV, whereas the charge of O_2 does not increase above two electrons, giving an adsorption potential energy of -1.7 eV, see Fig. 5.1a. However, if only two electrons are present, the adsorption potential energy of O_2 remains -1.7 eV, whereas the adsorption potential energy of the two oxygen atoms drop to -0.4 eV, so that dissociation is now endothermic by 1.3 eV, see Fig. 5.1b. As a consequence of the charge restrictions, the original O_2, which must be charged by at least one electron to be stable, needs three additional electrons from the surface to dissociate. As charge is limited on the surface, not all adsorbed molecules can dissociate. At 120 K, approximately one molecule per vacancy is found to dissociate. This lead us to suspect the surface of Henderson to contain some sub-surface vacancies, as each vacancy supplies at most two electrons. This is in agreement with findings by two-photon emission [67] for the surface treatment in question (sputtering).

Even without knowing precisely the adsorbate to vacancy ratio in Hendersons experiment, we can give a qualitative picture of what happens on the surface after oxygen exposure. The process is illustrated in Fig. 5.1c. As the surface is heated, as many molecules as the surface can supply with charge are converted to atomic oxygen. Since the dissociation rate is dependent on temperature, one would expect to find a temperature dependence of the ratio of atomic oxygen to molecular oxygen, because a dissociated molecule poisons the surface to additional oxygen adsorption four times as effectively as a molecularly adsorbed molecule, requiring four times as much charge. Above a certain temperature, dissociation should happen so fast that all oxygen dissociates instantly after adsorption, leading to a surface occupied only by oxygen atoms. This temperature dependence is indeed seen. The TPD desorption peak for O_2 desorption vanishes gradually as deposition temperature is increased from 100 K to 180 K. At 180 K, it has totally vanished. The dissociation now happens so quickly after adsorption that the surface is totally poisoned by atomic oxygen.

If the reaction $4O_2^-(\text{surf}) \rightarrow 3O_2(\text{gas})+2O^{2-}$ took place, the surface would be covered by atomic oxygen independent of adsorption temperature. This reaction is energetically allowed, but the transition state is not easily accessible; all three oxygen atoms

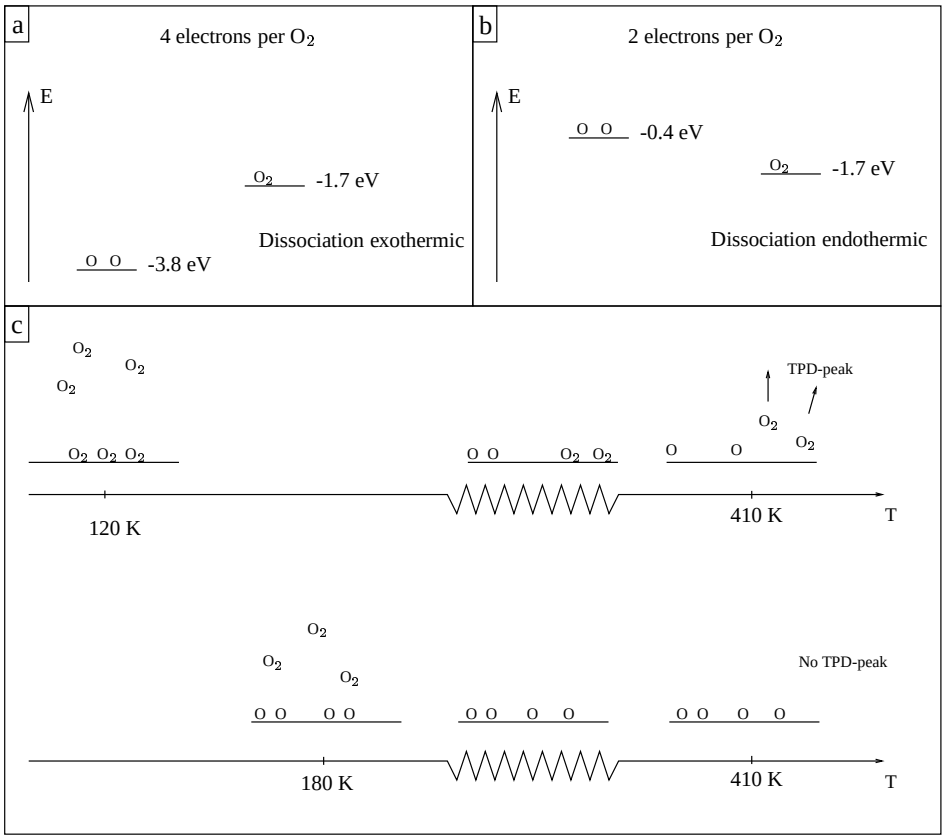

Figure 5.1: a) Adsorption potential energy of two oxygen atoms and one oxygen molecule, if four electrons can be supplied per oxygen molecule. Dissociation is exothermic. b) Adsorption potential energy of two oxygen atoms and one oxygen molecule, if only two electrons can be supplied per oxygen molecule. Dissociation is endothermic. c) The deposition temperature dependence of the adsorbed O_2/O ratio. At low temperatures, dissociation happens slowly enough that oxygen coverage exceeds one molecule per two vacancies. Thus not all oxygen acquires charge enough to dissociate and some desorb in a TPD peak at 410 K. At higher temperatures, dissociation happens effectively instantly, and only dissociated oxygen populates the surface, poisoning it to molecular oxygen adsorption.

have to desorb at exactly the same time, otherwise it is energetically prohibited. This may be why it does not occur.

5.2 STM measurements of vacancy diffusion

Schaub *et al.* [75] recently demonstrated that high oxygen vacancy mobility at and below room temperature is mediated by the presence of an adsorbate that they believe is adsorbed molecular oxygen. On a reduced surface, O_2 molecules were observed to bind in Ti rows and diffuse along them. According to the interpretations of the STM study [75] a diffusing O_2 molecule that encounters a bridging oxygen vacancy follows one of four different pathways:

- O_2 passes the vacancy with no apparent interaction.
- O_2 anneals the vacancy, leaving a transition state complex on the row. This recombines either with the original oxygen atom or with the one in the row on the other side of the Ti row, drawing it out onto the Ti row and leaving the vacancy. The latter process leads to the diffusion of the vacancy to a neighbouring row of bridging oxygen atoms.
- O_2 passes through the vacancy.
- O_2 passes through the vacancy. On the new titanium row, it anneals the vacancy, leaving a transition state complex on this row. It then recombines with a bridging oxygen atom, drawing it out onto the Ti row and leaving the vacancy. If it recombines with the one across the Ti row, the vacancy has diffused.

We have investigated the possibility of this process happening by ordinary phonon-mediated diffusion and by charge transfer mediated diffusion.

First, we briefly investigate the possibility of spontaneous vacancy creation. Simple constrained minimization, constraining the coordinate along the $[1\bar{1}0]$ direction (orthogonal to the bridging row, parallel to the surface), but leaving the atom free to relax both orthogonal to the surface plane and parallel to the row reveals a barrier of more than 4 eV for the process of spontaneous vacancy creation by bridging oxygen atoms relocating to the titanium row. A somewhat smaller, but still large, barrier of just above 2 eV is found to block vacancy creation by spontaneous diffusion of a bridging oxygen molecule to an in-plane oxygen. Wu *et al* [58] have done nudged elastic band calculations for this process and report a barrier of 2.87 eV.

For the diffusion through the vacancy and further along the row, we have done nudged elastic band calculations. Due to the size of the systems necessary to do converged calculations, we have been forced to modify the procedure somewhat. First, we do an ordinary NEB calculation in a small system of three tri-layers, one tri-layer relaxed and a surface unit cell of $p(3\times1)$. Then, we take the coordinates of the adsorbate in the critical points and transfer them to a larger system with four tri-layers, two relaxed. The adsorbate coordinates in the larger system are then kept fixed, while all other coordinates are allowed to relax. This gives us the adsorption energy in the critical points along the path. Then, we determine the force along the diffusion path from the new calculations and use it together with the energies to calculate splines connecting the points. The results are presented in Fig. 5.2b. The same procedure is used to obtain the barrier for dissociation in the vacancy, Fig. 5.2a.

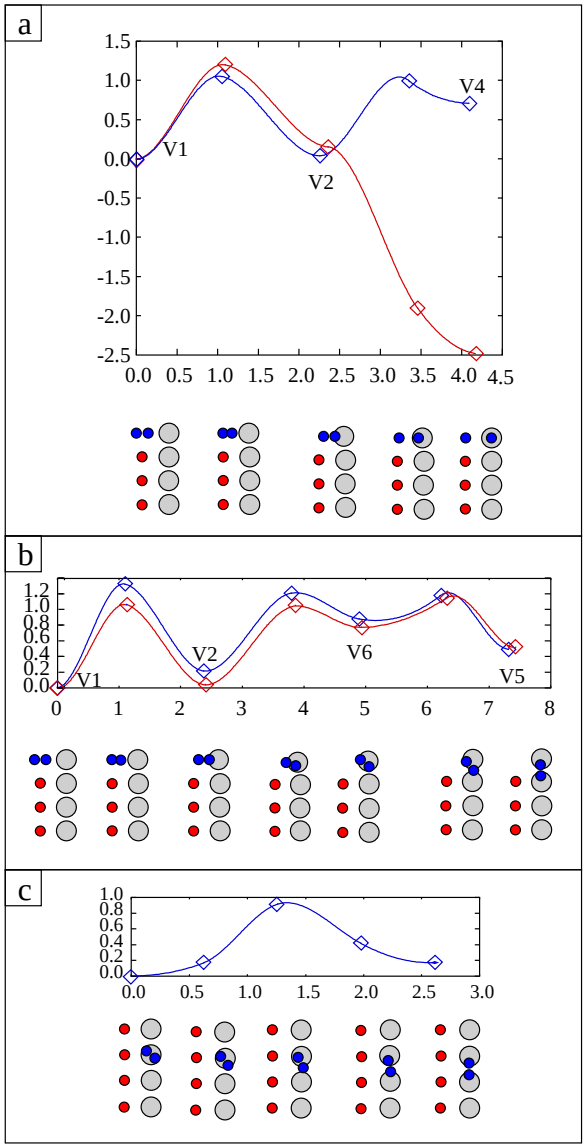

Figure 5.2: Barriers from NEB calculations (a and b) and constrained minimization (c). Diamonds represent calculated points; from the calculations we extract the force on the configurations and project it onto the path, thus deriving the negative energy gradient along the path. Using this information, we have connected the calculated points with cubic spline interpolations of the barriers, giving an estimate of the shape of the barriers. For a) and b), stable minima and transition states in the diffusion process have been recalculated in a $c(4\times2)$ (blue line) or a $c(6\times2)$ (red line) surface cell, four atomic layers slab, two relaxed. The $c(6\times2)$ contains two equidistant vacancies per surface cell, so that the vacancy structure is a $p(3\times1)$. For the constrained minimization scheme in c), see the text. Calculations were made in a $c(4\times2)$ surface unit cell.

The processes turn out to begin in the same way, following the same path to the stable V2 state. Here, the oxygen molecule binds both to the vacancy and to the titanium row atom. It is almost as highly charged as inside the vacancy. After this point, reached by crossing a barrier of 1.2 eV, the paths differ. Dissociation happens as the molecule extends the bond length until one atom is in the vacancy and one is adsorbed on the titanium row atom. Diffusion happens as the molecule instead begins rotating and moves outward towards the row. It encounters a shallow minimum sitting on the titanium atom directly in front of the vacancy, rotated by 45 degrees to the direction along the rows (V6). From there, it continues to its most stable configuration on the row, bridging two titanium atoms (V5). The barriers for both processes are almost the same as for the first step out of the vacancy, slightly smaller. Based on the assumption that the diffusing molecule is doubly charged, these barriers are calculated with no modifying donors in the cell, leading to doubly charged molecules with no spin. The reason for this choice of charge state is experimental indications that diffusion is activated by charge transfer to the adsorbate [83]. This point will be addressed in detail in section 5.3.

The diffusion along the row has a barrier of 0.6 eV if the molecule is doubly charged, see Fig. 5.2b. An estimate of the barrier for diffusion along the row if the molecule is singly charged can be made as follows. First, the diffusion path is assumed to be a straight line through configuration space. This path leads to unrealistically short bond lengths of the diffusing molecule in the transition state. Therefore, the path is modified by keeping the center of mass and the orientation of the diffusing molecule in all images, but changing the oxygen molecule bond length to increase linearly from the bridge to the top site. The molecule coordinates are then kept fixed and all other coordinates relaxed, just as in the modified NEB calculations above. This leads to a barrier of 0.9 eV for diffusion from the atop to the bridge site, see Fig. 5.2c. It is an upper estimate of the true barrier height but probably quite close to the real value.

In Chapter 4 it was demonstrated how very sensitive the stability of oxygen is to the surface valence. Therefore, we have investigated the barriers for diffusion and dissociation in both a $c(4\times2)$ unit cell with one vacancy (vanishing upon dissociation) and in a $c(6\times2)$ cell with two vacancies. In the case of diffusion, barriers change only very little, as expected since the molecule is already saturated with charge. Conversely, in the case of dissociation the barrier after the V2 configuration is reached vanishes altogether, and the reaction becomes very exothermic; 2.5 eV is gained, opposed to the loss of 0.6 eV in the case of no extra vacancy. The diffusion to the V2 state is then the limiting step. The diffusion along the row has a barrier of less than 0.5 eV. As a consequence, it appears possible that an oxygen molecule could diffuse along the row, encounter a vacancy, relax to the V2 state and from there dissociate with no barrier. 33 % is a large coverage of vacancies, though, and therefore the vanishing barrier only becomes relevant in the initial stages of adsorption when vacancies are abundant compared to the number of oxygen adsorbates. Also, it offers no explanation as to how an oxygen molecule would diffuse through the vacancy. The barrier for entering the vacancy would be less than 0.5 eV if the adsorbate never relaxed into the V2 state, simply passing it without releasing energy. Leaving it again, if once adsorbed there, would mean crossing a 1.2 eV barrier. This seems unrealistic. Nevertheless, no adsorbates are reported in the vacancies by Schaub *et al.*, and neither are defects that might be the V2 state. This opens the possibility that

diffusion is not phonon mediated but depends on another factor, for instance a charge transfer process.

5.3 STM measurements of diffusion on the rows

In a later paper, the same group (Wahlström *et al.* [83]) addresses the question of the diffusion mechanism of O_2 molecules on the TiO_2 surface. They report diffusion behavior apparently at variance with a simple phonon mediated diffusion. They have two pieces of evidence for this.

Firstly, in the conventional diffusion model, the hopping rate is described by

$$k = \frac{\omega_0}{2\pi} \exp\left(\frac{\Delta S}{k_\mathrm{b}}\right) \exp\left(-\frac{E_a}{k_\mathrm{b}T}\right) \tag{5.1}$$

where T is temperature, k_b is Boltzmann's constant, ΔS is the difference in entropy between the initial and final states, E_a is the energy in the transition state and ω_0 is the vibration frequency in the initial state. The prefactor, $\frac{\omega_0}{2\pi} \exp\left(\frac{\Delta S}{k_\mathrm{b}}\right)$, is normally of the order of 10^{12}-10^{14} s^{-1}. This number is inherent in the the shape of the barrier. The distance between initial and final states is usually a few Å and the barrier height 0.25-1.0 eV. As the vibration frequency is determined by the curvature of the potential, the frequency stays within this range. ΔS is normally approximated by 0, making the exponential 1. Wahlström *et al.* [83] find a prefactor of the order of 10^6.

Secondly, the scatter of hopping rates is rather large and turns out to be correlated to the coverage of vacancies.

The low prefactor and vacancy coverage dependence lead to the conclusion that diffusion is not well described by the conventional model. Instead the authors suggest a diffusion mechanism involving charge transfer, partially based on TiO_2 being used in photo-catalysis and known to catalyze a long range of interactions. In this model, the capture of an electron induces a jump to the neighbouring site. The simplest hypothesis is:

$$\begin{aligned}
\mathrm{O}_2^-(\mathrm{top}) + e^- &\rightarrow \mathrm{O}_2^{2-}(\mathrm{top})[\mathrm{metastable}] \\
&\rightarrow \mathrm{O}_2^{2-}(\mathrm{bridge}) \\
&\rightarrow \mathrm{O}_2^-(\mathrm{bridge}) + e^-[\mathrm{metastable}] \\
&\rightarrow \mathrm{O}_2^-(\mathrm{top}) + e^-.
\end{aligned}$$

Before the first electron capture, O_2 is singly charged, occupying the lowest energy configuration, the top site. Then, it captures an electron, becoming doubly charged. The electron capture happens fast, compared to the time scale of ionic movement. Therefore, O_2 is in a metastable state, its bond length still that of a singly charged molecule. The energy minimum for a doubly charged oxygen molecule is the bridge site; consequently, the adsorbate relaxes to this position. The energy released as the bond length accommodates to the new charge state helps overcome the barrier. In the bridge site it loses an electron again and relaxes to the top site. The adsorbate has now diffused one lattice

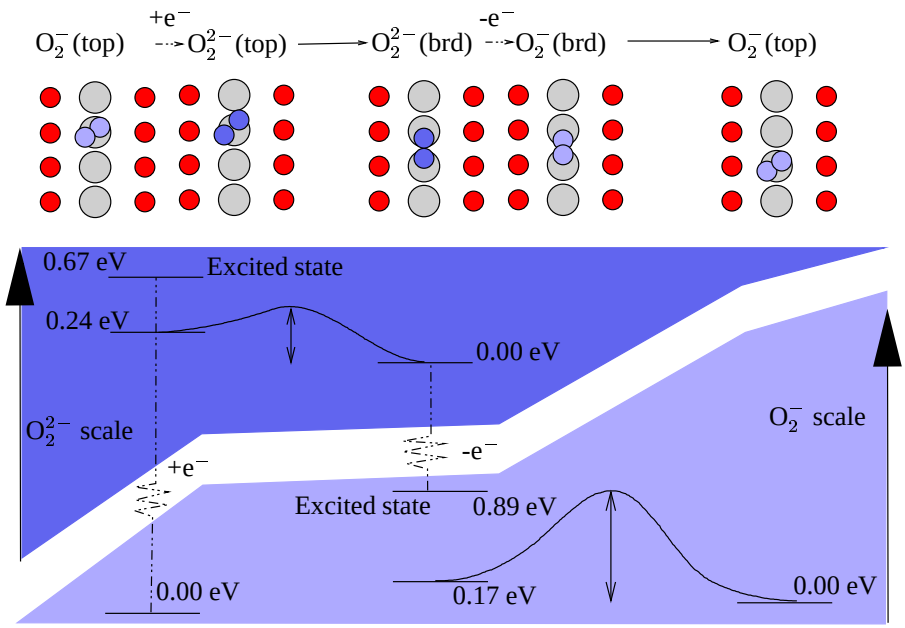

Figure 5.3: The diffusion hypothesis and corresponding calculated energies. Small red circles are bridging oxygen, larger grey circles are in-plane titanium atoms. Small, blue atoms are oxygen atoms being a part of a singly (lighter) or doubly (darker) charged adsorbate. Notice the difference in energy scales between doubly charged (dark blue area) and singly charged (light blue area) adsorbates. The longer bond lengths in the schematics of doubly charged states reflect the actual adsorbate lengthening.

spacing (or relaxed back to its original position). Fig. 5.3 shows this process, presenting the energy differences between top and bridge site and the barriers involved in crossing them, depending on the charge state of the molecule. The excited state energies are calculated by freezing all atoms in place and recalculating the energy for the configuration with the new charge state. This is likely to overestimate the energies slightly, as the relaxation energy from relaxations around the artificial dopant are included in the calculation. To make these kind of calculations possible at all, we have represented the singly charged case by a vacancy with an aluminum atom in the slab and the doubly charged case by a vacancy. The barrier for the doubly charged adsorbates has been calculated in a system containing one vacancy, whereas the singly charged adsorbates have been calculated in a system containing a phosphorus substituent, to simulate the stoichiometric surface as well as possible. Notice the difference in energy scales between dark and bright regions; systems containing different donor types cannot be directly compared.

It is very tempting to conclude that the change in site preference triggers the diffusion, as every time the adsorbate has lost or gained an electron, it is in an energetically prohibited site. However, the energy differences between sites are small compared to the differences in energy due to the different possible choices of exchange correlation

potential. Using RPBE reveals the same trends as PW-91, though it favours the top configuration slightly stronger than the bridge configuration, leading to an equal adsorption energy in the two configurations for a doubly charged molecule. Adsorption energies are also in general lowered between 0.4 and 0.7 eV. Most likely, diffusion is rather triggered by the adsorbate being in an unfavourable *configuration*. When the molecule accepts charge, it no longer has the optimal bond length and the energy released as the bond accommodates helps in the diffusion. Additionally, the barrier is lower in the doubly charged case.

A similar process allows diffusion through a vacancy:

$$\begin{aligned} \mathrm{O}_2^-(\mathrm{top}) + e^- &\rightarrow \mathrm{O}_2^{2-}(\mathrm{top}) \\ &\rightarrow \mathrm{O}_2^{2-}(\mathrm{vac}) \\ &\rightarrow \mathrm{O}_2^-(\mathrm{vac}) + e^- \\ &\rightarrow \mathrm{O}_2^-(\mathrm{top}) + e^-. \end{aligned}$$

The electron capture process now serves to drive the adsorbate into the vacancy, occupying the V1 configuration. As soon as the second electron is lost, however, this is no longer a stable position, and the adsorbate relaxes into either the row it came from or the one on the other side of the vacancy. Possibly some adsorbates relax while in the vacancy to the more favourable V3 state where the oxygen molecule is sitting orthogonal to the surface. The respective energy differences driving the diffusion are larger in this case, adsorption in the vacancy being favoured by 0.7 eV and prohibited by 0.4 eV in the divalent and monovalent vacancy, respectively, under the hypothesis that the adsorbate doesn't relax to the upright position in the vacancy. In the case of relaxation to the upright V3 configuration, the adsorbate is equally stable on the row and in the vacancy, and therefore the crossing of a barrier would be involved in leaving the vacancy. These values might describe only the qualitative trend that the monovalent vacancy is a much less favourable adsorption site than the divalent. As we have no exact knowledge of the surface charge state, this cannot be simulated.

5.4 STM measurements of different species

From the work of Henderson, two kinds of adsorbates are expected on the surface after low temperature oxygen exposure, atomic and molecular oxygen. Nevertheless, Vestergaard [102] observes a multitude of different species in STM, some of which can only be distinguished by their diffusion characteristics. The species group into two kinds, primary and conglomerates. The two primary species the author terms the β and γ species. γ diffuses at room temperature and mediates the diffusion of vacancies. The author assigns it to molecular oxygen, as described above. Its STM signature is small and centered on the atop position on the Ti rows. The β species has a larger STM signature and does not diffuse. A lot of other species are resolved by STM movies as conglomerates of γ and β species. Both the $\gamma\gamma$ and $\gamma\beta$ species diffuse. Vacancies are present on the surface, and the large conglomerates can react with these, following the reaction $\gamma\gamma \leftrightarrow \gamma\beta + \mathrm{vac}$. None of these species desorb in the TPD peak [132], and consequently,

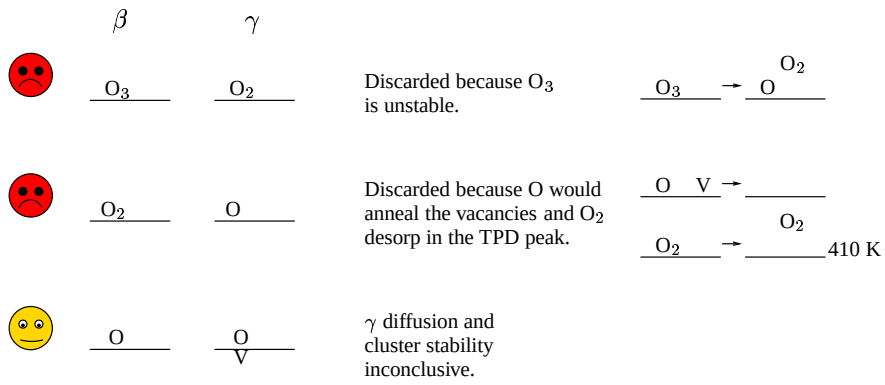

Figure 5.4: Different possibilities for the designation of β and γ species. The symbol V designates an oxygen vacancy.

another species has to exist. This invisible entity is termed α. To be consistent with the work of Henderson, it has to be an oxygen molecule, as the TPD peak is first order. In the following, we will attempt to give a consistent model of the oxygen content of these species.

5.4.1 Standard interpretation

γ as O_2, β as O_3

Vestergaard [102] designates γ as O_2. From the observed reaction $\gamma\gamma \leftrightarrow \gamma\beta + \text{vacancy}$, he deduces that β must contain one oxygen atom more than γ, as the number of oxygen atoms must be conserved. Unless charge is very scarce on the surface, we must discard this possibility on the basis of our calculations for ozone. Under charge rich conditions, the O_3 molecule is unstable towards dissociation and an oxygen molecule is unstable when located next to an oxygen atom. Thus, the β species would fall apart.

If charge is very scarce, it is hard to explain how ozone is created. A simple mechanism begins by one molecular oxygen dissociating on the surface. Subsequently, two additional oxygen molecules adsorb, one on either oxygen atom. This way, two ozone molecules would have formed. However, this picture does not hold. Charge has to be sufficiently ample to have the molecule dissociate in the first place. The two oxygen atoms on the surface are then doubly charged. Because doubly charged oxygen atoms are quite inert, they would never form ozone. It is very unlikely that they would become singly charged and reactive again, if they have at some point been doubly charged. This process would be similar to a molecule spontaneously breaking down into free radicals. Another way of forming ozone would be three oxygen molecules meeting and forming two ozone molecules. This cannot be ruled out but appears very unlikely.

Additionally, the β species are reported to adsorb in an atop site. Independent of charge state, we have been unable to find a configuration of ozone or any other complex containing three oxygen atoms which is more stable than the bridge ozone configuration.

Thus, we regard the assignment of β as ozone as questionable.

γ as O, β as O_2

Considering Hendersons results, the most inviting possibility is γ being atomic oxygen and β being molecular oxygen. Both these species are stable on the surface, if sufficient charge is present. However, this is problematic in the light of the vacancy diffusion mediating properties of the γ species. As described above, on encountering a vacancy, γ follows one of four pathways:

- γ passes the vacancy with no apparent interaction.
- γ anneals the vacancy, leaving a transition state complex on the row, which recombines either with the original oxygen atom or with the one in the row on the other side of the Ti row. The latter process leads to the diffusion of the vacancy to a neighbouring row of bridging oxygen atoms.
- γ passes through the vacancy.
- γ passes through the vacancy, and on the new titanium row anneals the vacancy, leaving a transition state complex on this row, and then recombining with a bridging oxygen vacancy.

The first (non)reaction is unproblematic. However, if an oxygen atom anneals a vacancy, there is nothing left to create a transition state complex, and the reaction would end there. The vacancy would simply be filled. Likewise, it is hard to imagine how an oxygen atom might diffuse through a bridging oxygen vacancy without simply thermalizing in the vacancy and annealing it. Thus, the possibility of γ being a single oxygen atom is discredited on this basis alone. The molecular oxygen as β is also problematic, as the barrier for thermal diffusion is around 0.5 eV, and the β is therefore likely to diffuse at room temperature. For a prefactor in the typical range of 10^{12}-10^{14} s^{-1}, the predicted hopping rate is of the order of 500-50000 s^{-1}. Additionally, β should be singly charged (if there is enough charge to supply them with two electrons, they would be more favourably residing in the vacancies). They then have an adsorption potential energies of -0.8 eV, and should then desorb at temperatures around 410 K - they ought to vanish in the desorption peak. Thus, this model is discarded.

γ as a Schottky defect, β as O

Discarding the two previous models forces us to look for a model where none of the species visible in STM are O_2. We have already ruled out the possibility that γ was an oxygen atom. From the work of Henderson, we expect that atomic oxygen is present on the surface. Thus, we now assign β to atomic oxygen. Because the reaction $\gamma\gamma \leftrightarrow \gamma\beta + \mathrm{vacancy}$ happens and is reversible, γ must contain one oxygen atom less than the β species. Consequently, γ should now contain no atoms. The only way of realizing this is letting γ be a perturbation of the surface. The most realistic is a Schottky defect, which is a sub-surface vacancy coupled with an O atom on the surface. If this is to appear as an

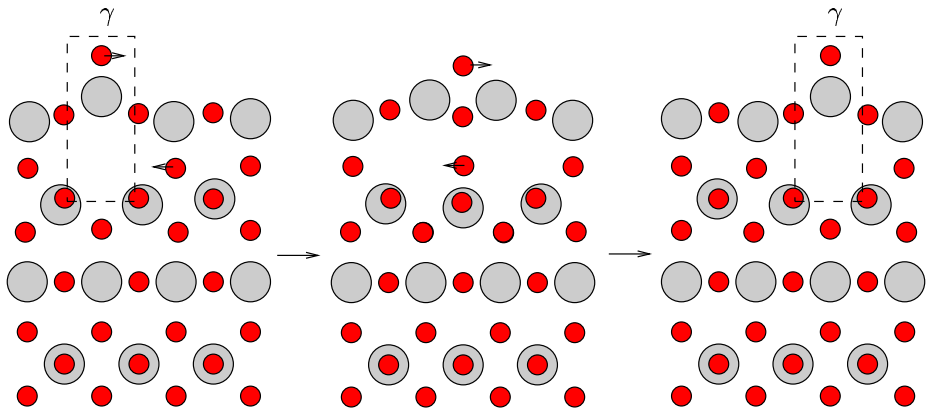

Figure 5.5: Schematic of a possible diffusion path for a Schottky defect along the titanium rows. In-plane oxygens has been indicated, even though they are out of the plane of the titanium row.

adsorbate adsorbed in the atop site on the row, the most likely possibility is an oxygen atom atop a second tri-layer bridging oxygen vacancy. This could be created in several different ways. Creation as a Schottky defect, moving the lattice oxygen to the surface, is endothermic by 2.60 eV. Therefore, these defects are unlikely to arise at temperatures below room temperature. However, if sub-surface vacancies exist already at oxygen exposure, as studies indicate [67], the presence of oxygen makes it favourable for them to diffuse to the surface. Therefore, a combination of an oxygen atom and a sub-surface vacancy could be created by a vacancy diffusing to the site beneath the atom, or the presence of the vacancy could induce the diffusion of the atom to the proper site. The defects may also be created at the time of adsorption by an oxygen molecule dissociating on top of a sub-surface vacancy, possibly drawing it up as part of the process.

As the creation of this kind of defect seems possible, we move to investigate whether this γ fulfills the criteria for diffusion. γ should be able to diffuse along the row. The most likely diffusion path (in the light of the diffusion of second tri-layer bridging oxygen vacancies described in Chapter 3) is the whole γ moving simultaneously, see Fig. 5.5. Here, the oxygen atom on the surface moves from one titanium atom to the next simultaneously as the second tri-layer oxygen atom beneath the final configuration titanium moves to occupy the original vacancy site. An estimate of the barrier for this diffusion is the energy difference between γ and a configuration with the adsorbed O moved to a bridge site and the diffusing lattice oxygen directly below, see Fig. 5.5. In a charge poor environment, simulated by adding an aluminum atom to the slab, the energy difference exceeds 3 eV. This effectively rules out the possibility for phonon induced diffusion. Since atomic oxygen is assumed to be present, we assume charge is relatively abundant. In a neutral environment, simulated by no artificial donors in the cell, the difference is 1.48 eV. This is still too large to allow phonon-induced diffusion. As can be seen from the Figure, the transition state essentially consists of two vacancies, rather than one, and thus, a barrier of the order of a vacancy creation energy could be expected.

Wahlström *et al* suggest the process to take place as a result of a charge transfer. It is unlikely that this diffusion is of the same kind as that illustrated above for oxygen molecules where the charge transfer makes the transition configuration more favourable than the initial configuration. More likely, the charge transfer is accompanied by an energy transfer as well. In light of the large change in barrier size above it seems likely that changing the charge of the surface would change the barrier. This may involve charge transfer to nearby vacancies or adsorbates. However, the investigation of this problem is so complicated that is has to be postponed, with regret, for later study.

The critical property of γ in the previous model was the diffusion through the vacancy. In this case, likewise. The process of γ annealing the vacancy, leaving a complex on the row, can be explained simply by the row oxygen atom jumping into the vacancy, leaving a highly reactive titanium atom just above the second tri-layer vacancy. The energy difference between these two configurations is only 0.19 eV, in favour of the γ configuration - it is more favourable to have the bridging oxygen vacancy and an adsorbate on the row titanium above the sub-surface vacancy than to anneal the bridging oxygen vacancy and leave the sub-surface vacancy uncovered! This is interesting in relation to the vacancy-creating reaction. Thus, vacancy diffusion is possible. The problem arises in the case of diffusion through the vacancy. As the adsorbed oxygen atom enters the vacancy simultaneous with the diffusion of the vacancy to the opposite titanium row, no driving force remains to recreate the γ on the other side. If the γ enters the vacancy by annealing the bridging oxygen vacancy and transferring the second tri-layer bridging oxygen vacancy to a second tri-layer layer in-plane oxygen vacancy, the energy gain is 0.93 eV, if no extra donors are present in the cell. If the vacancy diffuses to the first tri-layer sub-bridging vacancy, the energetic gain is even larger. However, these values may be misleading. If the surface is saturated by oxygen, the vacancies are empty of charge, and this may modify the picture. Envision that the charge from the original bridging oxygen vacancy is located on a nearby oxygen molecule. The bridging vacancy is annealed, and the oxygen molecule now receives charge only from the newly-created second tri-layer in-plane oxygen vacancy. This inhibits charge transfer. If the oxygen molecule now only has a charge of one electron, its binding energy decreases by roughly 0.9 eV. This binding energy decrease is exactly enough to make the two situations even out. If the bridging vacancy electrons were originally on an oxygen atom, the effect would be even more pronounced. This charge-buffer-function of adsorbates may be the reason that $\gamma\gamma \leftrightarrow \gamma\beta + \mathrm{vacancy}$ is seen, whereas $\gamma \leftrightarrow \beta + \mathrm{vacancy}$ is not. Thus, the evaluation of the diffusion properties of this choice for γ is inconclusive.

The γ and β species are observed to form larger clusters of molecules. The next step is to investigate whether these are stable. We first calculate the stability of these clusters in a relatively charge scarce environment, allowing only one electron per adsorbed oxygen atom. We do this by inserting an aluminum atom for every γ species and a phosphorus atom for each β species. Using a surface unit cell of $c(6\times2)$ to allow space between clusters, the $\gamma\gamma$ cluster is favourable by 0.31 eV, compared to two γ separated by one lattice constant. Thus, this cluster should be able to combine and dissolve as is is seen. The $\gamma\beta$ cluster is unstable by 0.49 eV, compared to a γ and a β, separated by one lattice constant. However, if the two top atoms recombine to a molecule in a bridging configuration, the cluster becomes favourable by 0.88 eV. We do not believe

charge is actually this scarce. Preliminary calculations using two phosphorus atoms in each cell indicate that the $\gamma\beta$ cluster is unstable if charge is ample. This is consistent with the calculations in the previous chapter. We know that molecular oxygen is stable against dissociation as long as charge is not ample but may dissociate if it is. This indicates that $\gamma\beta$ clusters probably form and disintegrate as a result of charge transfer processes to other surface species or defects. Another possibility is that the charge state is somewhere in between, so that the γ and β can form a pseudo-bond.

In this model, the α species, which desorb in the TPD peak, is simply singly charged oxygen molecules. As they have adsorption energies of approximately 0.8 eV and the TPD peak is found at a temperature equivalent to a desorption energy of 1.1 eV, this is consistent with experiment.

We conclude that a model having β as atomic oxygen and γ as a Schottky defect functions well in the description of the creation of the species on the surface during deposition. The formation of clusters is not sufficiently well described but seems consistent. We have only made very preliminary calculations analyzing the diffusion of the γ species on the surface. They indicate that a satisfactory treatment of the problem would involve nudged elastic band calculations to determine diffusion pathways as well as calculations with varying amount of accessible charge on the surface.

5.4.2 Alternative interpretation

In all of the models above, the β species has one oxygen atom more than the γ species, based on the observed reaction $\gamma\gamma \leftrightarrow \gamma\beta + \mathrm{vacancy}$. This critically depends on the point defects designated as vacancies actually being empty vacancies. Suppose that defect has some other character, F, the reaction becoming $\gamma\gamma \leftrightarrow \gamma\beta + \mathrm{F}$. We now find that $\beta = \gamma - \mathrm{F}$. If $\mathrm{F} = \mathrm{vacancy}$, then $\beta = \gamma + \mathrm{O}$, but other defects are also possible. We already know that the surface contains a number of invisible α species, which are molecular oxygen. It is possible that all vacancies are filled with such molecules, or even that they are invisible in the vacancies, so that vacancies with and without oxygen molecules cannot be distinguished. This way, there would be no possibility to resolve that some reactions happened only at vacancies filled with O_2. Supposing that the vacancies are filled with O_2, we get $\beta = \gamma - \mathrm{O}$, and can revisit the models above. The possibility of γ as O_3 is ruled out because the molecule is not stable on the surface.

γ as O_2, β as O

This model explains the diffusion of vacancies (with O_2 in them) reasonably well. The diffusion through the vacancy simply happens by γ jumping into the vacancy and the O_2 from the vacancy jumping out, becoming a new γ. The diffusion of the vacancy to the neighbouring row happens by one oxygen atom from the vacancy O_2 moving to the row γ, creating an O_3 complex. The O_3 complex created is only 0.12 eV more favourable than the initial configuration, thus making the process seem possible. The diffusion of γ along the rows have already been described in detail above as a charge transfer induced process, and the formation of the species is simply molecular and dissociative adsorption.

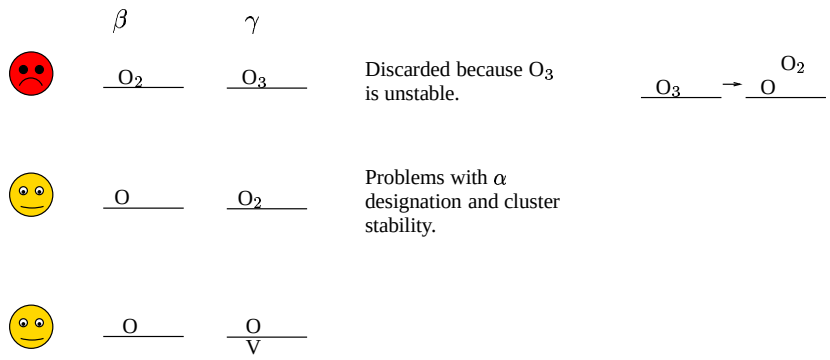

Figure 5.6: Different possibilities for the designation of β and γ species, if vacancies are filled with molecular oxygen. The symbol $\bar{\mathrm{V}}$ designates a second tri-layer bridging oxygen vacancy.

The main question in this case is the identity of the invisible α species. Vestergaard [102] attributes them to a physisorbed state, and this is of course a possibility. However, they would then be expected to desorb at lower temperatures. It could be that the difference is in the charge state, but this also does not seem plausible.

Turning to the creation of complexes in this model shows another weakness. In the section considering the co-adsorption of oxygen, we saw that atomic oxygen cannot coexist with molecular oxygen, unless charge is very ample. Thus, if one atomic oxygen species and one molecular oxygen species are present per vacancy, the molecular oxygen desorbs, meaning that the $\gamma\beta$ cluster is unstable. This would be remedied by introducing one vacancy per adsorbate. Consequently, this model describes a system with relatively few adsorbates, implying only few γ. From the data of Vestergaard, it seems unlikely, even if invisible sub-surface vacancies are present. He observes adsorbate-to-bridging vacancies ratios considerably above one.

γ as O, β as a Schottky defect

We already determined that it seems possible to create clusters from atomic oxygen atoms and Schottky defects. These would be $\gamma\beta$ clusters in this model also. $\gamma\gamma$ clusters could for instance be created by charge transfer processes. A $\gamma\gamma$ cluster could be a doubly charged oxygen molecule, which dissociates to two γ when sufficient charge is transfered.

One way for the vacancy diffusion to happen is by dissociating the oxygen in the vacancy, creating an oxygen molecule on the row. This molecule would likely be doubly charged, as this is the most likely charge state of the γ. The row O_2 would then dissociate, leaving one atom in the atop site and one on a bridging oxygen, leading the vacancy to diffuse. The diffusion through the vacancy would have to involve a ozone-like complex, because of symmetry. We have not yet done a systematic investigation of these processes.

5.4.3 Other models

If O_2 is truly invisible on the surface, vacancies with and without O_2 cannot be distinguished. Therefore, it is impossible to know if a process only happens if oxygen is already present in the vacancies. This opens the possibility that vacancy diffusion only happens at empty vacancies and vacancy creation and annihilation only happens if an oxygen molecule is present, and vice versa. In the 'γ as O, β as O_2' case, if vacancies only diffused when filled with O_2, the O would not necessarily anneal the vacancy. A mixed model would also present a very nice way of explaining the 'γ as O_2, β as O' case, if only empty vacancies diffused and only filled vacancies could be created and annealed. In neither case would it explain the elusive α-species.

It is also possible that the signatures attributed to vacancies are due to another kind of defect entirely, most probably involving hydrogen. This could be vacancies with a resident hydrogen atom or more likely a hydroxyl species. In this case, hydrogen may very well be present on the adsorbates also, changing oxygen atoms to hydroxyls and molecular oxygen to peroxide. Thoroughly investigating this eventuality is outside the scope of the present study.

CHAPTER 6

Conclusions and outlook

In this thesis, an investigation of the surface structure and oxygen chemistry of the rutile TiO_2(110) surface has been presented. The surface chemistry of oxygen turns out to be critically influenced by oxygen vacancies, the most favourable of which is the bridging oxygen vacancy. Relaxations around vacancies are large. They generally follow the pattern that nearby oxygen atoms relax towards the vacancies and titanium atoms away from it. When the vacancy is created, two electrons are freed to take part in different kinds of bonding. These electrons may leave the vacancy and relocate either to the titanium rows or to electrophillic adsorbates, such as oxygen. The relaxation around the vacancies is important to this property. If the atoms are not allowed to relax the charge transfer is inhibited. We have strong indications that the presence of oxygen on the surface induces the segregation of vacancies to the surface, as it has also been observed for sulfur.

Charge can travel along the titanium rows for great distances. As a consequence, the presence of vacancies activates the surface to oxygen adsorption for large areas. For typical experimental vacancy coverages, the whole surface should be activated. Oxygen adsorbs on the titanium rows or in the vacancies. Molecular oxygen can adsorb in two different charge states, either as a peroxo or superoxo species. These species are easily differentiated by evaluating bond length, magnetic moment and adsorption energy. The larger the adsorbate charge, the stronger is the binding. The trend is the same for atomic oxygen, but stronger. A singly charged oxygen atom on the surface appears to be very reactive. A given surface can only supply a certain amount of charge, typically determined by the number of surface and sub-surface defects. This amount of charge, rather than the number of free adsorption sites, determines how many adsorbates the surface can support, as adsorption as a neutral species is endothermic. Because dissociation of

a molecular species is only exothermic if the resulting oxygen atoms have a charge of two, a larger amount of oxygen can be adsorbed if it is adsorbed in molecular form. Consequently, if oxygen is adsorbed at low temperatures, more oxygen can be adsorbed than the surface can provide charge for the dissociation of. The adsorption energy for the stable molecular species having lowest charge is consistent with desorption around 410 K, as observed. If desorption happens at higher temperatures, dissociation can be expected to happen faster, and the surface never accepts molecular oxygen that it cannot provide charge to dissociate.

Observations using STM shows a lot of different oxygen species of the surface, some of which are conglomerates of other, less complicated species. The author of the study describes three primary species. He assigns them as O_3, chemisorbed O_2 and physisorbed O_2. We cannot support this assignment. We find that O_3 will dissociate if the surface is charge rich and is unlikely to form if it is charge poor. Assigning the species instead as atomic O, Schottky defects and superoxo species seems more promising. The creation of the Schottky defect is speculated to be possible by the oxygen induced vacancy diffusion. The diffusion characteristics are hard to evaluate, as experiment indicates that diffusion happens through a charge transfer process. This implies that the transition state complex is in an excited state. DFT gives information on the ground state only. However, we have presented a successful strategy for tailoring adsorbate charge by using donors and acceptors. We have strong indications that the diffusion barrier for the Schottky defect is highly sensitive to charge state. Because the diffusion path of the Schottky defect is expected to be complicated we are nevertheless not entirely satisfied with this. To improve the basis of the predictions we can give on Schottky defect diffusion characteristics, we believe NEB calculations should be done in systems of several different valences.

Some uncertainty exists as to the nature of the STM signature attributed to surface vacancies. Evidence exists that STM-invisible molecular oxygen is present on the surface. If these species remain invisible in the vacancies, species can be assigned in several different ways otherwise excluded. Here, the assignment of one species to molecular oxygen must be reconsidered. It appears promising, though problems arise in explaining the identity of the invisible state. Earlier work, both theoretical and experimental, have indicated that differentiating between e.g. bridging oxygen vacancies and bridging hydroxyls can be very difficult. If the vacancies are indeed filled with an adsorbate, the surface species may be contaminated by this adsorbate, and new calculations must be done to assign the species. In this context, it would be of great interest to obtain experimental evidence for the chemical nature of the species on the surface, as well as their charge state.

We must conclude from our results that intimate knowledge of the defects of the surface is needed to explain surface chemistry. Therefore, a great experimental effort lies ahead in determining how to prepare a crystal to obtain exactly the same kind of surface every time. These efforts are of course ongoing and indicate that it will prove a difficult and time demanding, yet feasible task.

This raises the question whether the study of single crystal surfaces will ever prove profitable in explaining catalysis in a production plant; will we ever be able to cross the gap to production conditions? In the present study, we have not even attempted to

address the influence of relatively simple defects such as step edges or dislocations. The influence of grain boundaries could be large, and the phase may even not be well known; what happens if the material becomes a mixture of anatase and rutile?

In the foreseeable future, we will be unable to know precisely what happens inside a reactor in a production plant. Nevertheless, information from single crystal studies can be of great value. An indication of this is that anatase and rutile appear to have many properties in common, even though the structure differs. On single crystals, we can establish the fundamental phenomena occurring. For instance, it is highly likely that when the charge state of the oxygen molecule is essential for the chemistry on the single crystal surface, it remains an important factor in a more complex system. It may be that high oxygen pressure will stabilize a neutral state on the surface. On the contrary, it is possible that high temperatures will boil oxygen molecules off. The latter question, we have already to some degree addressed by knowing the existence of the TPD peak. The ability of charge to travel for long distances along titanium rows is unlikely to change. Therefore, the charge state of the surface is likely to stay important. This charge state, our calculations indicate, can be tailored to the needs of the application. Indeed it is heavily influenced by the presence of metal particles (gold).

Since our approach still looks useful, future work presents itself. Self-interaction in our code may influence the charge transfer from the vacancies, because the self-interaction of vacancy electrons may induce them to leave the vacancy more easily. This question needs to be addressed. Therefore, the code should be rewritten, if possible, to allow for the exclusion of self-interaction. The diffusion of the Schottky defect should be investigated properly. Indeed, diffusion barriers between the different sub-surface vacancies should be established using NEB. All indications are that this will prove demanding in computational effort. Hoping to have understood the key features in the adsorption of oxygen on the surface, it would be highly interesting to delve into the chemistry of oxygen containing small molecules. Furthermore, it would be very useful to establish if the reactivity of the surface could be reliably tailored by using dopants. TiO_2 is far from the only oxide having a rutile phase. Making a comparison of the chemistry, in particular the charge transfer properties, of TiO_2 and SnO_2 would be of great interest because it would tell us how important the d-orbitals are in the charge transfer processes in TiO_2. Comparing to RuO_2 is also very likely to give important information. Therefore, a more systematic study of the rutile structure oxides would also pose a very interesting problem.

Acknowledgements

No thesis is written in a void; I am grateful to a number of people, who have helped and supported me through the last four years.

First and foremost, I am indebted to my supervisor, Bjørk Hammer. He has taken an active interest in all parts of my work and have always taken the time for questions and discussions. Likewise, he has been a source of inspiration and support in the periods where I felt my work appeared to be going nowhere, as well as in times when things were working out to my satisfaction.

During the four years of writing my thesis, several other theoreticians have worked in the group. I am grateful to Jakob Gottschalck and Zeljko Sljivancanin for helping me getting started using the DACAPO code and for fruitful discussions about theoretical surface science in general. On the TiO_2 system, I have worked closely together with Luis Miguel Molina and I am grateful for both his encouragement and his scientific input.

It has been a pleasure to work with the experimentalists from the CAMP group. In particular, I am grateful to Renald Schaub, Erik Wahlström, Ebbe Kruse Vestergaard, Anders Rønnau, Stefan Wendt and Flemming Besenbacher for explaining their work to me and voicing their opinions on mine. Being allowed to follow the experimental work so closely has been a unique experience and a continuing source of inspiration for my own work.

Several people are gratefully acknowledged for comments and suggestions during different stages of the making of my thesis. Bjørk Hammer, Luis Miguel Molina and Renald Schaub have all helped to enhance the clarity of the text by reading through parts of the thesis. Frauke Hümmelink, Birthe Rasmussen and Pelle Kofod have assisted in eradicating type errors and awkward grammar, and I am grateful for Peter Thostrup's help with Latex typesetting.

CHAPTER 7

Dansk resume

TiO_2 er et vigtigt materiale indenfor mange områder. Det er meget brugt i katalyse, både som support og katalyst. For eksempel er små guldklynger på TiO_2 meget lovende som katalyst for oxidering af CO. Mange eksperimentelle studier af iltkemien på enkeltkrystaloverflader har efterladt ubesvarede spørgsmål. Nogle af disse kan vi kun forvente besvaret ved at lave teoretiske modeller. Kvantemekanisk modellering har indtil videre givet gode resultater i beskrivelsen af overfladestruktur og -reaktivitet, og vi opmuntres derfor til anvende tæthedsfunktionalteori til at studere iltadsorption på (110) overfladen af rutil.

I følge Hohenberg og Kohns sætning er elektrontætheden af et bundet system i grundtilstanden entydigt bestemt af potentialet. Derfor er al information om systemet i princippet iboende i den elektroniske tæthed. Denne indsigt kan bruges til at konstruere en metode til selvkonsistent at bestemme elektrontætheden og dermed energien i grundtilstanden med meget mindre beregningsbyrde end der ville være involveret i at løse den tilsvarende mangelegeme Scrödingerligning. Hvis vi kendte den præcise form af exchange-correlation (ombytnings- og korrelationsenergien) for systemet ville metoden være eksakt. Da dette ikke er muligt, har der været forskellige forsøg på at konstruere en tilnærmet funktionsform for denne. Andre tilnærmelser er nødvendige for at kunne anvende beregningsproceduren i praksis. Når man ønsker at beskrive periodiske systemer er det en fordel at udvikle bølgefunktionen i planbølger og bruge Blochs sætning. Det er så kun nødvendigt at inkludere planbølger associeret med lavere kinetisk energi i beregningen. Da valenselektroner er stærkt dominerende i dannelsen af kemiske bånd kan beregningsbyrden lettes yderligere ved anvendelsen af pseudopotentialer.

Rutil er den mest stabile fase af TiO_2 og (110) overfladen den mest stabile overflade. Overfladen består af hele plan af TiO_2 enheder, stablet ovenpå hinanden. Disse

benævnes trilag. De primære karakteristika er rækker af titanium atomer, skiftevis med rækker af iltatomer, der stikker ud af overfladens plan. Overfladerelaksationen stikker dybt ned i overfladen og beregninger må derfor inkludere tilsvarende mange trilag. Iltvakancer dannes let; den laveste vakancedannelsesvarme på 3.0 eV har vakancer i de udstikkende iltrækker. Disse vakancer vekselvirker stærkt langs rækkerne, i mindre grad vinkelret på dem. Under vakancedannelsen frigøres elektroner via båndbrydningen, som derefter er frie til at tage del i binding andre steder. Hvis ingen adsorbater er til stede, forbliver de delvis lokaliseret omkring vakancen, delvis flytter de til titaniumrækkerne. Herfra kan de relokere til elektrofile adsorbater. Denne ladningstransport langs titaniumrækkerne er vidtrækkende og overstiger let 10 Å.

Vakancer kan også dannes i trilagene umiddelbart under overfladen. De har højere dannelsesvarme end vakancer i de udstikkende iltrækker. Tilstedeværelsen af iltadsorbater på overfladen letter dannelsen af vakancer med mindst 2 eV. Ladningsoverførsel fra vakancen til adsorbatet er kritisk for denne stabilisering af vakancen i overfladeregionen. Ligeledes letter tilstedeværelsen af ilt segreringen af vakancer til overfladen.

Ilt kan ikke adsorbere på den defektfrie overflade. Dannelsen af vakancer ændrer overfladekemien drastisk. Iltadsorption bliver varmeudviklende med så meget som 2.2 eV i vakancen og 1.7 eV på titaniumrækken. Den stabiliserende faktor er overførslen af to elektroner til adsorbatet, hvilket gør iltmolekylet dobbeltladet. Dobbeltladede iltmolekyler er karakteriseret ved bindingslængder på 1.40 Å og derover, ligesom i brintoveriltemolekylet. Det magnetiske moment er forsvindende. Overfladevalensen kan skræddersyes til at motivere dannelsen af enkeltladede iltmolekyler. Det kan opnås på flere måder, f.eks. ved at adsorbere mere end et iltmolekyle per vakance eller ved at dopere krystallen med acceptoratomer. Enkeltladede iltmolekyler karakteriseres ved bindingslængder omkring 1.35 Å og magnetiske momenter omkring 1 Bohr magneton. O_2 og CO kan sameksistere på overfladen, hvor de kan danne et pseudobånd. Dette bekræfter muligheden af, at CO kan oxideres på overfladen. Hvis vakancerne ikke beskyttes, f.eks. ved at adsorbere et guldatom i dem, er reaktionen tilbøjelig til at forbruge vakancerne, hvorved videre reaktion umuliggøres. Ozon kan adsorbere på overfladen. Hvis overfladen kan levere mange elektroner, vil ozon dissociere og efterlade et iltatom på overfladen. Hvis kun få elektroner er til rådighed er ozon stabil på overfladen.

Ladningstilstanden af overfladen og den relative elektrofilicitet adsorbaterne imellem er nøglen til at forklare TPD spektra. Ilt adsorberer molekylært på overfladen. Efter adsorption dissocierer molekylerne, hvis tilstrækkeligt mange elektroner er tilstede til at de resulterende iltatomer hver kan få to elektroner. Da dissociation sker med forskellig hastighed ved forskellige temperaturer ses forskellige blandingsforhold mellem adsorberede iltatomer og -molekyler. I et forsøg på at forklare STMobservationer er diffusionen af iltmolekyler forsøgt beskrevet ved en ladningsmedieret proces. Denne model støttes i nogen grad af beregninger. Derimod støtter beregninger ikke eksistensen af ozon på overfladen, som foreslået for at forklare STMmålinger. I stedet kan de samme signaturer forklares ved adsorberede iltatomer og Schottkydefekter. Dette spørgsmål er stadig åbent.

Bibliography

[1] M. Ramamoorthy, D. Vanderbilt, and R. D. King-Smith, "First-principles calculations of the energetics of stoichiometric TiO_2 surfaces," Phys. Rev. B **49,** 16721–16727 (1994).

[2] D. Ollis and H. Al-Ekabi, *Photocatalytic Purification and Treatment of Water and Air* (Elsevier, Amsterdam, 1993).

[3] M. Haruta, "Catalysis of Gold Nanoparticles Deposited on Metal Oxides," CATTECH **6,** 102–115 (2002).

[4] M. Valden, X. Lai, and D. W. Goodman, "Onset of Catalytic Activity of Gold Clusters on Titania with the Appearance of Nonmetallic Properties," Science **281,** 1647–1650 (1998).

[5] O. K. Tan, W. Cao, Y. Hu, and W. Zhu, "Nano-structured oxide semiconductor materials for gas-sensing applications," Ceramics International **30,** 1127–1133 (2004).

[6] S. Yoo, S. A. Akbar, and K. H. Sandhage, "Nanocarving of titania (TiO_2): a novel approach for fabricating chemical sensing platform," Ceramics International **30,** 1121–1126 (2004).

[7] H. Li, K. A. Khor, and P. Cheang, "Titanium dioxide reinforced hydroxyapatite coatings deposited by high velocity oxy-fuel (HVOF) spray," Biomaterials **23,** 85–91 (2002).

[8] Y. Kikuchi, K. Sunada, T. Iyoda, K. Hashimoto, and A. Fujishima, "Photocatalytic bactericidal effect of TiO_2 thin films: Dynamic view of the active oxygen species responsible for the effect," J. Photochem. Photobiol. A: Chem. **106,** 51–56 (1997).

[9] A. Linsebigler, G. Lu, and J. T. J. Yates, "Photocatalysis on TiO_2 Surfaces: Principles, Mechanisms, and Selected Results," Chem. Rev. **95,** 735–758 (1995).

[10] A. Frank, N. Kopidakis, and J. van de Lagemaat, "Electrons in nanostructured TiO_2 solar cells: transport, recombination and photovoltaic properties," Coor. Chem. Rev. **248,** 1165–1179 (2004).

[11] R. Wang, K. Hashimoto, A. Fujishima, M. Chikuni, E. Kojima, A. Kitamura, M. Shimohigoshi, and T. Watanabe, "Light-induced amphiphilic surfaces," Nature **388,** 431–432 (1997).

[12] R. Schaub, P. Thostrup, N. Lopez, E. Lægsgaard, I. Stensgaard, J. K. Nørskov, and F. Besenbacher, "Oxygen vacancies as active sites for water dissociation on rutile $TiO_2(110)$," Phys. Rev. Lett. **87,** 266104 (2001).

[13] S. D. Elliott and S. P. Bates, "Assigment the (1×2) surface of rutile from first principles," Phys. Rev. B **65,** 245415 (2002).

[14] D. Vogtenhuber, R. Podloucky, J. Redinger, E. L. D. Hebenstreit, W. Hebenstreit, and U. Diebold, "*Ab initio* and experimental studies of chlorine adsorption on the rutile $TiO_2(110)$ surface," Phys. Rev. B **65,** 125411 (2002).

[15] J. A. Rodriguez, G. Liu, T. Jirsak, J. Hrbek, Z. Chang, J. Dvorak, and A. Maiti, "Activation of Gold on Titania: Adsorption and Reaction of SO_2 on Au/$TiO_2(110)$," J. Am. Chem. Soc. **124,** 5242–5250 (2002).

[16] J. A. Rodriguez, J. Hrbek, Z. Chang, J. Dvorak, and T. Jirsak, "Importance of O vacancies in the behavior of oxide surfaces: Adsorption of sulfur on $TiO_2(110)$," Phys. Rev. B **65,** 235414 (2002).

[17] P. Hohenberg and W. Kohn, "Inhomogeneous Electron Gas," Phys. Rev. **136,** B864–B871 (1964).

[18] W. Kohn, "Density Functional Theory: fundamentals and applications," In *Proceedings of the international school of physics *Enrico Fermi*, Course LXXXIX, Highlights of Condensed-Matter Theory*, F. Bassami, F. Fumi, and M. P. Tosi, eds., pp. 1–13 (1985).

[19] W. Kohn, "Nobel Lecture: Electronic structure of matter — wave functions and density functionals," Rev. Mod. Phys. **71,** 1253–1266 (1999).

[20] M. Levy, "Electron densities in search of Hamiltonians," Phys. Rev. A **26,** 1200–1208 (1982).

[21] E. Lieb, "Density Functionals for Coulomb Systems," In *Physics as Natural Philosophy: Essays in honor of Laszlo Tisza on his 75th Birthday*, A. Shimony and H. Feshbach, eds., pp. 111–149 (1982).

[22] P. L. Taylor and O. Heinonen, *A Quantum Approach to Condensed Matter Physics* (Cambridge University Press, Cambridge, 2002).

[23] B. Hammer and J. K. Nørskov, "Theoretical Surface Science and Catalysis—Calculation and Concepts," Adv. Catal. **45,** 71–130 (2000).

[24] A. Roudgar and A. Gross, "Local reactivity of metal overlayers: Density functional theory calculations of Pd on Au," Phys. Rev. B **67,** 033409 (2003).

[25] R. O. Jones and O. Gunnarson, "The density functional formalism, its applications and prospects," Rev. Mod. Phys. **61,** 689–746 (1989).

[26] J. P. Perdew, "Unified theory of exchange and correlation beyond the local density approximation," In *Electronic Structure of Solids '91*, P. Ziesche and H. Eschrig, eds., Physical Research **17,** 11–20 (Akademie Verlag, Berlin, 1991).

[27] B. Hammer, L. B. Hansen, and J. K. Nørskov, "Improved adsorption energetics within density-functional theory using revised Perdew-Burke-Ernzerhof functionals," Phys. Rev. B **59,** 7413–7421 (1999).

[28] J. P. Perdew, K. Burke, and M. Ernzerhof, "Generalized Gradient Approximation Made Simple," Phys. Rev. Lett. **77,** 3865–3868 (1996).

[29] M. C. Payne, M. P. Teter, D. C. Allan, T. A. Arias, and J. D. Joannopoulos, "Iterative minimization techniques for *ab initio* total-energy calculations: molecular dynamics and conjugate gradients," Rev. Mod. Phys. **64,** 1045–1097 (1992).

[30] N. W. Ashcroft and N. D. Mermin, *Solid State Physics* (Saunders College Publishing, New York, 1976).

[31] A. Gross, *Theoretical Surface Science: A Microscopic Perspective* (Springer-Verlag, Berlin Heidelberg, 2003).

[32] D. J. Chadi and M. L. Cohen, "Special Points in the Brillouin Zone," Phys. Rev. B **8,** 5747–5753 (1973).

[33] H. J. Monkhorst and J. D. Pack, "Special points for Brillouin-zone integrations," Phys. Rev. B **13,** 5188–5192 (1976).

[34] D. Vanderbilt, "Soft self-consistent pseudopotentials in a generalized eigenvalue formalism," Phys. Rev. B **41,** 7892–7895 (1990).

[35] D. R. Hamann, M. Schlüter, and C. Chiang, "Norm-Conserving Pseudopotentials," Phys. Rev. Lett. **43,** 1494–1497 (1979).

[36] P. Hänggi and P. Talkner, "Reaction-rate theory: fifty years after Kramers," Rev. Mod. Phys. **62,** 251–341 (1990).

[37] H. Jónsson, G. Mills, and K. W. Jakobsen, "Nudged Elastic Band Method," In *Classical and Quantum Dynamics in Condensed Phase Simulation. Proceedings of the School of Physics "Computer Simulation of Rare Events and the Dynamics of Classical and Quantum Dynamics in Condensed Phase Systems"*, B. J. Berne, G. Ciccotti, and D. F. Coker, eds., pp. 386–404 (1997).

[38] S. P. Bates, G. Kresse, and M. J. Gillan, "A systematic study of the surface energetics and structure of $TiO_2(110)$ by first-principles calculations," Surf. Sci. **385,** 386–394 (1997).

[39] G. Charlton *et al.*, "Relaxation of TiO_2(110)-(1×1) Using Surface X-Ray Diffraction," Phys. Rev. Lett. **78,** 495–498 (1997).

[40] N. M. Harrison, X.-G. Wang, J. Muscat, and M. Scheffler, "The influence of soft vibrational modes on our understanding of oxide surface structure," Faraday Discuss. **114,** 305–312 (1999).

[41] T. Bredow, L. Giordano, F. Cinquini, and G. Pacchioni, "Electronic properties of rutile TiO_2 ultrathin films : Odd-even oscillations with the number of layers," Phys. Rev. B. **70,** 035419 (2004).

[42] H. Onishi and Y. Iwasawa, "Reconstruction of TiO_2(110) surface: STM study with atomic-scale resolution," Surf. Sci. **313,** L783–L789 (1994).

[43] M. Li, W. Hebenstreit, and U. Diebold, "Oxygen-induced restructuring of the rutile TiO_2(110)(1×1) surface," Surf. Sci. **414,** L951–L956 (1998).

[44] M. Li, W. Hebenstreit, L. Gross, U. Diebold, M. A. Henderson, D. R. Jennison, P. A. Schultz, and M. P. Sears, "Oxygen-induced restructuring of the TiO_2(110) surface: a comprehensive study," Surf. Sci. **437,** 173–190 (1999).

[45] M. Li, W. Hebenstreit, U. Diebold, M. A. Henderson, and D. R. Jennison, "Oxygen-induced restructuring of rutile formation TiO_2(110) : mechanism, atomic models, and influence on surface chemistry," Faraday Discuss. **114,** 245–258 (1999).

[46] M. Li, W. Hebenstreit, U. Diebold, A. M. Tyryshkin, M. K. Bowman, G. G. Dunham, and M. A. Henderson, "The Influence of the Bulk Reduction State on the Surface Structure and Morphology of Rutile TiO_2(110) Single Crystals," J. Phys. Chem. B **104,** 4944–4950 (2000).

[47] M. Li, W. Hebenstreit, and U. Diebold, "Morphology change of oxygen-restructured TiO_2(110) surfaces by UHV annealing: Formation of a low-temperature (1×2) structure," Phys. Rev. B **61,** 4926–4933 (2000).

[48] S. D. Elliott and S. P. Bates, "A first principles survey of stoichiometric (1×2) reconstructions on the rutile surface," Surf. Sci. **495,** 211–233 (2001).

[49] S. D. Elliott and S. P. Bates, "Assigning the (1×2) surface reconstructions on reduced rutile by first-principles energetics," Phys. Rev. B **65,** 245415 (2002).

[50] U. Diebold, "The surface science of titanium dioxide," Surf. Sci. Rep. **48,** 53–229 (2003).

[51] P. J. D. Lindan, N. M. Harrison, M. J. Gillan, and J. A. White, "First-principles spin-polarized calculations on the reduced and reconstructed TiO_2(110) surface," Phys. Rev. B **55,** 15919–15927 (1997).

[52] A. T. Paxton and L. Thiên-Nga, "Electronic structure of reduced titanium dioxide," Phys. Rev. B **57,** 1579–1584 (1998).

[53] Personal comunication between Dr. Bjørk Hammer and Dr. Philip Lindan.

[54] T. Bredow and G. Pacchioni, "Electronic structure of an isolated oxygen vacancy at the TiO_2(110) surface," Chem. Phys. Lett. **355,** 417–423 (2002).

[55] M. Menetrey, A. Markovits, C. Minot, and G. Pacchioni, "Formation of Schottky Defects at the Surface of MgO, TiO_2(110) and SiO_2(110): A Comparative Density Functional Study," J. Phys. Chem. **108,** 12858–12864 (2004).

[56] M. P. de Lara-Castells and J. L. Krause, "Periodic Hartree-Fock study of the adsorption of molecular oxygen on a reduced TiO_2 (110) surface," J. Chem. Phys. **115,** 4798–4810 (2001).

[57] M. P. de Lara-Castells and J. L. Krause, "Theoretical study of the interaction of molecular oxygen with a reduced TiO_2 surface," Chem. Phys. Lett. **354,** 483–490 (2002).

[58] X. Wu, A. Selloni, M. Lazzeri, and S. K. Nayak, "Oxygen vacancy mediated adsorption and reactions of molecular oxygen on the TiO_2(110) surface," Phys. Rev. B **68,** 241402 (2003).

[59] D. Vogtenhuber, R. Podloucky, and J. Redinger, "Ab initio study of atomic Cl adsorption on stoichiometric and reduced rutile TiO_2(110) surfaces," Surf. Sci. **454-456,** 369–373 (2000).

[60] Y. Wang, D. Pillay, and G. S. Wang, "Dynamics of oxygen species on reduced TiO_2," Phys. Rev. B **70,** 193410 (2004).

[61] S. C. Abrahams and J. L. Bernstein, "Rutile: Normal Probability Plot Analysis and Accurate Measurement of Crystal Structure," J. Chem. Phys. **55,** 3206–3211 (1971).

[62] V. E. Henrich and P. A. Cox, *The surface science of metal oxides* (Cambridge University Press, Cambridge, 1996).

[63] J. P. LaFemina, "Total Energy Computaions of Oxide Surface Reconstructions," Crit. Rev. Surf. Chem. **3,** 297–386 (1994).

[64] P. W. Tasker, "The stability of ionic crystal surfaces," J. Phys. C **12,** 4977–4984 (1979).

[65] R. Lindsay, A. Wander, A. Ernst, B. Montanari, C. Thornton, and N. Harrison, "Revisiting the surface structure of TiO_2(110): A not so simple LEED investigation," In *VIII European Conference on Surface Crystallography and Dynamcs ECSCD-8*, (2004).

[66] M. Ramamoorthy, R. D. King-Smith, and D. Vanderbilt, "Defects on TiO_2(110) surfaces," Phys. Rev. B **49,** 7709–7715 (1994).

[67] K. Onda, B. Lin, and H. Petek, "Two-photon photoemission spectroscopy of TiO_2(110) surfaces modified by defects and O_2 or H_2O adsorbates," Phys. Rev. B **70,** 045415 (2004).

[68] U. Diebold, J. Lehman, T. Mahmoud, M. Kuhn, G. Leonardelli, W. Hebenstreit, M. Schmid, and P. Varga, "Intrinsic defects on a TiO_2(110)(1$\times$1) surface and their reaction with oxygen: a scanning tunneling microscopy study," Surf. Sci. **411,** 137–153 (1998).

[69] E. L. D. Hebenstreit, W. Hebenstreit, H. Geisler, J. C. A. Ventrice, P. T. Sprunger, and U. Diebold, "Bulk-defect dependent adsorption on a metal oxide surface: S/TiO_2(110)," Surf. Sci. **486,** L467–L474 (2001).

[70] U. Diebold, M. Li, O. Dulub, E. L. D. Hebenstreit, and W. Hebenstreit, "The relationship between bulk and surface properties of rutile TiO_2(110)," Surf. Rev. Lett. **7,** 613–617 (2000).

[71] M. A. Henderson, "Mechanism for the bulk-assisted reoxidation of ion sputtered TiO_2 surfaces: Diffusion of oxygen to the surface or titanium to the bulk?," Surf. Sci. **343,** L1156–L1160 (1995).

[72] M. A. Henderson, "A surface perspective on self-diffusion in rutile TiO_2," Surf. Sci. **419,** 174–187 (1999).

[73] J. A. Rodriguez, T. Jirsak, G. Liu, J. Hrbek, J. Dvorak, and A. Maiti, "Chemistry of NO_2 on Oxide Surfaces: Formation of NO_3 on TiO_2(110) and $NO_2 \leftrightarrow$O Vacancy Interactions," J. Am. Chem. Soc. **123,** 9597–9605 (2001).

[74] J. Oviedo, M. A. S. Miguel, and J. F. Sanz, "Oxygen vacancies on TiO_2 (110) from first principles calculations," J. Chem. Phys. **121,** 7427–7433 (2004).

[75] R. Schaub, E. Wahlström, A. Rønnau, E. Lægsgaard, I. Stensgaard, and F. Besenbacher, "Oxygen-Mediated Diffusion of Oxygen Vacancies on the TiO_2(110) Surface," Science **299,** 377–379 (2003).

[76] G. Q. Lu, A. Linsebigler, and J. T. Yates, "The Photochemical Identification of 2 Chemisorption States for Molecular-Oxygen on TiO_2(110)," J. Chem. Phys. **102,** 3005–3008 (1995).

[77] C. N. Rusu and J. T. J. Yates, "Defect Sites on TiO_2(110). Detection by O_2 Photodesorption," Langmuir **13,** 4311–4316 (1997).

[78] W. S. Epling, C. H. F. Peden, M. A. Henderson, and U. Diebold, "Evidence for oxygen adatoms on TiO_2(110) resulting from O_2 dissociation at vacancy sites," Surf. Sci. **412-413,** 333–343 (1998).

[79] R. Souda, "Resonant ion stimulated desorption of O^+ and H^+: A probe of interactions of oxygen and hydrogen with TiO_2," J. Chem. Phys. **111,** 10652 (1999).

[80] C. Shu, N. Sukumar, and C. P. Ursenbach, "Adsorption of O_2 on TiO_2(110): A theoretical study," J. Chem. Phys. **110,** 10539–10544 (1999).

[81] M. A. Henderson, W. S. Epling, C. L. Perkins, C. H. F. Peden, and U. Diebold, "Interaction of Molecular Oxygen with the Vacuum-Annealed TiO_2(110) Surface: Molecular and Dissociative Channels," J. Phys. Chem. B **103,** 5328–5337 (1999).

[82] M. P. de Lara-Castells and J. L. Krause, "Theoretical study of the UV-induced desorption of molecular oxygen from the reduced TiO_2 surface," J. Chem. Phys **118,** 5098–5105 (2003).

[83] E. Wahlström, E. Vestergaard, R. Schaub, A. Rønnau, M. Vestergaard, E. Lægsgaard, I. Stensgaard, and F. Besenbacher, "Electron Transfer-Induced Dynamics of Oxygen Molecules on the TiO_2(110) Surface," Science **303,** 511–513 (2004).

[84] T. L. Thompson, O. Diwald, and J. T. Yates, "Molecular oxygen-mediated vacancy diffusion on TiO_2(110)-new studies of the proposed mechanism," Chem. Phys. Lett. **393,** 28–30 (2004).

[85] C. Zhang and P. J. D. Lindan, "A density functional study of the coadsorption of water and oxygen on TiO_2," J. Chem. Phys. **121,** 3811–3815 (2004).

[86] X. Wu, A. Selloni, and S. K. Nayak, "First principles study of CO oxidation on TiO_2(110): The role of surface oxygen vacancies," J. Chem. Phys **120,** 4512–4516 (2004).

[87] D. C. Sorescu and J. J. T. Yates, "Adsorption of CO on the TiO_2(110) Surface: A Theoretical Study," J. Phys. Chem. B **102,** 4556–4565 (1998).

[88] D. C. Sorescu and J. J. T. Yates, "First Principles Calculations of the Adsorption Properties of CO and NO on the Defective TiO_2(110) Surface," J. Phys. Chem. B **106,** 6184–6199 (2002).

[89] J. Li, L. Wu, and Y. Zhang, "Theoretical study of adsorbed-decomposition of NO, CO and CH_2O on a TiO_2(110) (1×1) defect surface," Chem. Phys. Lett. **342,** 249–258 (2001).

[90] D. C. Sorescu, C. N. Rusu, and J. J. T. Yates, "Adsorption of NO on the TiO_2(110) Surface: An Experimental and Theoretical Study," J. Phys. Chem. B **104,** 4408–4417 (2000).

[91] A. N. Shultz, W. M. Hetherington, III, D. R. Baer, L.-Q. Wang, and M. H. Engelhard, "Comparative SHG and XPS studies of interactions between defects and N_2O on (110) rutile TiO_2surfaces," Surf. Sci. **392,** 1–7 (1997).

[92] A. Eichler and J. Hafner, "Adsorbate-induced vacancy formation and substrate relaxation on Cr(100)," Phys. Rev. Lett. **79,** 4481–4484 (1997).

[93] W. Göpel, G. Rocker, and R. Feierabend, "Intrinsic defects of TiO_2(110): Interaction with chemisorbed O_2, H_2, CO, and CO_2," Phys. Rev. B **28,** 3427–3438 (1983).

[94] M. Okumura, J. M. Coronado, J. Soria, M. Haruta, and J. C. Conesay, "EPR Study of CO and O_2 Interaction with Supported Au Catalysts," J. Catal. **203,** 168–174 (2001).

[95] S. G. Bratsch, "Revised Mulliken Electronegativities," J. Chem. Edu. **65,** 34–41 (1988).

[96] U. Gesenhues and T. Rentschler, "Crystal growth and defect structure of Al^{3+}-doped rutile," J. Solid State Chem. **143,** 210–218 (1999).

[97] G. Rayner-Canham, *Descriptive Inorganic Chemistry* (W. H. Freeman and Company, New York, 1999).

[98] M. Menetrey, A. Markovits, and C. Minot, "Reactivity of a reduced metal oxide surface: hydrogen, water and carbon monoxide adsorption on oxygen defective rutile TiO_2(110)," Surf. Sci. **524,** 49–62 (2003).

[99] M. A. Henderson, W. S. Epling, C. H. F. Peden, and C. L. Perkins, "Insights into Photoexcited Electron Scavenging Processes on TiO_2 Obtained from Studies of the Reaction of O_2 with OH Groups Adsorbed at Electronic Defects on TiO_2(110)," J. Phys. Chem. B **107,** 534–545 (2003).

[100] P. J. D. Lindan, N. M. Harrison, and M. J. Gillan, "Mixed Dissociative and Molecular Adsorption of Water on the Rutile (110) Surface," Phys. Rev. Lett. **80,** 762–765 (1998).

[101] W. Langel, "Car-Parrinello simulation of H_2O dissociation on rutile," Surf. Sci. **496,** 141–150 (2002).

[102] E. K. Vestergaard, Ph.D. thesis, Department of Physics and Astronomy, University of Århus, Denmark, 2004.

[103] T. Beck, A. Klust, M. Batzill, U. Diebold, C. D. Valentin, and A. Selloni, "Surface Structure of TiO_2(011)-(2×1)," Phys. Rev. Lett. **93,** 036104 (2004).

[104] M. Haruta, "Size- and support-dependency in the catalysis of gold," Catal. Today **36,** 153–166 (1997).

[105] M. S. Chen and D. W. Goodman, "The Structure of Catalytically Active Gold on Titania," Science **206,** 252–255 (2004).

[106] F. Cosandey and T. E. Madey, "Growth, morphology, interfacial effects and catalytic properties of Au on TiO_2," Surf. Rev. Lett. **8,** 73–93 (2001).

[107] Y. W. Devina Pillay and G. S. Hwang, "A Comparative Theoretical Study of Au, Ag and Cu Adsorption on TiO_2 (110) Rutile Surfaces," Korean J. Chem. Eng. **21,** 537–547 (2003).

[108] N. Lopez, J. K. Nørskov, T. Janssens, A. Carlsson, A. Puig-Molina, B. Clausen, and J. D. Grunwaldt, "The adhesion and shape of nanosized Au particles in a Au/TiO_2(110) catalyst," J. Catal. **225,** 86–94 (2004).

[109] N. Lopez and J. K. Nørskov, "Theoretical study of the Au/TiO_2(110) interface," Surf. Sci. **515,** 175–186 (2002).

[110] E.Wahlström, N. Lopez, R. Schaub, P. Thostrup, A. Rønnau, C. Africh, E. Lægsgaard, J. K. Nørskov, and F. Besenbacher, "Bonding of Gold Nanoclusters to Oxygen Vacancies on Rutile TiO2(110)," Phys. Rev. Lett. **90,** 026101 (2003).

[111] Z.-P. Liu, X. Gong, J. Kohanoff, C. Sanches, and P. Hu, "Catalytic role of Metal Oxides in Gold-Based Catalysts: A First Principles Study of CO Oxidation on TiO_2 Supported Au," Phys. Rev. Lett. **91,** 266102 (2003).

[112] K. Okazaki, Y. Morikawi, S. Tanaka, K. Tanaka, and M. Kohyyama, "Electronic structures of Au on TiO_2 by first-principles calculations," Phys. Rev. B **69,** 235404 (2004).

[113] A. Vijay, G. Mills, and H. Metiu, "Adsorption of gold on stoichiometric and reduced rutile TiO_2(110) surfaces," J. Chem. Phys. **118,** 6536–6551 (2003).

[114] Z.-P. Liu, P. Hu, and A. Alavi, "Catalytic role of Gold in Gold-Based Catalysts: A Density Functional Theory Study on the CO Oxidation on Gold," J. Am. Chem. Soc. **124,** 14770–14779 (2002).

[115] A. Vittadini and A. Selloni, "Small gold clusters on stoichiometric and defected anatase (101) and their interaction with CO: A density functional study," J. Chem. Phys. **117,** 353–361 (2002).

[116] Q. Fujishima, H. Saltsburg, and M. Flytzani-Stephanopoulos, "Active Nonmetallic Au and Pt Species on Ceria-Based Water-Gas Shift Catalysts," Science **301,** 935–938 (2003).

[117] W. Wang, L. W. Chiang, and Y. Ku, "Decomposition of benzene in air streams by UV/TiO_2 process," Journal of Hazardous Materials **101,** 133–146 (2003).

[118] K. Sekiguchi, A. Sanada, and K. Sakamoto, "Degradation of toluene with an ozone-decomposition catalyst in the presence of ozone, and the combined effect of TiO_2 addition," Catalysis Communications **4,** 247–252 (2003).

[119] L. S. Li, W. P. Zhu, P. Y. Zhang, Z. Y. Chen, and W. Y. Han, "Photocatalytic oxidation and ozonation of catechol over carbon-black-modified nano-TiO_2 thin films supported on A1 sheet," Water Research **37,** 3646–3651 (2003).

[120] P. Y. Zhang, F. Y. Liang, G. Yu, Q. Chen, and W. P. Zhu, "A comparative study on decomposition of gaseous toluene by O-3/UV, TiO_2/UV and O-3/TiO_2/UV," J. Photochem. Photobiol. A: Chem. **156,** 189–194 (2003).

[121] A. Kerc, M. Bekbolet, and M. A. Saatci, "Effect of partial oxidation by ozonation on the photocatalytic degradation of humic acids," Internationel Journal of Photoenergy **5,** 75–80 (2003).

[122] M. D. Hernandez-Alsonso, J. M. Coronado, A. J. Maira, J. Soria, V. Loddo, and V. Augugliaro, "Ozone enhanced activity of aqueous titanium dioxide suspensions for photocatalytic oxidation of free cyanide ions," Applied Catalysis B - Environmental **39,** 257–267 (2002).

[123] H. Suty, C. D. Traversay, and M. Cost, "Applications of advanced oxidation processes: present and future," Water Science and Technology **49,** 227–233 (2004).

[124] C. Tizaoui and M. J. Slater, "Uses of ozone in a three-phase system for water treatment: Ozone adsorption," Ozone-Science and Engineering **25,** 315–322 (2003).

[125] P. R. Gogate and A. B. Pandit, "A review of imperative technologies for wastewater treatment I: oxidation technologies at ambient conditions," Advances in Environmental Reasearch **8,** 501–551 (2004).

[126] F. J. Beltran, F. J. Rivas, and R. M. de Espinosa, "A TiO_2/Al_2O_3 catalyst to improve the ozonation of oxalic acid in water," Applied Catalysis B - Environmental **47,** 101–109 (2004).

[127] G. Ciardelli, I. Ciabatti, L. Ranieri, G. Capannelli, and A. Bottino, "Membrane contactors for textile wastewater ozonation," Advanced Membrane Technology **984,** 29–38 (2003).

[128] J. Arana, J. A. H. Melian, J. M. D. Rodriguez, O. G. Diaz, A. Viera, J. P. Pena, P. P. M. Sosa, and V. E. Jimenez, "TiO_2-photocatalysis as a tertiary treatment of naturally treated wastewater," Catalysis Today **76,** 279–289 (2002).

[129] K. C. Cho, K. C. Hwang, T. Sano, K. Takeuchi, and S. Matsuzawa, "Photocatalytic performance of Pt-loaded TiO_2 in the decomposition of gaseous ozone," J. Photochem. Photobiol. A: Chem. **161,** 155–161 (2004).

[130] A. Mills, S. K. Lee, and A. Lepre, "Photodecomposition of ozone sensitised by a film of titanium dioxide on glass," J. Photochem. Photobiol. A: Chem. **155,** 199–205 (2003).

[131] J. J. Lin, A. Kawai, and T. Nakajima, "Effective catalysts for decomposition of aqueous ozone," Applied Catalysis B- Environmental **39,** 157–165 (2002).

[132] Personal comunication with Dr. Renald Schaub.